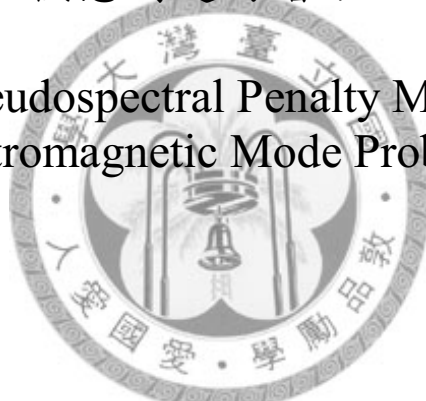


國立臺灣大學電機資訊學院光電工程學研究所
碩士論文

Graduate Institute of Photonics and Optoelectronics
College of Electrical Engineering and Computer Science
National Taiwan University
Master Thesis

解電磁模態問題的譜方法新模型

New Pseudospectral Penalty Models for
Electromagnetic Mode Problems



江舜凡

Chiang, Shun-Fan

指導教授：張宏鈞 博士

Advisor: Hung-chun Chang, Ph.D.

中華民國97年7月
July, 2008

摘要

在本篇論文中，我們發展了新的電磁解析模型來分析一維波導、二維波導和光子晶體結構。同時，我們也推導了新的同步近似項的邊界條件來配合新的方程式。另外，由於樂勤得 (Legendre) 內差方程式準確的近似特性，我們也使用了譜方法中的樂勤得法來對空間分割。

不同於大部分是以赫姆霍茲 (Helmholtz) 方程式為基礎來解波導模態，我們提出了一種綜合了馬克斯威爾旋度以及散度方程式的新模型來產生特徵值 (eigenvalue) 問題的方法。對於在介面的邊界條件，我們則是使用了同步近似項的邊界條件，這種邊界條件可以在數學上證明具有穩定數值的效果。雖然在時域上，使用同步近似項邊界條件的譜方法是一個被證實具有不錯收斂性質的數值方法，但其使用的方程式跟本篇研究所發展的、在頻域使用的方程式有本質上的不同。在時域上我們所考慮的電磁場一律是實數，但在頻域上因為使用相位法的因素，所有的電磁場必須使用複數來表示。所以我們重新推導了分別給一維波導、二維波導和光子晶體使用的同步近似項邊界條件。

而為了確認新提出演算法的效率程度和數值收斂性，我們做了一些數值實例分析。這些光實例包括平板波導、部份填滿波導、圓柱形波導、具有尖角的埋入式波導、肋型波導以及四角晶格和三角晶格這兩種光子晶體結構。利用新的演算法來解這些結構時，我們可以得到高精度的傳播常數和特徵頻率以及觀察到指數收斂的特性。另外要特別說明的是，對於有尖角的介質波導，我們在沒有對邊界作任何特殊處理的情況下，得到了比以往更準確的數值解，這代表了在光波導分析領域的一項重大突破。

Abstract

In this thesis, mode solvers for one-dimensional (1D) and 2D waveguides, and photonic crystals (PCs) with new electromagnetic formulations are developed. The new penalty-type boundary conditions are derived to work with new formulations, and the pseudospectral Legendre method is adopted to perform spatial discretization for its accurate approximation property.

Unlike many waveguide mode solvers which are based on Helmholtz equations, we propose new formulations which combine Maxwell's curl and divergence equations to derive the eigenvalue problem. For the interface boundary condition treatment, penalty-type boundary conditions are employed and mathematically proved that they can stabilize the scheme. Although pseudospectral time-domain (PSTD) methods with penalty-type boundary conditions have been known to offer good convergence property, the related frequency-domain formulations developed in this work possess intrinsic difference. In time-domain simulations, the electromagnetic fields considered are all real quantities, while in frequency-domain analysis, the fields are complex ones with the phasor technique. And new penalty-type boundary conditions in the frequency-domain mode analysis of 1D and 2D waveguides, and PCs, are respectively derived.

Numerical examples are considered to examine the efficiency and numerical convergence property of the proposed algorithms. Optical structures in these examples include slab waveguides, partial-filled waveguide, fiber waveguides, channel waveguides with sharp corners, rib waveguides, PCs with square lattice, and PCs with triangular lattice. Spectral convergence property with very high-accuracy modal effective index and eigenfrequency calculation is achieved. In particular, for the dielectric waveguide with corners, higher numerical accuracy than reported results is obtained without doing field singularity treatment at the corners as in the latter. This represents significant advancement in the numerical analysis of optical waveguide problems.

Contents

1	Introduction	1
1.1	Motivations	1
1.2	Chapter Outline	3
2	Mathematical Formulation for 1D Waveguide Analysis	5
2.1	Equations Used for 1D Waveguide Structure	5
2.2	Well-posedness Analysis	6
2.3	The Energy Method	9
2.4	Characteristic Representations of Physical Boundary Condition	10
2.5	Design of the Scheme	12
2.6	Final Form of the Formulation	14
3	Mathematical Formulation for 2D Waveguide Analysis	18
3.1	Equations Used for 2D Waveguide Structure	18
3.2	Well-posedness Analysis	20
3.3	The Energy Method	23
3.4	Characteristic Representations of Physical Boundary Conditions	25
3.5	Design of the Scheme	27
3.6	The Final Form of The Six-Equation Version	29
3.7	The Final Form of Three-Equation Version	31

4	Mathematical Formulation for 2D Photonic Crystal Analysis	35
4.1	Equations Used for PC Structure	35
4.2	Well-posedness Analysis	36
4.3	The Energy Method	37
4.4	Characteristic Representations of Physical Boundary Condtions	38
4.5	Design of the Scheme	40
4.6	The Final Form of The Three-Equation Version	42
4.7	The Final Form of the One-Equation Version	43
5	Pseudospectral Method and Shifted Inverse Power Method	45
5.1	The Pseudospectral Method	45
5.1.1	Overview of the Pseudospectral Method	45
5.1.2	The Pseudospectral Legendre Method	46
5.1.3	Curvilinear Representation of The Pseudospectral Method	48
5.2	The Shifted Inverse Power Method	51
5.2.1	The Algorithm of SIPM	51
5.2.2	The Iterative Method	52
5.2.3	Guessing the Initial Eigenvector Using Former Data	54
6	Numerical Results For Waveguide Problems	57
6.1	Symmetric Slab Waveguides	57
6.2	Asymmetric Slab Waveguides	58
6.3	Partially Filled Metallic Waveguides	58
6.4	Circular Metallic Waveguides	59
6.5	Fiber Waveguides	60
6.6	Channel Waveguides with Sharp Corners	61
6.7	Rib Waveguides	62

7	Numerical Results For Photonic Crystal Problems	86
7.1	Square-Lattice Photonic Crystals	86
7.2	Triangular-Lattice Photonic Crystals	87
8	Conclusion	96



List of Figures

2.1	Transformation between global and local coordinates.	17
2.2	The grid points in domain M.	17
3.1	Transformation between global and local coordinates.	34
3.2	The characteristic of $l_0(x)$	34
5.1	Using former data to interpolate initial eigenvector	56
6.1	Sketch of a slab waveguide.	64
6.2	Field profile for the TE mode of the symmetric waveguide.	64
6.3	Relative errors in the effective index for the TE and TM modes of symmetric slab waveguide with respect to the degree of polynomial in each domain.	65
6.4	Field profile for TE mode of the asymmetric waveguide.	66
6.5	Field profile for TM mode of the asymmetric waveguide.	66
6.6	Relative errors in the effective index for the TE and TM modes of asymmetric slab waveguide with respect to the degree of polynomial in each domain.	67
6.7	Cross-section of a partially filled metallic waveguide.	68
6.8	Mesh division of the partially filled metallic waveguide of Fig. 6.6. . .	68
6.9	Relative error in the effective index for the fundamental LSE ₁₀ mode of the partially filled metallic waveguide of Fig. 6.7.	69
6.10	Sketch of a quarter of the cross-section of a circular metallic waveguide.	70
6.11	Mesh division for the structure of Fig. 6.10.	70

6.12	Relative errors in the effective index for the fundamental TE_{11} mode of the circular metallic waveguide of Fig. 6.10.	71
6.13	Distributions of the six field components of the fundamental (TE_{11}) mode of the circular metallic waveguide of Fig. 6.10.	72
6.14	Sketch of a quarter of the cross-section of a circular fiber waveguide. . .	73
6.15	Mesh division of for the structure of Fig. 6.14.	73
6.16	Relative errors in the effective index for the fundamental (HE_{11}) mode of the circular fiber waveguide of Fig. 6.14.	74
6.17	Distributions of the six field components of the fundamental (HE_{11}) mode of the circular fiber waveguide of Fig. 6.14.	75
6.18	Sketch of a quarter of the cross-section of the channel waveguide. . .	76
6.19	Mesh division for the structure of Fig. 6.18.	76
6.20	Relative errors in the effective index for the fundamental mode of the channel waveguide of Fig. 6.18, as compared to <i>Hadley's</i> results [<i>Hadley, 2002</i>] ($n_{eff} = 1.27627404$).	77
6.21	Same as Fig. 6.20 but with the reference effective index value being that calculated with degree-45 polynomials ($n_{eff} = 1.27627403774$). . .	78
6.22	Field profiles of E_x along $\phi = 45^\circ$ for the channel waveguide of Fig. 6.18 calculated using various degrees of polynomial.	79
6.23	Field profiles of E_y along $\phi = 45^\circ$ for the channel waveguide of Fig. 6.18 calculated using various degrees of polynomial.	79
6.24	Field profiles of E_z along $\phi = 45^\circ$ for the channel waveguide of Fig. 6.18 calculated using various degrees of polynomial.	80
6.25	Field profiles of H_x along $\phi = 45^\circ$ for the channel waveguide of Fig. 6.18 calculated using various degrees of polynomial.	80
6.26	Field profiles of H_y along $\phi = 45^\circ$ for the channel waveguide of Fig. 6.18 calculated using various degrees of polynomial.	81

6.27	Field profiles of H_z along $\phi = 45^\circ$ for the channel waveguide of Fig. 6.18 calculated using various degrees of polynomial.	81
6.28	Distributions of the six field components of the fundamental mode of the channel waveguide of Fig. 6.18.	82
6.29	Sketch of a half of the cross-section of the rib waveguide.	83
6.30	Mesh division for the structure of Fig. 6.29.	83
6.31	Relative error in the effective index for the fundamental mode of the rib waveguide of Fig. 6.29, as compared to <i>Hadley's</i> result [<i>Hadley, 2002</i>].	84
6.32	Distributions of the six field components of the fundamental mode of the rib waveguide of Fig. 6.29.	85
7.1	Sketch of the cross-section of a PC with square lattice.	88
7.2	Mesh division of the unit cell in Fig. 7.1.	88
7.3	Band diagram for TE modes of the square-lattice PC of Fig. 7.1.	89
7.4	Band diagram for TM modes of the square-lattice PC of Fig. 7.1.	89
7.5	Relative errors in the calculated eigen frequency versus the degree of polynomial for the first TE and TM modes of the square-lattice PC of Fig. 7.1 at the M point using the degree-21 three-equation formulation result as reference.	90
7.6	(a)(b)(c) Field distributions of the first TE mode at the M point for the square-lattice PC of Fig. 7.1. (d)(e)(f) Field distributions of the first TM mode at the M point for the same PC.	91
7.7	Sketch of the cross-section of a PC with triangular lattice.	92
7.8	Mesh division of the unit cell in Fig. 7.7.	92
7.9	Band diagram for TE modes of the triangle-lattice PC of Fig. 7.7.	93
7.10	Band diagram for TM modes of the triangular-lattice PC of Fig. 7.7.	93

7.11 Relative errors in the calculated eigen function versus the degree of polynomial of the triangular-lattice PC of Fig. 7.7 at the K point using the degree-21 three-equation formulation result as the reference. 94

7.12 (a)(b)(c) Field distributions of the first TE mode at the K point for the triangular-lattice PC of 7.7. (d)(e)(f) Field distributions of the first TM mode of PC at the K point for the same PC. 95





Chapter 1

Introduction

1.1 Motivations

For constructing various guided-wave devices and components in optical communication systems, optical waveguides and, in recent years, photonic crystals (PCs) have been played important roles. In the design of these waveguides and PCs, it is important to understand accurate propagation characteristics of electromagnetic waves in these structures. But unfortunately, according to Maxwell's equations, it is impossible to have analytical solutions for most waveguides and PCs with various cross-sections and materials, and we often need computer numerical analysis to understand the performance of many new types of these structures.

There are various types of numerical analysis methods for waveguide analysis, which directly solve the eigenvalue problems associated with the corresponding problems. Typical methods include the spectral index method (SIM) [*Stern et al.*, 1990], the finite element methods (FEMs) [*Cendes and Silvester*, 1970; *Rahman and Davis*, 1984; *Lee et al.*, 1991], the finite difference methods (FDMs)[*Bierwirth et al.* 1986; *Lüsse et al.*, 1994; *Hadley and Smith*, 1995], and the integral equation methods [*Sphicopoulos et al.*, 1985; *Baken et al.*, 1990]. Although the SIM is easy to use, it is not adequate for solving more and more sophisticated structures. And although both the FEM and FDM are well developed and robust methods, they often need a lot of mesh grids for obtaining better numerical results. Comparing with these numerical methods, spectral methods to be employed in this research can offer more

precise solutions with the same amount of mesh grids.

The prototype of spectral methods for the solution of differential equation problems is the well-known Fourier method in fluid mechanics. In 1970s, the Fourier method was first applied to direct numerical simulation of turbulence [*Orszag and Patterson, 1972*]. This success was fundamental for a fast calculation technique of the nonlinear terms through the “pseudospectral” methods (PSMs). In the Fourier method, the differentiations are made in the spectral space (the space of the expansion coefficients) and the products are performed in the physical space (the space of the values of the unknowns). But the Fourier method is unable to handle non-periodic problems due to the nonuniform convergence of the Fourier series at the extremities of the domain, known as the Gibbs oscillation. So for the nonperiodic problems, the Chebyshev and Legendre polynomials [*Boyd, 1999*] are used. Through the PSMs based on Fourier, Chebyshev, and Legendre polynomials, we can transfer differential operators into high-order numerical differential matrices.

In recent years, PSMs have been extended to the analysis of electromagnetic problems both in time-domain [*Yang et al., 1999; Hesthaven et al., 1999*] and frequency-domain [*Wu, 2003; Chiang, 2007*]. In frequency-domain, *Chiang* [2007] has developed mode solvers for two-dimensional (2D) waveguides and 2D PCs using PSMs, in which conventional-type boundary conditions were used. However, conventional-type boundary conditions can not be proved to stabilize numerical scheme. Although *Wu* [2003] used penalty-type boundary conditions [*Funaro and Gottlieb, 1988*] for 1D-waveguide analysis, which can be mathematically proved to stabilize numerical scheme, he used the boundary conditions derived in time-domain. But there exists intrinsic difference between time-domain and frequency-domain methods in that the electromagnetic fields considered are all real quantities in time-domain simulations, while in frequency-domain analysis, the fields are complex ones with the phasor technique. In this thesis, we have redrived the penalty-type boundary conditions for frequency-domain in details.

Channel waveguides have been known hard to solve due to the presence of corners and the associated singular field behavior [Sudbo, 1992]. According to the previous works conducted by Hadley [2002] and Thomas *et al.* [2007], it was reported that a local expansion of the field near the corners was required to produce higher order numerical convergence. In this thesis, we propose a new algorithm which can achieve high order convergence without doing special treatment around corner points.

1.2 Chapter Outline

There are seven chapters following this chapter.

In Chapter 2, we derive the formulation for the transverse electric (TE) mode for 1D (slab) waveguides. The boundary conditions are imposed by using the penalty method with characteristic variables. The three different types of boundary conditions, including perfect electric conductor (PEC), perfect magnetic conductor (PMC), and dielectric boundary conditions will be shown. Since the transverse magnetic (TM) mode can be derived in the same way, we do not show its details.

In Chapter 3, we derive the formulation for the 2D waveguides. And just as in Chapter 2, the boundary conditions are also imposed by using the penalty method with characteristic variables. The derivation will be combined with the transfinite element method. How to decrease the number of equations from six to three is discussed in the last section.

In Chapter 4, we derive the formulation for 2D PCs. Since the derivation is very similar to the one for 2D waveguides, we will not present it in details. Readers can refer to Chapter 3 for relevant formulae. The TM mode can be derived in the same way, and only the final results are given in the last two sections.

In Chapter 5, we introduce the fundamental concepts of the collocation methods and the pseudospectral Legendre method [Teng *et al.*, 2008] which we use to analyze problems. In the second part of this chapter, we introduce the shifted inverse power method (SIPM) which we will use to solve eigenvalue problems. We have done some

modification on the SIPM in our applications.

In Chapter 6, 1D and 2D optical waveguides are numerically analyzed. Numerical results for several types of waveguides, including slab waveguides, fiber waveguides, channel waveguides, and rib waveguides are examined for examining the accuracy of the mode solver.

In Chapter 7, PC structures are numerically analyzed. Band diagrams of typical square-lattice and triangular-lattice PCs are examined. Since the modified SIPM is employed for solving eigenvalue problems, we can save much memory space.

The conclusion of this work is summarized in Chapter 8.



Chapter 2

Mathematical Formulation for 1D Waveguide Analysis

This chapter is devoted to explain the whole process of deriving the formulation for the 1D waveguide structure from Maxwell's equations.

2.1 Equations Used for 1D Waveguide Structure

From Maxwell's curl equations, we have the equations for the transverse electric (TE) case assuming the material structure is uniform in the y direction:

$$\mu_0 \frac{\partial \tilde{H}_x}{\partial t} = \frac{\partial \tilde{E}_y}{\partial z} \quad (2.1a)$$

$$\mu_0 \frac{\partial \tilde{H}_z}{\partial t} = -\frac{\partial \tilde{E}_y}{\partial x} \quad (2.1b)$$

$$\epsilon \frac{\partial \tilde{E}_y}{\partial t} = \frac{\partial \tilde{H}_x}{\partial z} - \frac{\partial \tilde{H}_z}{\partial x} \quad (2.1c)$$

where \tilde{H}_x and \tilde{H}_z are the magnetic field components while \tilde{E}_y represents the electric field, μ_0 is the permeability of non-magnetic material, ϵ is the permittivity, and z is the propagation direction. We have just used Maxwell's curl equations so far. There exists a Maxwell's divergence equation written as

$$\frac{\partial \tilde{H}_x}{\partial x} + \frac{\partial \tilde{H}_z}{\partial z} = 0. \quad (2.2)$$

Therefore there are four equations for the 1D TE waveguide structure. Prior works used to take the three Maxwell's curl equations as the basic equations for analysis.

In this work, we replace (2.1b) with (2.2). Then the new three equations appear to be

$$\frac{\partial \tilde{H}_x}{\partial z} = \epsilon \frac{\partial \tilde{E}_y}{\partial t} + \frac{\partial \tilde{H}_z}{\partial x} \quad (2.3a)$$

$$\frac{\partial \tilde{H}_z}{\partial z} = -\frac{\partial \tilde{H}_x}{\partial x} \quad (2.3b)$$

$$\frac{\partial \tilde{E}_y}{\partial z} = \mu_0 \frac{\partial \tilde{H}_x}{\partial t}. \quad (2.3c)$$

Before proceeding to the next section, we find it is more convenient to deal with the equations if we apply the following transformation

$$\tilde{H}_x = \frac{1}{\sqrt{\mu_0/\epsilon_0}} H_x, \quad \tilde{H}_z = \frac{1}{\sqrt{\mu_0/\epsilon_0}} H_z, \quad \tilde{E}_y = E_y.$$

This transformation makes (2.3) appear as

$$\frac{\partial H_x}{\partial z} = \frac{\epsilon_r}{c} \frac{\partial E_y}{\partial t} + \frac{\partial H_z}{\partial x} \quad (2.4a)$$

$$\frac{\partial H_z}{\partial z} = -\frac{\partial H_x}{\partial x} \quad (2.4b)$$

$$\frac{\partial E_y}{\partial z} = \frac{1}{c} \frac{\partial H_x}{\partial t} \quad (2.4c)$$

where ϵ_r is the relative permittivity defined as $\epsilon_r = \epsilon/\epsilon_0$ and c is the speed of light in vacuum.

2.2 Well-posedness Analysis

Rewriting (2.4) into the complex form, we have

$$\frac{\partial}{\partial z}(H_{xr} + iH_{xi}) = \frac{\epsilon_{rr} + i\epsilon_{ri}}{c} \frac{\partial}{\partial t}(E_{yr} + iE_{yi}) + \frac{\partial}{\partial x}(H_{zr} + iH_{zi}) \quad (2.5a)$$

$$\frac{\partial}{\partial z}(H_{zr} + iH_{zi}) = -\frac{\partial}{\partial x}(H_{xr} + iH_{xi}) \quad (2.5b)$$

$$\frac{\partial}{\partial z}(E_{yr} + iE_{yi}) = \frac{1}{c} \frac{\partial}{\partial t}(H_{xr} + iH_{xi}) \quad (2.5c)$$

where the subscripts r and i denote the corresponding real and imaginary compo-

nents. Equation (2.5) can then be written as

$$\frac{\partial}{\partial z} H_{xr} = \frac{1}{c} \frac{\partial}{\partial t} (\epsilon_{rr} E_{yr} - \epsilon_{ri} E_{yi}) - \frac{\partial}{\partial x} (-H_{zr}) \quad (2.6a)$$

$$\frac{\partial}{\partial z} H_{xi} = \frac{1}{c} \frac{\partial}{\partial t} (\epsilon_{rr} E_{yi} - \epsilon_{ri} E_{yr}) - \frac{\partial}{\partial x} (-H_{zi}) \quad (2.6b)$$

$$\frac{\partial}{\partial z} (-H_{zr}) = -\frac{\partial}{\partial x} H_{xr} \quad (2.6c)$$

$$\frac{\partial}{\partial z} (-H_{zi}) = -\frac{\partial}{\partial x} H_{xi} \quad (2.6d)$$

$$\frac{\partial}{\partial z} E_{yr} = \frac{1}{c} \frac{\partial}{\partial t} H_{xr} \quad (2.6e)$$

$$\frac{\partial}{\partial z} E_{yi} = \frac{1}{c} \frac{\partial}{\partial t} H_{xi}. \quad (2.6f)$$

Equation (2.6) can be expressed in the matrix form:

$$\frac{\partial \hat{q}}{\partial z} = \frac{M}{c} \cdot \frac{\partial \hat{q}}{\partial t} + A_x \cdot \frac{\partial \hat{q}}{\partial x} \quad (2.7)$$

where $\hat{q} = [H_{xr} \ H_{xi} \ -H_{zr} \ -H_{zi} \ E_{yr} \ E_{yi}]^T$, M is the material matrix defined as

$$M = \begin{bmatrix} 0 & 0 & 0 & 0 & \epsilon_{rr} & -\epsilon_{ri} \\ 0 & 0 & 0 & 0 & \epsilon_{ri} & \epsilon_{rr} \\ 0 & 0 & 0 & 0 & 0 & 0 \\ 0 & 0 & 0 & 0 & 0 & 0 \\ 1 & 0 & 0 & 0 & 0 & 0 \\ 0 & 1 & 0 & 0 & 0 & 0 \end{bmatrix} \quad (2.8)$$

and

$$A_x = \begin{bmatrix} 0 & 0 & -1 & 0 & 0 & 0 \\ 0 & 0 & 0 & -1 & 0 & 0 \\ -1 & 0 & 0 & 0 & 0 & 0 \\ 0 & -1 & 0 & 0 & 0 & 0 \\ 0 & 0 & 0 & 0 & 0 & 0 \\ 0 & 0 & 0 & 0 & 0 & 0 \end{bmatrix}. \quad (2.9)$$

Let $\hat{q}(x, z, t) = q(x, z) \cdot e^{i(\omega t - \beta z)}$, where β is propagation constant, (2.7) becomes

$$-i\beta q = i\frac{\omega}{c} M \cdot q + A_x \cdot \frac{\partial q}{\partial x} = ik_0 M \cdot q + A_x \cdot \frac{\partial q}{\partial x} \quad (2.10)$$

where k_0 is the wavenumber in free space. Since $-i\beta q$ and $ik_0 M q$ are low-order terms, they can be eliminated from the well-posedness analysis, as will be done below.

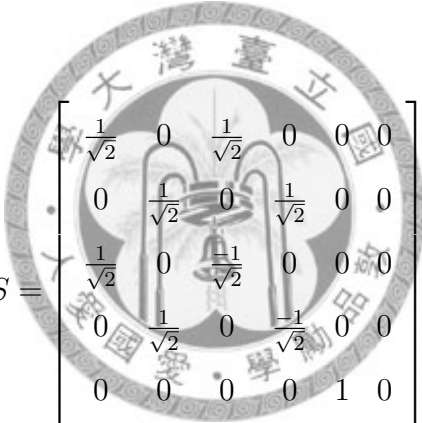
Since $A_x = A_x^T$, where the superscript denotes the transpose, there exists a matrix S such that

$$S^T \cdot A_x \cdot S = \Lambda \quad (2.11)$$

where S^T represents the transpose matrix of S . From linear algebra, we know that for an symmetric matrix A_x , we can create such matrix S by arranging all eigenvectors of A_x , $\{s_i | i = 1, \dots, 6\}$, in the form:

$$S = [s_1 \quad s_2 \quad s_3 \quad s_4 \quad s_5 \quad s_6] \quad (2.12)$$

which is found to be



$$S = \begin{bmatrix} \frac{1}{\sqrt{2}} & 0 & \frac{1}{\sqrt{2}} & 0 & 0 & 0 \\ 0 & \frac{1}{\sqrt{2}} & 0 & \frac{1}{\sqrt{2}} & 0 & 0 \\ \frac{1}{\sqrt{2}} & 0 & \frac{-1}{\sqrt{2}} & 0 & 0 & 0 \\ 0 & \frac{1}{\sqrt{2}} & 0 & \frac{-1}{\sqrt{2}} & 0 & 0 \\ 0 & 0 & 0 & 0 & 1 & 0 \\ 0 & 0 & 0 & 0 & 0 & 1 \end{bmatrix}. \quad (2.13)$$

Notice that $S^T = S$ and

$$S^T S = \begin{bmatrix} \frac{1}{\sqrt{2}} & 0 & \frac{1}{\sqrt{2}} & 0 & 0 & 0 \\ 0 & \frac{1}{\sqrt{2}} & 0 & \frac{1}{\sqrt{2}} & 0 & 0 \\ \frac{1}{\sqrt{2}} & 0 & \frac{-1}{\sqrt{2}} & 0 & 0 & 0 \\ 0 & \frac{1}{\sqrt{2}} & 0 & \frac{-1}{\sqrt{2}} & 0 & 0 \\ 0 & 0 & 0 & 0 & 1 & 0 \\ 0 & 0 & 0 & 0 & 0 & 1 \end{bmatrix} \cdot \begin{bmatrix} \frac{1}{\sqrt{2}} & 0 & \frac{1}{\sqrt{2}} & 0 & 0 & 0 \\ 0 & \frac{1}{\sqrt{2}} & 0 & \frac{1}{\sqrt{2}} & 0 & 0 \\ \frac{1}{\sqrt{2}} & 0 & \frac{-1}{\sqrt{2}} & 0 & 0 & 0 \\ 0 & \frac{1}{\sqrt{2}} & 0 & \frac{-1}{\sqrt{2}} & 0 & 0 \\ 0 & 0 & 0 & 0 & 1 & 0 \\ 0 & 0 & 0 & 0 & 0 & 1 \end{bmatrix} = I \quad (2.14)$$

where I is the identity matrix and

$$S^T A_x S = \begin{bmatrix} \frac{1}{\sqrt{2}} & 0 & \frac{1}{\sqrt{2}} & 0 & 0 & 0 \\ 0 & \frac{1}{\sqrt{2}} & 0 & \frac{1}{\sqrt{2}} & 0 & 0 \\ \frac{1}{\sqrt{2}} & 0 & \frac{-1}{\sqrt{2}} & 0 & 0 & 0 \\ 0 & \frac{1}{\sqrt{2}} & 0 & \frac{-1}{\sqrt{2}} & 0 & 0 \\ 0 & 0 & 0 & 0 & 1 & 0 \\ 0 & 0 & 0 & 0 & 0 & 1 \end{bmatrix} \begin{bmatrix} 0 & 0 & -1 & 0 & 0 & 0 \\ 0 & 0 & 0 & -1 & 0 & 0 \\ -1 & 0 & 0 & 0 & 0 & 0 \\ 0 & -1 & 0 & 0 & 0 & 0 \\ 0 & 0 & 0 & 0 & 0 & 0 \\ 0 & 0 & 0 & 0 & 0 & 0 \end{bmatrix} \cdot \quad (2.15)$$

$$\begin{bmatrix} \frac{1}{\sqrt{2}} & 0 & \frac{1}{\sqrt{2}} & 0 & 0 & 0 \\ 0 & \frac{1}{\sqrt{2}} & 0 & \frac{1}{\sqrt{2}} & 0 & 0 \\ \frac{1}{\sqrt{2}} & 0 & \frac{-1}{\sqrt{2}} & 0 & 0 & 0 \\ 0 & \frac{1}{\sqrt{2}} & 0 & \frac{-1}{\sqrt{2}} & 0 & 0 \\ 0 & 0 & 0 & 0 & 1 & 0 \\ 0 & 0 & 0 & 0 & 0 & 1 \end{bmatrix} = \begin{bmatrix} -1 & 0 & 0 & 0 & 0 & 0 \\ 0 & -1 & 0 & 0 & 0 & 0 \\ 0 & 0 & 1 & 0 & 0 & 0 \\ 0 & 0 & 0 & 1 & 0 & 0 \\ 0 & 0 & 0 & 0 & 0 & 0 \\ 0 & 0 & 0 & 0 & 0 & 0 \end{bmatrix} = \Lambda.$$

Before we proceed, we define a new vector R for latter use

$$R = S^T \cdot q = \begin{bmatrix} \frac{1}{\sqrt{2}} H_{xr} - \frac{1}{\sqrt{2}} H_{zr} \\ \frac{1}{\sqrt{2}} H_{xi} - \frac{1}{\sqrt{2}} H_{zi} \\ \frac{1}{\sqrt{2}} H_{xr} + \frac{1}{\sqrt{2}} H_{zr} \\ \frac{1}{\sqrt{2}} H_{xi} + \frac{1}{\sqrt{2}} H_{zi} \\ E_{yr} \\ E_{yi} \end{bmatrix} = \begin{bmatrix} R_1 \\ R_2 \\ R_3 \\ R_4 \\ R_5 \\ R_6 \end{bmatrix} \quad (2.16)$$

which is called the characteristic state vector with its elements named as the characteristic variables.

2.3 The Energy Method

If we multiply q^T from the left to (2.10), we have

$$0 = q^T A_x \frac{\partial q}{\partial x}. \quad (2.17a)$$

Then, if we adopt local coordinate transformation defined in Fig. 2.1 and integrate over $\xi \in [-1, 1]$, the equation becomes

$$\begin{aligned}
0 &= \int_{-1}^1 q^T A_\xi \frac{\partial q}{\partial \xi} \cdot d\xi & (2.18a) \\
&= \int_{-1}^1 \frac{1}{2} \frac{\partial}{\partial \xi} (q^T A_\xi q) \cdot d\xi \\
&= \frac{1}{2} \left[(q^T A_\xi q) \Big|_{\xi=1} + (-1) (q^T A_\xi q) \Big|_{\xi=-1} \right] \\
&= \frac{1}{2} \left[\frac{\partial \xi / \partial x}{|\partial \xi / \partial x|} \Big|_{\xi=1} \frac{\partial \xi}{\partial x} (q^T A_x q) \Big|_{\xi=1} + \frac{-\partial \xi / \partial x}{|\partial \xi / \partial x|} \Big|_{\xi=-1} \frac{\partial \xi}{\partial x} (q^T A_x q) \Big|_{\xi=-1} \right] \\
&= \frac{1}{2} \left[n_x \Big|_{\xi=1} \frac{\partial \xi}{\partial x} (q^T A_x q) \Big|_{\xi=1} + n_x \Big|_{\xi=-1} \frac{\partial \xi}{\partial x} (q^T A_x q) \Big|_{\xi=-1} \right] \\
&= \frac{n_x \Big|_{\xi=1}}{2} \Big|_{\xi=1} \frac{\partial \xi}{\partial x} (q^T S \cdot S^T A_x S \cdot S^T q) \Big|_{\xi=1} + \frac{n_x \Big|_{\xi=-1}}{2} \Big|_{\xi=-1} \frac{\partial \xi}{\partial x} (q^T S \cdot S^T A_x S \cdot S^T q) \Big|_{\xi=-1} \\
&= \frac{n_x \Big|_{\xi=1}}{2} \Big|_{\xi=1} \frac{\partial \xi}{\partial x} (R^T \cdot \Lambda \cdot R) \Big|_{\xi=1} + \frac{n_x \Big|_{\xi=-1}}{2} \Big|_{\xi=-1} \frac{\partial \xi}{\partial x} (R^T \cdot \Lambda \cdot R) \Big|_{\xi=-1} \\
&= \frac{n_x \Big|_{\xi=1}}{2} \Big|_{\xi=1} \frac{\partial \xi}{\partial x} \left[-(R_1^T R_1) - (R_2^T R_2) + (R_3^T R_3) + (R_4^T R_4) \right] \Big|_{\xi=1} \\
&\quad + \frac{n_x \Big|_{\xi=-1}}{2} \Big|_{\xi=-1} \frac{\partial \xi}{\partial x} \left[-(R_1^T R_1) - (R_2^T R_2) + (R_3^T R_3) + (R_4^T R_4) \right] \Big|_{\xi=-1}
\end{aligned}$$

where $A_\xi = A_x \frac{\partial \xi}{\partial x}$ and n_x is the unit outward vector at boundary points. Note that the eigenvalues corresponding to R_5 and R_6 are zeros, as seen in (2.15). Closely looking at (2.18), since the left side is zero, for the equation to be meaningful, the right side should be zero, or we need the conditions

$$R_1^T R_1 + R_2^T R_2 = R_3^T R_3 + R_4^T R_4 \quad \text{at } \xi = 1 \quad (2.19a)$$

$$R_1^T R_1 + R_2^T R_2 = R_3^T R_3 + R_4^T R_4 \quad \text{at } \xi = -1. \quad (2.19b)$$

We must follow (2.19) when designing the boundary conditions to make the equations be well-posed.

2.4 Characteristic Representations of Physical Boundary Condition

We now consider the representation of physical boundary conditions. Since for 1D structures, we define y and z directions as tangential directions and the x direction

as the normal direction, the characteristic variables can be represented in this way:

$$R_1 = \frac{1}{\sqrt{2}}\text{Re}(\vec{n} \cdot \vec{H}) - \frac{1}{\sqrt{2}}\text{Re}(\vec{n} \times \vec{H}) \quad (2.20a)$$

$$R_2 = \frac{1}{\sqrt{2}}\text{Im}(\vec{n} \cdot \vec{H}) - \frac{1}{\sqrt{2}}\text{Im}(\vec{n} \times \vec{H}) \quad (2.20b)$$

$$R_3 = \frac{1}{\sqrt{2}}\text{Re}(\vec{n} \cdot \vec{H}) + \frac{1}{\sqrt{2}}\text{Re}(\vec{n} \times \vec{H}) \quad (2.20c)$$

$$R_4 = \frac{1}{\sqrt{2}}\text{Im}(\vec{n} \cdot \vec{H}) + \frac{1}{\sqrt{2}}\text{Im}(\vec{n} \times \vec{H}) \quad (2.20d)$$

where \vec{n} denotes the unit normal vector in the x direction. Because the corresponding eigenvalues of R_5 and R_6 are zeros, we just neglect them.

For the perfect electric conductor (PEC) boundary condition, there are two conditions the fields should satisfy (considering isotropic non-magnetic media):

$$\vec{n} \times \vec{E} = 0 \quad (2.21a)$$

$$\vec{n} \cdot \vec{H} = 0. \quad (2.21b)$$

Closely looking at (2.20), we observe

$$R_1 + R_3 = \sqrt{2}\text{Re}(\vec{n} \cdot \vec{H}) \quad (2.22a)$$

$$R_2 + R_4 = \sqrt{2}\text{Im}(\vec{n} \cdot \vec{H}). \quad (2.22b)$$

Then the PEC boundary condition has a characteristic representation as

$$\begin{pmatrix} R_{1BC} = -R_3, & R_{2BC} = -R_4 \\ R_{3BC} = -R_1, & R_{4BC} = -R_2 \end{pmatrix}. \quad (2.23)$$

For the perfect magnetic conductor (PMC) boundary condition, there are also two conditions needed to be satisfied:

$$\vec{n} \cdot \vec{E} = 0 \quad (2.24a)$$

$$\vec{n} \times \vec{H} = 0. \quad (2.24b)$$

Again, from (2.20), we have

$$R_1 - R_3 = -\sqrt{2}\text{Re}(\vec{n} \times \vec{H}) \quad (2.25a)$$

$$R_2 - R_4 = -\sqrt{2}\text{Im}(\vec{n} \times \vec{H}) \quad (2.25b)$$

and the characteristic representation for the PMC boundary condition is

$$\begin{pmatrix} R_{1BC} = R_3, & R_{2BC} = R_4 \\ R_{3BC} = R_1, & R_{4BC} = R_2 \end{pmatrix}. \quad (2.26)$$

For source-free dielectric media, the physical boundary conditions are

$$\vec{n} \times \vec{E}^I = \vec{n} \times \vec{E}^{II} \quad (2.27a)$$

$$\vec{n} \cdot \epsilon_I \vec{E}^I = \vec{n} \cdot \epsilon_{II} \vec{E}^{II} \quad (2.27b)$$

$$\vec{n} \times \vec{H}^I = \vec{n} \times \vec{H}^{II} \quad (2.27c)$$

$$\vec{n} \cdot \vec{H}^I = \vec{n} \cdot \vec{H}^{II} \quad (2.27d)$$

with the superscripts I and II denoting different dielectric regions on the two sides of the interface, respectively. From (2.20), we have

$$R_1^I = \frac{1}{\sqrt{2}} \text{Re}(\vec{n}^I \cdot \vec{H}^I) - \frac{1}{\sqrt{2}} \text{Re}(\vec{n}^I \times \vec{H}^I) \quad (2.28a)$$

$$R_1^{II} = \frac{1}{\sqrt{2}} \text{Re}(\vec{n}^{II} \cdot \vec{H}^{II}) - \frac{1}{\sqrt{2}} \text{Re}(\vec{n}^{II} \times \vec{H}^{II}). \quad (2.28b)$$

Because \vec{n}^I and \vec{n}^{II} are in opposite directions, let $\vec{n}^I = -\vec{n}^{II} = \vec{n}$ and add (2.28a) to (2.28b) to obtain

$$R_1^I + R_1^{II} = \frac{1}{\sqrt{2}} \text{Re}(\vec{n} \cdot (\vec{H}^I - \vec{H}^{II})) - \frac{1}{\sqrt{2}} \text{Re}(\vec{n} \times (\vec{H}^I - \vec{H}^{II})) \quad (2.29)$$

which through (2.27) yields

$$R_1^I = -R_1^{II}. \quad (2.30)$$

By doing the same procedure to R_2 , R_3 , and R_4 , we can get

$$\begin{pmatrix} R_{1BC}^{I/II} = -R_1^{II/I}, & R_{2BC}^{I/II} = -R_2^{II/I} \\ R_{3BC}^{I/II} = -R_3^{II/I}, & R_{4BC}^{I/II} = -R_4^{II/I} \end{pmatrix}. \quad (2.31)$$

2.5 Design of the Scheme

In this section, we will add boundary conditions to the governing equations for analysis. Starting from (2.10) with some boundary terms, we have at grid point i ,

$i = 0, \dots, N$, within the representation domain M as shown in Fig. 2.2,

$$\begin{aligned}
-i\beta q|_i = ik_0 M q|_i + A_x \frac{\partial q}{\partial x} \Big|_i - \delta_{0i} \tau^- S B^- (R|_{x=a} - R_{BC}) \\
- \delta_{Ni} \tau^+ S B^+ (R|_{x=b} - R_{BC}).
\end{aligned} \tag{2.32}$$

The symbols and variables in (2.32) are explained as follows. δ_{ij} is the Kronecker delta function defined as

$$\delta_{ij} = \begin{cases} 1, & \text{if } i = j \\ 0, & \text{if } i \neq j. \end{cases} \tag{2.33}$$

τ^- and τ^+ are constant numbers and their values will be delivered latter. S is the matrix defined in (2.13). a and b are lower and upper limits plotted in Fig. 2.1. B^- and B^+ are boundary inflow/outflow operators defined as

$$B^- = \begin{bmatrix} b_1^- & 0 & 0 & 0 & 0 & 0 \\ 0 & b_2^- & 0 & 0 & 0 & 0 \\ 0 & 0 & b_3^- & 0 & 0 & 0 \\ 0 & 0 & 0 & b_4^- & 0 & 0 \\ 0 & 0 & 0 & 0 & 0 & 0 \\ 0 & 0 & 0 & 0 & 0 & 0 \end{bmatrix}, B^+ = \begin{bmatrix} b_1^+ & 0 & 0 & 0 & 0 & 0 \\ 0 & b_2^+ & 0 & 0 & 0 & 0 \\ 0 & 0 & b_3^+ & 0 & 0 & 0 \\ 0 & 0 & 0 & b_4^+ & 0 & 0 \\ 0 & 0 & 0 & 0 & 0 & 0 \\ 0 & 0 & 0 & 0 & 0 & 0 \end{bmatrix} \tag{2.34}$$

R is the characteristic state vector defined in (2.16) and R_{BC} is defined in the previous section for every physical boundary condition.

Next, we write the energy rate equation (2.18) in the discrete form and add the boundary terms

$$\begin{aligned}
0 &= \sum_{i=0}^N w_i \left[q_i^T A_x \frac{\partial q}{\partial x} \Big|_i - \delta_{0i} \tau^- (R^T B^- R)|_{x=a} - \delta_{Ni} \tau^+ (R^T B^+ R)|_{x=b} \right] \\
&= \sum_{i=0}^N w_i q_i^T A_x \frac{\partial q}{\partial x} \Big|_i - w_0 \tau^- (R^T B^- R)|_{x=a} - w_N \tau^+ (R^T B^+ R)|_{x=b}
\end{aligned} \tag{2.35a}$$

where \sum is the discrete form of integral, and w_i is the weight of the discrete integral.

The value of w_i will be delivered in Chapter 5. From (2.18), we can obtain

$$\begin{aligned}
0 &= \frac{n_x|_{x=b}}{2} \left| \frac{\partial \xi}{\partial x} \right|_{x=b} [-(R_1^T R_1) - (R_2^T R_2) + (R_3^T R_3) + (R_4^T R_4)]|_{x=b} \quad (2.36a) \\
&+ \frac{n_x|_{x=a}}{2} \left| \frac{\partial \xi}{\partial x} \right|_{x=a} [-(R_1^T R_1) - (R_2^T R_2) + (R_3^T R_3) + (R_4^T R_4)]|_{x=a} \\
&- w_0 \tau^- (R^T B^- R)|_{x=a} - w_N \tau^+ (R^T B^+ R)|_{x=b} \\
&= (R_1^T R_1)|_{x=b} \left(\frac{-1}{2} \left| \frac{\partial \xi}{\partial x} \right|_{x=b} - w_N \tau^+ b_1^+ \right) + (R_2^T R_2)|_{x=b} \left(\frac{-1}{2} \left| \frac{\partial \xi}{\partial x} \right|_{x=b} - w_N \tau^+ b_2^+ \right) \\
&+ (R_3^T R_3)|_{x=b} \left(\frac{1}{2} \left| \frac{\partial \xi}{\partial x} \right|_{x=b} - w_N \tau^+ b_3^+ \right) + (R_4^T R_4)|_{x=b} \left(\frac{1}{2} \left| \frac{\partial \xi}{\partial x} \right|_{x=b} - w_N \tau^+ b_4^+ \right) \\
&- (R_1^T R_1)|_{x=a} \left(\frac{-1}{2} \left| \frac{\partial \xi}{\partial x} \right|_{x=a} + w_0 \tau^- b_1^- \right) - (R_2^T R_2)|_{x=a} \left(\frac{-1}{2} \left| \frac{\partial \xi}{\partial x} \right|_{x=a} + w_0 \tau^- b_2^- \right) \\
&- (R_3^T R_3)|_{x=a} \left(\frac{1}{2} \left| \frac{\partial \xi}{\partial x} \right|_{x=a} + w_0 \tau^- b_3^- \right) - (R_4^T R_4)|_{x=a} \left(\frac{1}{2} \left| \frac{\partial \xi}{\partial x} \right|_{x=a} + w_0 \tau^- b_4^- \right).
\end{aligned}$$

which means

$$\frac{-1}{2} \left| \frac{\partial \xi}{\partial x} \right|_{x=b} - w_N \tau^+ b_1^+ = 0, \quad \frac{-1}{2} \left| \frac{\partial \xi}{\partial x} \right|_{x=b} - w_N \tau^+ b_2^+ = 0 \quad (2.37a)$$

$$\frac{1}{2} \left| \frac{\partial \xi}{\partial x} \right|_{x=b} - w_N \tau^+ b_3^+ = 0, \quad \frac{1}{2} \left| \frac{\partial \xi}{\partial x} \right|_{x=b} - w_N \tau^+ b_4^+ = 0 \quad (2.37b)$$

$$\frac{-1}{2} \left| \frac{\partial \xi}{\partial x} \right|_{x=a} + w_0 \tau^- b_1^- = 0, \quad \frac{-1}{2} \left| \frac{\partial \xi}{\partial x} \right|_{x=a} + w_0 \tau^- b_2^- = 0 \quad (2.37c)$$

$$\frac{1}{2} \left| \frac{\partial \xi}{\partial x} \right|_{x=a} + w_0 \tau^- b_3^- = 0, \quad \frac{1}{2} \left| \frac{\partial \xi}{\partial x} \right|_{x=a} + w_0 \tau^- b_4^- = 0. \quad (2.37d)$$

From (2.37), we define

$$\left(\tau^+ = \frac{1}{2w_N} \left| \frac{\partial \xi}{\partial x} \right|_{x=b}, \quad \tau^- = \frac{1}{2w_0} \left| \frac{\partial \xi}{\partial x} \right|_{x=a} \right) \quad (2.38)$$

and

$$\begin{pmatrix} b_1^+ = -1, & b_2^+ = -1, & b_3^+ = 1, & b_4^+ = 1 \\ b_1^- = 1, & b_2^- = 1, & b_3^- = -1, & b_4^- = -1 \end{pmatrix}. \quad (2.39)$$

Substituting the values in (2.39) into (2.34), we thus determine matrices B^- and B^+ .

2.6 Final Form of the Formulation

There is only one step left: making the equations become a standard eigenvalue problem. Here we just take the PEC boundary condition as an example. The other two boundary types can be derived in the same manner.

We start from (2.32). By substituting the matrices M , A_x , S , and B , and replacing $(R-R_{BC})$ with the condition (2.23), we can get the following six equations:

$$-i\beta H_{xr}|_i = ik_0(\epsilon_{rr} E_{yr}|_i - \epsilon_{ri} E_{yi}|_i) + \left. \frac{\partial H_{zr}}{\partial x} \right|_i \quad (2.40a)$$

$$-i\beta H_{xi}|_i = ik_0(\epsilon_{rr} E_{yi}|_i + \epsilon_{ri} E_{yr}|_i) + \left. \frac{\partial H_{zi}}{\partial x} \right|_i \quad (2.40b)$$

$$\begin{aligned} -i\beta H_{zr}|_i = & - \left. \frac{\partial H_{xr}}{\partial x} \right|_i - \delta_{i0}\tau^- \left. \frac{\partial \xi}{\partial x} \right|_{\xi=-1} \left[2 H_{xr}|_{\xi=-1} \right] \\ & + \delta_{iN}\tau^+ \left. \frac{\partial \xi}{\partial x} \right|_{\xi=1} \left[2 H_{xr}|_{\xi=1} \right] \end{aligned} \quad (2.40c)$$

$$\begin{aligned} -i\beta H_{zi}|_i = & - \left. \frac{\partial H_{xi}}{\partial x} \right|_i - \delta_{i0}\tau^- \left. \frac{\partial \xi}{\partial x} \right|_{\xi=-1} \left[2 H_{xi}|_{\xi=-1} \right] \\ & + \delta_{iN}\tau^+ \left. \frac{\partial \xi}{\partial x} \right|_{\xi=1} \left[2 H_{xi}|_{\xi=1} \right] \end{aligned} \quad (2.40d)$$

$$-i\beta E_{yr}|_i = ik_0 H_{xr}|_i \quad (2.40e)$$

$$-i\beta E_{yi}|_i = ik_0 H_{xi}|_i \quad (2.40f)$$

Then multiplying (2.40b), (2.40d), and (2.40f) by $i(\equiv \sqrt{-1})$ and adding them to (2.40a), (2.40c), and (2.40e), respectively. We obtain

$$-i\beta H_x|_i = ik_0\epsilon_r E_y + \left. \frac{\partial H_z}{\partial x} \right|_i \quad (2.41a)$$

$$\begin{aligned} -i\beta H_z|_i = & - \left. \frac{\partial H_x}{\partial x} \right|_i - \delta_{i0}\tau^- \left. \frac{\partial \xi}{\partial x} \right|_{\xi=-1} \left[2 H_x|_{\xi=-1} \right] \\ & + \delta_{iN}\tau^+ \left. \frac{\partial \xi}{\partial x} \right|_{\xi=1} \left[2 H_x|_{\xi=1} \right] \end{aligned} \quad (2.41b)$$

$$-i\beta E_y|_i = ik_0 H_x|_i \quad (2.41c)$$

where $H_x = H_{xr} + iH_{xi}$, and so on. Equation (2.41) represents a standard eigenvalue problem.

For the case of the dielectric boundary condition, the eigenvalue formulation

with the following equations can be derived:

$$-i\beta H_x^I|_i = ik_0 \epsilon_r E_y^I + \left. \frac{\partial H_z^I}{\partial x} \right|_i + \delta_{i0} \tau^- \left. \frac{\partial \xi}{\partial x} \right|_{\xi^I=-1} \left[H_z^I|_{\xi^I=-1} - H_z^{II}|_{\xi^{II}=1} \right] \quad (2.42a)$$

$$- \delta_{iN} \tau^+ \left. \frac{\partial \xi}{\partial x} \right|_{\xi^I=1} \left[H_z^I|_{\xi^I=1} - H_z^{II}|_{\xi^{II}=-1} \right]$$

$$-i\beta H_z^I|_i = - \left. \frac{\partial H_x^I}{\partial x} \right|_i - \delta_{i0} \tau^- \left. \frac{\partial \xi}{\partial x} \right|_{\xi^I=-1} \left[H_x^I|_{\xi^I=-1} - H_x^{II}|_{\xi^{II}=1} \right] \quad (2.42b)$$

$$+ \delta_{iN} \tau^+ \left. \frac{\partial \xi}{\partial x} \right|_{\xi^I=1} \left[H_x^I|_{\xi^I=1} - H_x^{II}|_{\xi^{II}=-1} \right]$$

$$-i\beta E_y^I|_i = ik_0 H_x^I|_i. \quad (2.42c)$$



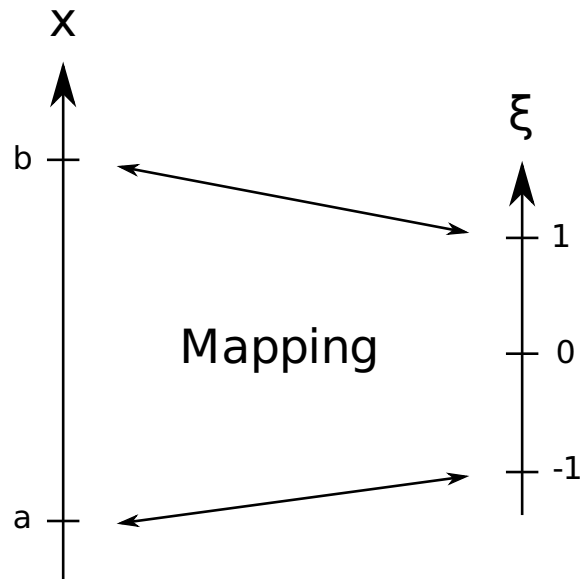


Figure 2.1: Transformation between global and local coordinates.

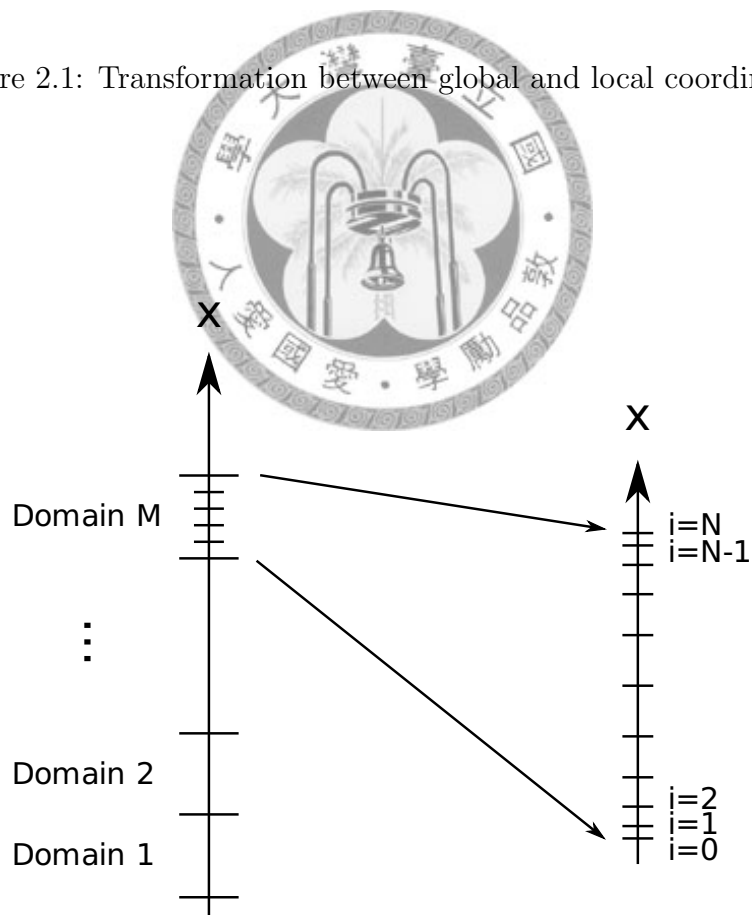


Figure 2.2: The grid points in domain M.

Chapter 3

Mathematical Formulation for 2D Waveguide Analysis

This chapter is devoted to, just like in the previous chapter, the process of derivation of formulation for 2D waveguide problem.

3.1 Equations Used for 2D Waveguide Structure

From the Maxwell's curl equations


$$\epsilon \frac{\partial \tilde{E}_x}{\partial t} = \frac{\partial \tilde{H}_z}{\partial y} - \frac{\partial \tilde{H}_y}{\partial z} \quad (3.1a)$$

$$\epsilon \frac{\partial \tilde{E}_y}{\partial t} = \frac{\partial \tilde{H}_x}{\partial z} - \frac{\partial \tilde{H}_z}{\partial x} \quad (3.1b)$$

$$\epsilon \frac{\partial \tilde{E}_z}{\partial t} = \frac{\partial \tilde{H}_y}{\partial x} - \frac{\partial \tilde{H}_x}{\partial y} \quad (3.1c)$$

$$\mu_0 \frac{\partial \tilde{H}_x}{\partial t} = \frac{\partial \tilde{E}_y}{\partial z} - \frac{\partial \tilde{E}_z}{\partial y} \quad (3.1d)$$

$$\mu_0 \frac{\partial \tilde{H}_y}{\partial t} = \frac{\partial \tilde{E}_z}{\partial x} - \frac{\partial \tilde{E}_x}{\partial z} \quad (3.1e)$$

$$\mu_0 \frac{\partial \tilde{H}_z}{\partial t} = \frac{\partial \tilde{E}_x}{\partial y} - \frac{\partial \tilde{E}_y}{\partial x} \quad (3.1f)$$

where \tilde{E}_x , \tilde{E}_y , and \tilde{E}_z are the electric field components while \tilde{H}_x , \tilde{H}_y , and \tilde{H}_z represent the magnetic field components, μ_0 is the permeability of non-magnetic material, ϵ is the permittivity, and z is the propagation direction. And as in the 1D formulation, we replace (3.1c) and (3.1f) with the other two divergence equations to

get the following equations, with the order of equations being rearranged:

$$\frac{\partial \tilde{E}_x}{\partial z} = -\mu_0 \frac{\partial \tilde{H}_y}{\partial t} + \frac{\partial \tilde{E}_z}{\partial x} \quad (3.2a)$$

$$\frac{\partial \tilde{E}_y}{\partial z} = \mu_0 \frac{\partial \tilde{H}_x}{\partial t} + \frac{\partial \tilde{E}_z}{\partial y} \quad (3.2b)$$

$$\frac{\partial \tilde{E}_z}{\partial z} = -\frac{\partial \tilde{E}_x}{\partial x} - \frac{\partial \tilde{E}_y}{\partial y} \quad (3.2c)$$

$$\frac{\partial \tilde{H}_x}{\partial z} = \epsilon \frac{\partial \tilde{E}_y}{\partial t} + \frac{\partial \tilde{H}_z}{\partial x} \quad (3.2d)$$

$$\frac{\partial \tilde{H}_y}{\partial z} = -\epsilon \frac{\partial \tilde{E}_x}{\partial t} + \frac{\partial \tilde{H}_z}{\partial y} \quad (3.2e)$$

$$\frac{\partial \tilde{H}_z}{\partial z} = -\frac{\partial \tilde{H}_x}{\partial x} - \frac{\partial \tilde{H}_y}{\partial y}. \quad (3.2f)$$

Before proceeding to next section, we do the following transformation to make the derivation easier

$$\tilde{H}_x = \frac{1}{\sqrt{\mu_0/\epsilon_0}} H_x, \quad \tilde{H}_y = \frac{1}{\sqrt{\mu_0/\epsilon_0}} H_y, \quad \tilde{H}_z = \frac{1}{\sqrt{\mu_0/\epsilon_0}} H_z,$$

$$\tilde{E}_x = E_x, \quad \tilde{E}_y = E_y, \quad \tilde{E}_z = E_z.$$

This transformation makes (3.2) appear as

$$\frac{\partial E_x}{\partial z} = -\frac{1}{c} \frac{\partial H_y}{\partial t} + \frac{\partial E_z}{\partial x} \quad (3.4a)$$

$$\frac{\partial E_y}{\partial z} = \frac{1}{c} \frac{\partial H_x}{\partial t} + \frac{\partial E_z}{\partial y} \quad (3.4b)$$

$$\frac{\partial E_z}{\partial z} = -\frac{\partial E_x}{\partial x} - \frac{\partial E_y}{\partial y} \quad (3.4c)$$

$$\frac{\partial H_x}{\partial z} = \frac{\epsilon_r}{c} \frac{\partial E_y}{\partial t} + \frac{\partial H_z}{\partial x} \quad (3.4d)$$

$$\frac{\partial H_y}{\partial z} = -\frac{\epsilon_r}{c} \frac{\partial E_x}{\partial t} + \frac{\partial H_z}{\partial y} \quad (3.4e)$$

$$\frac{\partial H_z}{\partial z} = -\frac{\partial H_x}{\partial x} - \frac{\partial H_y}{\partial y} \quad (3.4f)$$

where ϵ_r is the relative permittivity defined as $\epsilon_r = \epsilon/\epsilon_0$ and c is the speed of light in vaccum.

3.2 Well-posedness Analysis

First, rewriting (3.4) in the following form on purpose:

$$\frac{1}{\epsilon_r} \frac{\partial}{\partial z} (\epsilon_r E_x) = -\frac{1}{c} \frac{\partial}{\partial t} (H_y) + \frac{\partial}{\partial x} (E_z) \quad (3.5a)$$

$$\frac{1}{\epsilon_r} \frac{\partial}{\partial z} (\epsilon_r E_y) = \frac{1}{c} \frac{\partial}{\partial t} (H_x) + \frac{\partial}{\partial y} (E_z) \quad (3.5b)$$

$$-\epsilon_r \frac{\partial}{\partial z} (E_z) = \frac{\partial}{\partial x} (\epsilon_r E_x) + \frac{\partial}{\partial y} (\epsilon_r E_y) \quad (3.5c)$$

$$\frac{\partial}{\partial z} (H_x) = \frac{1}{c} \frac{\partial}{\partial t} (\epsilon_r E_y) + \frac{\partial}{\partial x} (H_z) \quad (3.5d)$$

$$\frac{\partial}{\partial z} (H_y) = -\frac{1}{c} \frac{\partial}{\partial t} (\epsilon_r E_x) + \frac{\partial}{\partial y} (H_z) \quad (3.5e)$$

$$-\frac{\partial}{\partial z} (H_z) = \frac{\partial}{\partial x} (H_x) + \frac{\partial}{\partial y} (H_y). \quad (3.5f)$$

Next, we write (3.5) in the matrix form:

$$M_1 \frac{\partial \hat{q}}{\partial z} = \frac{M_2}{c} \cdot \frac{\partial \hat{q}}{\partial t} + A_x \cdot \frac{\partial \hat{q}}{\partial x} + A_y \cdot \frac{\partial \hat{q}}{\partial y} \quad (3.6)$$

where $\hat{q} = [\epsilon_r E_x \ \epsilon_r E_y \ E_z \ H_x \ H_y \ H_z]^T$ and M_1 , M_2 , A_x , and A_y are defined as

$$M_1 = \begin{bmatrix} \frac{1}{\epsilon_r} & 0 & 0 & 0 & 0 & 0 \\ 0 & \frac{1}{\epsilon_r} & 0 & 0 & 0 & 0 \\ 0 & 0 & -\epsilon_r & 0 & 0 & 0 \\ 0 & 0 & 0 & 1 & 0 & 0 \\ 0 & 0 & 0 & 0 & 1 & 0 \\ 0 & 0 & 0 & 0 & 0 & -1 \end{bmatrix}, M_2 = \begin{bmatrix} 0 & 0 & 0 & 0 & -1 & 0 \\ 0 & 0 & 0 & 1 & 0 & 0 \\ 0 & 0 & 0 & 0 & 0 & 0 \\ 0 & 1 & 0 & 0 & 0 & 0 \\ -1 & 0 & 0 & 0 & 0 & 0 \\ 0 & 0 & 0 & 0 & 0 & 0 \end{bmatrix}$$

and

$$A_x = \begin{bmatrix} 0 & 0 & 1 & 0 & 0 & 0 \\ 0 & 0 & 0 & 0 & 0 & 0 \\ 1 & 0 & 0 & 0 & 0 & 0 \\ 0 & 0 & 0 & 0 & 0 & 1 \\ 0 & 0 & 0 & 0 & 0 & 0 \\ 0 & 0 & 0 & 1 & 0 & 0 \end{bmatrix}, A_y = \begin{bmatrix} 0 & 0 & 0 & 0 & 0 & 0 \\ 0 & 0 & 1 & 0 & 0 & 0 \\ 0 & 1 & 0 & 0 & 0 & 0 \\ 0 & 0 & 0 & 0 & 0 & 0 \\ 0 & 0 & 0 & 0 & 0 & 1 \\ 0 & 0 & 0 & 0 & 1 & 0 \end{bmatrix}.$$

Let $\hat{q}(x, y, z, t) = q(x, y) \cdot e^{i(\omega t - \beta z)}$, then (3.6) becomes

$$-i\beta M_1 \cdot q = ik_0 M_2 \cdot q + A_x \cdot \frac{\partial q}{\partial x} + A_y \cdot \frac{\partial q}{\partial y} \quad (3.7)$$

where k_0 is the wavenumber in free space defined as $k_0 = \omega/c$.

If we use the same process as in the previous chapter to conduct the wellposedness analysis, we must deal with a 12×12 matrix. Instead of dealing with 12×12 matrix, we take another way do the prove.

Since the low order term does not affect the wellposedness of the original problem we thus neglect the term in the following analysis

$$0 = A_x \cdot \frac{\partial q}{\partial x} + A_y \cdot \frac{\partial q}{\partial y}. \quad (3.8)$$

We define a new matrix $A(n)$, which will be used in the next section:

$$A(n) = n_x A_x + n_y A_y \quad (3.9)$$

with $\vec{n} = (n_x, n_y)$ representing a unit normal vector directed outward on the boundary of a considered domain. Since $A(n) = A(n)^T$, there exists a matrix S such that

$$S^T \cdot A(n) \cdot S = \Lambda \quad (3.10)$$

where S^T is the transpose matrix of S . From linear algebra, we know that for a symmetric matrix $A(n)$, we can create such matrix S by arranging all of the eigenvectors of $A(n)$ as

$$S = [s_1 \quad s_2 \quad s_3 \quad s_4 \quad s_5 \quad s_6] \quad (3.11)$$

where $\{s_i | i = 1, \dots, 6\}$ are the eigenvectors of $A(n)$. The matrix S is obtained as

$$S = \begin{bmatrix} \frac{n_x}{\sqrt{2}} & \frac{n_x}{\sqrt{2}} & n_y & 0 & 0 & 0 \\ \frac{n_y}{\sqrt{2}} & \frac{n_y}{\sqrt{2}} & -n_x & 0 & 0 & 0 \\ \frac{-1}{\sqrt{2}} & \frac{1}{\sqrt{2}} & 0 & 0 & 0 & 0 \\ 0 & 0 & 0 & n_y & \frac{n_x}{\sqrt{2}} & \frac{n_x}{\sqrt{2}} \\ 0 & 0 & 0 & -n_x & \frac{n_y}{\sqrt{2}} & \frac{n_y}{\sqrt{2}} \\ 0 & 0 & 0 & 0 & \frac{1}{\sqrt{2}} & \frac{-1}{\sqrt{2}} \end{bmatrix} \quad (3.12)$$

and

$$S^T S = \begin{bmatrix} \frac{n_x}{\sqrt{2}} & \frac{n_y}{\sqrt{2}} & \frac{-1}{\sqrt{2}} & 0 & 0 & 0 \\ \frac{n_x}{\sqrt{2}} & \frac{n_y}{\sqrt{2}} & \frac{1}{\sqrt{2}} & 0 & 0 & 0 \\ n_y & -n_x & 0 & 0 & 0 & 0 \\ 0 & 0 & 0 & n_y & -n_x & 0 \\ 0 & 0 & 0 & \frac{n_x}{\sqrt{2}} & \frac{n_y}{\sqrt{2}} & \frac{1}{\sqrt{2}} \\ 0 & 0 & 0 & \frac{n_x}{\sqrt{2}} & \frac{n_y}{\sqrt{2}} & \frac{-1}{\sqrt{2}} \end{bmatrix} \cdot \begin{bmatrix} \frac{n_x}{\sqrt{2}} & \frac{n_x}{\sqrt{2}} & n_y & 0 & 0 & 0 \\ \frac{n_y}{\sqrt{2}} & \frac{n_y}{\sqrt{2}} & -n_x & 0 & 0 & 0 \\ \frac{-1}{\sqrt{2}} & \frac{1}{\sqrt{2}} & 0 & 0 & 0 & 0 \\ 0 & 0 & 0 & n_y & \frac{n_x}{\sqrt{2}} & \frac{n_x}{\sqrt{2}} \\ 0 & 0 & 0 & -n_x & \frac{n_y}{\sqrt{2}} & \frac{n_y}{\sqrt{2}} \\ 0 & 0 & 0 & 0 & \frac{1}{\sqrt{2}} & \frac{-1}{\sqrt{2}} \end{bmatrix} = I.$$

Notice that $(n_x^2 + n_y^2)^{1/2} = 1$ and

$$S^T A(n) S = \begin{bmatrix} \frac{n_x}{\sqrt{2}} & \frac{n_y}{\sqrt{2}} & \frac{-1}{\sqrt{2}} & 0 & 0 & 0 \\ \frac{n_x}{\sqrt{2}} & \frac{n_y}{\sqrt{2}} & \frac{1}{\sqrt{2}} & 0 & 0 & 0 \\ n_y & -n_x & 0 & 0 & 0 & 0 \\ 0 & 0 & 0 & n_y & -n_x & 0 \\ 0 & 0 & 0 & \frac{n_x}{\sqrt{2}} & \frac{n_y}{\sqrt{2}} & \frac{1}{\sqrt{2}} \\ 0 & 0 & 0 & \frac{n_x}{\sqrt{2}} & \frac{n_y}{\sqrt{2}} & \frac{-1}{\sqrt{2}} \end{bmatrix} \cdot \begin{bmatrix} 0 & 0 & n_x & 0 & 0 & 0 \\ 0 & 0 & n_y & 0 & 0 & 0 \\ n_x & n_y & 0 & 0 & 0 & 0 \\ 0 & 0 & 0 & 0 & 0 & n_x \\ 0 & 0 & 0 & 0 & 0 & n_y \\ 0 & 0 & 0 & n_x & n_y & 0 \end{bmatrix}. \quad (3.13)$$

$$= \begin{bmatrix} \frac{n_x}{\sqrt{2}} & \frac{n_x}{\sqrt{2}} & n_y & 0 & 0 & 0 \\ \frac{n_y}{\sqrt{2}} & \frac{n_y}{\sqrt{2}} & -n_x & 0 & 0 & 0 \\ \frac{-1}{\sqrt{2}} & \frac{1}{\sqrt{2}} & 0 & 0 & 0 & 0 \\ 0 & 0 & 0 & n_y & \frac{n_x}{\sqrt{2}} & \frac{n_x}{\sqrt{2}} \\ 0 & 0 & 0 & -n_x & \frac{n_y}{\sqrt{2}} & \frac{n_y}{\sqrt{2}} \\ 0 & 0 & 0 & 0 & \frac{1}{\sqrt{2}} & \frac{-1}{\sqrt{2}} \end{bmatrix} = \begin{bmatrix} -1 & 0 & 0 & 0 & 0 & 0 \\ 0 & 1 & 0 & 0 & 0 & 0 \\ 0 & 0 & 0 & 0 & 0 & 0 \\ 0 & 0 & 0 & 0 & 0 & 0 \\ 0 & 0 & 0 & 0 & 1 & 0 \\ 0 & 0 & 0 & 0 & 0 & -1 \end{bmatrix} = \Lambda.$$

Before we proceed, we define a new vector R , the characteristic state vector, for

latter use:

$$R = S^T \cdot q = \begin{bmatrix} \frac{n_x}{\sqrt{2}}\epsilon_r E_x + \frac{n_y}{\sqrt{2}}\epsilon_r E_y - \frac{1}{\sqrt{2}}E_z \\ \frac{n_x}{\sqrt{2}}\epsilon_r E_x + \frac{n_y}{\sqrt{2}}\epsilon_r E_y + \frac{1}{\sqrt{2}}E_z \\ n_y\epsilon_r E_x - n_x\epsilon_r E_y \\ n_y H_x - n_x H_y \\ \frac{n_x}{\sqrt{2}}H_x + \frac{n_y}{\sqrt{2}}H_y + \frac{1}{\sqrt{2}}H_z \\ \frac{n_x}{\sqrt{2}}H_x + \frac{n_y}{\sqrt{2}}H_y - \frac{1}{\sqrt{2}}H_z \end{bmatrix} = \begin{bmatrix} R_1 \\ R_2 \\ R_3 \\ R_4 \\ R_5 \\ R_6 \end{bmatrix} \quad (3.14)$$

3.3 The Energy Method

Based on (3.8), we can create the following equations:

$$0 = A_x \frac{\partial q}{\partial x} + A_y \frac{\partial q}{\partial y} \quad (3.15a)$$

$$0 = q^* A_x \frac{\partial q}{\partial x} + q^* A_y \frac{\partial q}{\partial y} \quad (3.15b)$$

$$0 = \frac{\partial q^*}{\partial x} A_x^* + \frac{\partial q^*}{\partial y} A_y^* = \frac{\partial q^*}{\partial x} A_x + \frac{\partial q^*}{\partial y} A_y \quad (3.15c)$$

$$0 = \frac{\partial q^*}{\partial x} A_x q + \frac{\partial q^*}{\partial y} A_y q. \quad (3.15d)$$

where q^* is the Hermitian of q . Summing up (3.15b) and (3.15d) and using the local coordinates (ξ, η) transformation plotted in Fig. 3.1, we have

$$0 = q^* A_\xi \frac{\partial q}{\partial \xi} + q^* A_\eta \frac{\partial q}{\partial \eta} + \frac{\partial q^*}{\partial \xi} A_\xi q + \frac{\partial q^*}{\partial \eta} A_\eta q \quad (3.16)$$

$$= \frac{\partial}{\partial \xi} (q^* A_\xi q) + \frac{\partial}{\partial \eta} (q^* A_\eta q) \quad (3.17)$$

where

$$A_\xi = A_x \frac{\partial \xi}{\partial x} + A_y \frac{\partial \xi}{\partial y}, \quad A_\eta = A_x \frac{\partial \eta}{\partial x} + A_y \frac{\partial \eta}{\partial y}.$$

Integrating over $\Omega \in \{-1 \leq \xi \leq 1, -1 \leq \eta \leq 1\}$, (4.16) becomes

$$0 = \int_{S=\Omega} \left[\frac{\partial}{\partial \xi} (q^* A_\xi q) + \frac{\partial}{\partial \eta} (q^* A_\eta q) \right] \cdot dS \quad (3.18a)$$

$$= \int_{l=\delta\Omega} q^* (n_\xi A_\xi + n_\eta A_\eta) q \cdot dl \quad (3.18b)$$

$$= \begin{cases} \int_{l=\delta\Omega} q^* \left[n_\eta \left(\frac{\partial \eta}{\partial x}, \frac{\partial \eta}{\partial y} \right) \cdot (A_x, A_y) \right] q \cdot dl & \text{if } n_\xi = 0 \\ \int_{l=\delta\Omega} q^* \left[n_\xi \left(\frac{\partial \xi}{\partial x}, \frac{\partial \xi}{\partial y} \right) \cdot (A_x, A_y) \right] q \cdot dl & \text{if } n_\eta = 0 \end{cases} \quad (3.18c)$$

$$= \begin{cases} \int_{l=\delta\Omega} n_\eta |\nabla \eta| q^* A(n) q \cdot dl & \text{if } n_\xi = 0 \\ \int_{l=\delta\Omega} n_\xi |\nabla \xi| q^* A(n) q \cdot dl & \text{if } n_\eta = 0 \end{cases} \quad (3.18d)$$

$$= \begin{cases} \int_{l=\delta\Omega} n_\eta |\nabla \eta| (q^* S) \Lambda(S^* q) \cdot dl & \text{if } n_\xi = 0 \\ \int_{l=\delta\Omega} n_\xi |\nabla \xi| (q^* S) \Lambda(S^* q) \cdot dl & \text{if } n_\eta = 0 \end{cases} \quad (3.18e)$$

$$= \int_{-1}^1 |\nabla \eta| [-R_1^* R_1 + R_2^* R_2 + R_5^* R_5 - R_6^* R_6]_{\eta=-1} \cdot d\xi \quad (3.18f)$$

$$+ \int_{-1}^1 |\nabla \eta| [-R_1^* R_1 + R_2^* R_2 + R_5^* R_5 - R_6^* R_6]_{\eta=1} \cdot d\xi$$

$$+ \int_{-1}^1 |\nabla \xi| [-R_1^* R_1 + R_2^* R_2 + R_5^* R_5 - R_6^* R_6]_{\xi=-1} \cdot d\eta$$

$$+ \int_{-1}^1 |\nabla \xi| [-R_1^* R_1 + R_2^* R_2 + R_5^* R_5 - R_6^* R_6]_{\xi=1} \cdot d\eta$$

where (n_ξ, n_η) is a unit normal vector directed outward at the boundary $\delta\Omega$ of Ω .

Note that the eigenvalues corresponding to R_3 and R_4 are zeros, as seen in (3.13).

Closely looking at (3.18), since the left side is zero, for the equation to be meaningful,

the right side should be zero, or we need the condition

$$R_1^* R_1 + R_2^* R_2 = R_3^* R_3 + R_4^* R_4 \quad \text{at the boundary.} \quad (3.19)$$

We must follow (3.19) when designing the boundary conditions to make the equations be well-posed.

3.4 Characteristic Representations of Physical Boundary Conditions

We now consider the representations of physical boundary conditions for 2D structure. Assume there is an interface separating two domains. At this interface, we define the unit vector $\vec{n} = (n_x, n_y)$ pointing outward from the first domain to the second domain. Then from (3.14), the R variables can be represented in this way

$$R_1 = \frac{1}{\sqrt{2}} \vec{n} \cdot (\epsilon_r \vec{E}_{\parallel}) - \frac{1}{\sqrt{2}} \vec{E}_{\perp} \quad (3.20a)$$

$$R_2 = \frac{1}{\sqrt{2}} \vec{n} \cdot (\epsilon_r \vec{E}_{\parallel}) + \frac{1}{\sqrt{2}} \vec{E}_{\perp} \quad (3.20b)$$

$$R_5 = \frac{1}{\sqrt{2}} \vec{n} \cdot \vec{H}_{\parallel} + \frac{1}{\sqrt{2}} \vec{H}_{\perp} \quad (3.20c)$$

$$R_6 = \frac{1}{\sqrt{2}} \vec{n} \cdot \vec{H}_{\parallel} - \frac{1}{\sqrt{2}} \vec{H}_{\perp} \quad (3.20d)$$

where the subscript of the \vec{E}_{\parallel} means the direction of the electric field is in the x - y plane and the subscript of \vec{E}_{\perp} means the direction of the electric field is perpendicular to the x - y plane. Because the corresponding eigenvalues of R_3 and R_4 are zeros, they are ignored.

For the PEC boundary condition, we have (considering isotropic non-magnetic media)

$$\vec{n} \times \vec{E}_{\parallel} = 0, \quad \vec{E}_{\perp} = 0 \quad (3.21a)$$

$$\vec{n} \cdot \vec{H}_{\parallel} = 0. \quad (3.21b)$$

From (3.20), we can obtain

$$R_1 - R_2 = -\sqrt{2} \vec{E}_{\perp} \quad (3.22a)$$

$$R_5 + R_6 = \sqrt{2} \vec{n} \cdot \vec{H}_{\parallel}. \quad (3.22b)$$

Then with (3.21) the PEC boundary condition has a characteristic representation as

$$\begin{pmatrix} R_{1BC} = R_2, & R_{2BC} = R_1 \\ R_{5BC} = -R_6, & R_{6BC} = -R_5 \end{pmatrix}. \quad (3.23)$$

For the PMC boundary condition, we have

$$\vec{n} \cdot \vec{E}_{\parallel} = 0 \quad (3.24a)$$

$$\vec{n} \times \vec{H}_{\parallel} = 0, \quad \vec{H}_{\perp} = 0. \quad (3.24b)$$

From (3.20), we have

$$R_1 + R_2 = \sqrt{2} \vec{n} \cdot (\epsilon_r \vec{E}_{\parallel}) \quad (3.25a)$$

$$R_5 - R_6 = \sqrt{2} \vec{H}_{\perp} \quad (3.25b)$$

leading the characteristic representation for the PMC boundary condition as

$$\begin{pmatrix} R_{1BC} = -R_2, & R_{2BC} = -R_1 \\ R_{5BC} = R_6, & R_{6BC} = R_5 \end{pmatrix}. \quad (3.26)$$

For source-free dielectric media, the physical boundary conditions between two domains are

$$\vec{n} \times \vec{E}_{\parallel}^I = \vec{n} \times \vec{E}_{\parallel}^{II}, \quad \vec{E}_{\perp}^I = \vec{E}_{\perp}^{II} \quad (3.27a)$$

$$\vec{n} \cdot \epsilon_I \vec{E}_{\parallel}^I = \vec{n} \cdot \epsilon_{II} \vec{E}_{\parallel}^{II} \quad (3.27b)$$

$$\vec{n} \times \vec{H}_{\parallel}^I = \vec{n} \times \vec{H}_{\parallel}^{II}, \quad \vec{H}_{\perp}^I = \vec{H}_{\perp}^{II} \quad (3.27c)$$

$$\vec{n} \cdot \vec{H}_{\parallel}^I = \vec{n} \cdot \vec{H}_{\parallel}^{II} \quad (3.27d)$$

where the superscripts I and II denoting different dielectric regions on the two sides or two domains of the surface interface, respectively. From (3.20), we have

$$R_1^I = \frac{1}{\sqrt{2}} \vec{n}^I \cdot (\epsilon_{rI} \vec{E}_{\parallel}^I) - \frac{1}{\sqrt{2}} \vec{E}_{\perp}^I \quad (3.28a)$$

$$R_2^{II} = \frac{1}{\sqrt{2}} \vec{n}^{II} \cdot (\epsilon_{rII} \vec{E}_{\parallel}^{II}) + \frac{1}{\sqrt{2}} \vec{E}_{\perp}^{II}. \quad (3.28b)$$

Because \vec{n}^I and \vec{n}^{II} are in opposite directions, let $\vec{n}^I = -\vec{n}^{II} = \vec{n}$. Then, adding (3.28a) to (3.28b), we obtain

$$R_1^I + R_2^{II} = \frac{1}{\sqrt{2}} \vec{n} \cdot (\epsilon_{rI} \vec{E}_{\parallel}^I - \epsilon_{rII} \vec{E}_{\parallel}^{II}) - \frac{1}{\sqrt{2}} (\vec{E}_{\perp}^I - \vec{E}_{\perp}^{II}). \quad (3.29)$$

Using (3.27), (3.29) yields

$$R_1^I = -R_2^{II}. \quad (3.30)$$

After doing the same procedure to $R_2, R_5,$ and $R_6,$ we can get the characteristic representation as

$$\left(\begin{array}{l} R_{1BC}^{I/II} = -R_2^{II/I}, \quad R_{2BC}^{I/II} = -R_1^{II/I} \\ R_{5BC}^{I/II} = -R_6^{II/I}, \quad R_{6BC}^{I/II} = -R_5^{II/I} \end{array} \right). \quad (3.31)$$

3.5 Design of the Scheme

In this section, we will add boundary conditions to the governing equations. Consider (3.7) with boundary terms for grid point (x_i, y_j)

$$\begin{aligned} -i\beta M_1 \cdot q|_{(x_i, y_j)} &= ik_0 M_2 \cdot q|_{(x_i, y_j)} + A_x \frac{\partial q}{\partial x} \Big|_{(x_i, y_j)} + A_y \frac{\partial q}{\partial y} \Big|_{(x_i, y_j)} \\ &\quad - \delta(x_i, y_j) \tau SB(R - R_{BC}) \end{aligned} \quad (3.32)$$

where $i, j \in \{0, 1, \dots, N\}$ represents the numbering of grid points, $\delta(x_i, y_j)$ is defined as

$$\delta(x_i, y_j) = \delta_{0i} + \delta_{Ni} + \delta_{0j} + \delta_{Nj}.$$

τ is a real constant number with its values to be delivered latter, S is the matrix defined in (3.12), B is the boundary inflow/outflow operator defined as

$$B = \begin{bmatrix} b_1 & 0 & 0 & 0 & 0 & 0 \\ 0 & b_2 & 0 & 0 & 0 & 0 \\ 0 & 0 & 0 & 0 & 0 & 0 \\ 0 & 0 & 0 & 0 & 0 & 0 \\ 0 & 0 & 0 & 0 & b_5 & 0 \\ 0 & 0 & 0 & 0 & 0 & b_6 \end{bmatrix} \quad (3.33)$$

where $b_1, b_2, b_5,$ and b_6 are all real, R is the characteristic state vector defined in (3.14), and R_{BC} is defined in the previous section for every physical boundary condition.

Next, we ignore the low-order terms of (3.32). And like the low-order terms, the inhomogeneous term R_{BC} can be neglected. Using (3.15b) and (3.15d) to obtain

$$0 = q^*|_{(x_i, y_j)} A_x \frac{\partial q}{\partial x} \Big|_{(x_i, y_j)} + q^*|_{(x_i, y_j)} A_y \frac{\partial q}{\partial y} \Big|_{(x_i, y_j)} - \delta(x_i, y_j) \tau(R^* B R) \quad (3.34)$$

$$0 = \frac{\partial q}{\partial x} \Big|_{(x_i, y_j)} A_x q^*|_{(x_i, y_j)} + \frac{\partial q}{\partial y} \Big|_{(x_i, y_j)} A_y q^*|_{(x_i, y_j)} - \delta(x_i, y_j) \tau(R^* B R). \quad (3.35)$$

Summing up (3.34) and (3.35), integrating the equation in the discrete form, and basing on (3.18), we have

$$\begin{aligned} 0 &= \sum_{j=0}^N w_{\eta j} \sum_{i=0}^N w_{\xi i} \left[\frac{\partial}{\partial x} (q^* A_x q) + \frac{\partial}{\partial y} (q^* A_y q) - 2\delta(x_i, y_j) \tau(R^* B R) \right] \\ &= \left(\sum_{\substack{i=0 \\ \eta=-1}}^N + \sum_{\substack{i=0 \\ \eta=1}}^N \right) w_{\xi i} |\nabla \xi| [-R_1^* R_1 + R_2^* R_2 + R_5^* R_5 - R_6^* R_6] \\ &\quad + \left(\sum_{\substack{j=0 \\ \xi=-1}}^N + \sum_{\substack{j=0 \\ \xi=1}}^N \right) w_{\eta j} |\nabla \eta| [-R_1^* R_1 + R_2^* R_2 + R_5^* R_5 - R_6^* R_6] \\ &\quad - \left(w_{\eta 0} \sum_{\substack{i=0 \\ \eta=-1}}^N + w_{\eta N} \sum_{\substack{i=0 \\ \eta=1}}^N \right) w_{\xi i} 2\tau(R^* B R) \\ &\quad - \left(w_{\xi 0} \sum_{\substack{j=0 \\ \xi=-1}}^N + w_{\xi N} \sum_{\substack{j=0 \\ \xi=1}}^N \right) w_{\eta j} 2\tau(R^* B R) \end{aligned} \quad (3.36)$$

where \sum is the discrete form of integral and w_{xi} and w_{yj} are the weights of the discrete integrals (which will be delivered in Chapter 5). The values of w_{xi} and w_{yj}

depend on the numerical method employed. Write (3.36) as

$$\begin{aligned}
0 = & \sum_{\substack{i=0 \\ \eta=-1}}^N w_{\xi i} [(-|\nabla\xi| - 2w_{\eta 0}\tau b_1)R_1^*R_1 + (|\nabla\xi| - 2w_{\eta 0}\tau b_2)R_2^*R_2 \\
& + (|\nabla\xi| - 2w_{\eta 0}\tau b_5)R_5^*R_5 + (-|\nabla\xi| - 2w_{\eta 0}\tau b_6)R_6^*R_6] \\
& + \sum_{\substack{i=0 \\ \eta=1}}^N w_{\xi i} [(-|\nabla\xi| - 2w_{\eta N}\tau b_1)R_1^*R_1 + (|\nabla\xi| - 2w_{\eta N}\tau b_2)R_2^*R_2 \\
& + (|\nabla\xi| - 2w_{\eta N}\tau b_5)R_5^*R_5 + (-|\nabla\xi| - 2w_{\eta N}\tau b_6)R_6^*R_6] \\
& + \sum_{\substack{j=0 \\ \xi=-1}}^N w_{\eta j} [(-|\nabla\eta| - 2w_{\xi 0}\tau b_1)R_1^*R_1 + (|\nabla\eta| - 2w_{\xi 0}\tau b_2)R_2^*R_2 \\
& + (|\nabla\eta| - 2w_{\xi 0}\tau b_5)R_5^*R_5 + (-|\nabla\eta| - 2w_{\xi 0}\tau b_6)R_6^*R_6] \\
& + \sum_{\substack{j=0 \\ \xi=1}}^N w_{\eta j} [(-|\nabla\eta| - 2w_{\xi N}\tau b_1)R_1^*R_1 + (|\nabla\eta| - 2w_{\xi N}\tau b_2)R_2^*R_2 \\
& + (|\nabla\eta| - 2w_{\xi N}\tau b_5)R_5^*R_5 + (-|\nabla\eta| - 2w_{\xi N}\tau b_6)R_6^*R_6]. \tag{3.37}
\end{aligned}$$

In order to make the right side of (3.37) to be zero, we define

$$\tau = \begin{cases} \frac{1}{2w_{\eta 0}} |\nabla\xi|, & \text{when } \eta = -1 \\ \frac{1}{2w_{\eta N}} |\nabla\xi|, & \text{when } \eta = 1 \\ \frac{1}{2w_{\xi 0}} |\nabla\eta|, & \text{when } \xi = -1 \\ \frac{1}{2w_{\xi N}} |\nabla\eta|, & \text{when } \xi = 1 \end{cases} \tag{3.38}$$

and

$$\left(b_1 = -1, \quad b_2 = 1, \quad b_5 = 1, \quad b_6 = -1 \right). \tag{3.39}$$

Substituting the values in (3.39) into (3.33), the matrix B is determined.

3.6 The Final Form of The Six-Equation Version

The boundary conditions have been discussed in detail in previous sections. Now we substitute all variables obtained to form a standard eigenvalue problem.

We start with the case of the PEC boundary condition. First, substituting the matrices M_1 , M_2 , A_x , A_y , S , and B into (3.32), and replacing $(R - R_{BC})$ with (3.23), we can obtain the following six equations:

$$-i\beta E_x = -ik_0 H_y + \frac{\partial}{\partial x} E_z - \delta(x_i, y_j) \tau [2n_x E_z] \quad (3.40a)$$

$$-i\beta E_y = ik_0 H_x + \frac{\partial}{\partial y} E_z - \delta(x_i, y_j) \tau [2n_y E_z] \quad (3.40b)$$

$$-i\beta E_z = -\frac{\partial}{\partial x} E_x - \frac{\partial}{\partial y} E_y \quad (3.40c)$$

$$-i\beta H_x = ik_0 \epsilon_r E_y + \frac{\partial}{\partial x} H_z \quad (3.40d)$$

$$-i\beta H_y = -ik_0 \epsilon_r E_x + \frac{\partial}{\partial y} H_z \quad (3.40e)$$

$$-i\beta H_z = -\frac{\partial}{\partial x} H_x - \frac{\partial}{\partial y} H_y + \delta(x_i, y_j) \tau [2(n_x H_x + n_y H_y)]. \quad (3.40f)$$

For the case of the PMC boundary condition, by replacing $(R - R_{BC})$ with (3.26), we can get the following equations:

$$-i\beta E_x = -ik_0 H_y + \frac{\partial}{\partial x} E_z \quad (3.41a)$$

$$-i\beta E_y = ik_0 H_x + \frac{\partial}{\partial y} E_z \quad (3.41b)$$

$$-i\beta E_z = -\frac{\partial}{\partial x} E_x - \frac{\partial}{\partial y} E_y + \delta(x_i, y_j) \tau [2(n_x E_x + n_y E_y)] \quad (3.41c)$$

$$-i\beta H_x = ik_0 \epsilon_r E_y + \frac{\partial}{\partial x} H_z - \delta(x_i, y_j) \tau [2n_x H_z] \quad (3.41d)$$

$$-i\beta H_y = -ik_0 \epsilon_r E_x + \frac{\partial}{\partial y} H_z - \delta(x_i, y_j) \tau [2n_y H_z] \quad (3.41e)$$

$$-i\beta H_z = -\frac{\partial}{\partial x} H_x - \frac{\partial}{\partial y} H_y. \quad (3.41f)$$

Finally, by replacing $(R - R_{BC})$ with (3.31), we have the following equations for

the dielectric boundary condition:

$$-i\beta E_x^I = -ik_0 H_y^I + \frac{\partial}{\partial x} E_z^I - \delta^I(x_i, y_j) \tau^I [n_x^I (E_z^I - E_z^{II})] \quad (3.42a)$$

$$-i\beta E_y^I = ik_0 H_x^I + \frac{\partial}{\partial y} E_z^I - \delta^I(x_i, y_j) \tau^I [n_y^I (E_z^I - E_z^{II})] \quad (3.42b)$$

$$\begin{aligned} -i\beta E_z^I = & -\frac{\partial}{\partial x} E_x^I - \frac{\partial}{\partial y} E_y^I \\ & + \delta^I(x_i, y_j) \tau^I \left[n_x^I (E_x^I - \frac{\epsilon_{rII}}{\epsilon_{rI}} E_x^{II}) + n_y^I (E_y^I - \frac{\epsilon_{rII}}{\epsilon_{rI}} E_y^{II}) \right] \end{aligned} \quad (3.42c)$$

$$-i\beta H_x^I = ik_0 \epsilon_{rI} E_y^I + \frac{\partial}{\partial x} H_z^I - \delta^I(x_i, y_j) \tau^I [n_x^I (H_z^I - H_z^{II})] \quad (3.42d)$$

$$-i\beta H_y^I = -ik_0 \epsilon_{rI} E_x^I + \frac{\partial}{\partial y} H_z^I - \delta^I(x_i, y_j) \tau^I [n_y^I (H_z^I - H_z^{II})] \quad (3.42e)$$

$$\begin{aligned} -i\beta H_z^I = & -\frac{\partial}{\partial x} H_x^I - \frac{\partial}{\partial y} H_y^I \\ & + \delta^I(x_i, y_j) \tau^I [n_x^I (H_x^I - H_x^{II}) + n_y^I (H_y^I - H_y^{II})]. \end{aligned} \quad (3.42f)$$

3.7 The Final Form of Three-Equation Version

We have demonstrated the formulations for 2D waveguide problems in the previous section. In fact, we can decrease the number of equations from six to three. First, we start from (3.40) by writing it in the continuous form:

$$-i\beta E_x(x, y) = -ik_0 H_y(x, y) + \frac{\partial}{\partial x} E_z(x, y) - \delta(x, y) \tau [2n_x E_z] \quad (3.43a)$$

$$-i\beta E_y(x, y) = ik_0 H_x(x, y) + \frac{\partial}{\partial y} E_z(x, y) - \delta(x, y) \tau [2n_y E_z] \quad (3.43b)$$

$$-i\beta E_z(x, y) = -\frac{\partial}{\partial x} E_x(x, y) - \frac{\partial}{\partial y} E_y(x, y) \quad (3.43c)$$

$$-i\beta H_x(x, y) = ik_0 \epsilon_r E_y(x, y) + \frac{\partial}{\partial x} H_z(x, y) \quad (3.43d)$$

$$-i\beta H_y(x, y) = -ik_0 \epsilon_r E_x(x, y) + \frac{\partial}{\partial y} H_z(x, y) \quad (3.43e)$$

$$-i\beta H_z(x, y) = -\frac{\partial}{\partial x} H_x(x, y) - \frac{\partial}{\partial y} H_y(x, y) + \delta(x, y) \tau [2(n_x H_x + n_y H_y)] \quad (3.43f)$$

where $\delta(x, y)$ is defined as

$$\delta(x, y) = l_0(x) + l_N(x) + l_0(y) + l_N(y).$$

Here, the l function, for example, $l_0(x)$, is the basis function we use to interpolate an unknown function. $l_0(x)$ will look like as shown in Fig. 3.2 which is equal to 1 at $x = x_0$ and 0 at other grid points.

We multiply (3.43d), (3.43e), and (3.43c) with $i\beta$ and replace $i\beta E_x(x, y)$, $i\beta E_y(x, y)$, and $i\beta H_z(x, y)$ with (3.43a), (3.43b), and (3.43f), respectively, to obtain

$$-\beta^2 H_x(x, y) = -k_0^2 \epsilon_r H_x(x, y) - \frac{\partial^2}{\partial x^2} H_x(x, y) - \frac{\partial^2}{\partial x \partial y} H_y(x, y) \quad (3.44)$$

$$+ ik_0 \epsilon_r \frac{\partial}{\partial y} E_z(x, y) + \frac{\partial}{\partial x} \delta(x, y) \tau [2(n_x H_x + n_y H_y)]$$

$$- ik_0 \epsilon_r \delta(x, y) \tau [2n_y E_z]$$

$$-\beta^2 H_y(x, y) = -k_0^2 \epsilon_r H_y(x, y) - \frac{\partial^2}{\partial x \partial y} H_x(x, y) - \frac{\partial^2}{\partial y^2} H_y(x, y) \quad (3.45)$$

$$- ik_0 \epsilon_r \frac{\partial}{\partial x} E_z(x, y) + \frac{\partial}{\partial y} \delta(x, y) \tau [2(n_x H_x + n_y H_y)]$$

$$+ ik_0 \epsilon_r \delta(x, y) \tau [2n_x E_z]$$

$$-\beta^2 E_z(x, y) = -ik_0 \frac{\partial}{\partial y} H_x(x, y) + ik_0 \frac{\partial}{\partial x} H_y(x, y) - \frac{\partial^2}{\partial x^2} E_z(x, y) \quad (3.46)$$

$$- \frac{\partial^2}{\partial y^2} E_z(x, y) + \tau \left[n_x \frac{\partial}{\partial x} \delta(x, y) + n_y \frac{\partial}{\partial y} \delta(x, y) \right] [2E_z].$$

Finally, we rewrite (3.44)–(3.46) in discrete form as

$$-\beta^2 H_x = -k_0^2 \epsilon_r H_x - \frac{\partial^2}{\partial x^2} H_x - \frac{\partial^2}{\partial x \partial y} H_y + ik_0 \epsilon_r \frac{\partial}{\partial y} E_z \quad (3.47)$$

$$+ \frac{\partial}{\partial x} \delta(x_i, y_j) \tau [2(n_x H_x + n_y H_y)] - ik_0 \epsilon_r \delta(x_i, y_j) \tau [2n_y E_z]$$

$$-\beta^2 H_y = -k_0^2 \epsilon_r H_y - \frac{\partial^2}{\partial x \partial y} H_x - \frac{\partial^2}{\partial y^2} H_y - ik_0 \epsilon_r \frac{\partial}{\partial x} E_z \quad (3.48)$$

$$+ \frac{\partial}{\partial y} \delta(x_i, y_j) \tau [2(n_x H_x + n_y H_y)] + ik_0 \epsilon_r \delta(x_i, y_j) \tau [2n_x E_z]$$

$$-\beta^2 E_z = -ik_0 \frac{\partial}{\partial y} H_x + ik_0 \frac{\partial}{\partial x} H_y - \frac{\partial^2}{\partial x^2} E_z - \frac{\partial^2}{\partial y^2} E_z \quad (3.49)$$

$$+ \tau \left[n_x \frac{\partial}{\partial x} \delta(x_i, y_j) + n_y \frac{\partial}{\partial y} \delta(x_i, y_j) \right] [2E_z].$$

For the case of the PMC boundary condition, we can derive

$$-\beta^2 H_x = -k_0^2 \epsilon_r H_x - \frac{\partial^2}{\partial x^2} H_x - \frac{\partial^2}{\partial x \partial y} H_y + ik_0 \epsilon_r \frac{\partial}{\partial y} E_z \quad (3.50)$$

$$+ \delta(x_i, y_j) \tau \left[2n_x \left(\frac{\partial}{\partial x} H_x + \frac{\partial}{\partial y} H_y \right) \right]$$

$$-\beta^2 H_y = -k_0^2 \epsilon_r H_y - \frac{\partial^2}{\partial x \partial y} H_x - \frac{\partial^2}{\partial y^2} H_y - ik_0 \epsilon_r \frac{\partial}{\partial x} E_z \quad (3.51)$$

$$+ \delta(x_i, y_j) \tau \left[2n_y \left(\frac{\partial}{\partial x} H_x + \frac{\partial}{\partial y} H_y \right) \right]$$

$$-\beta^2 E_z = -ik_0 \frac{\partial}{\partial y} H_x + ik_0 \frac{\partial}{\partial x} H_y - \frac{\partial^2}{\partial x^2} E_z - \frac{\partial^2}{\partial y^2} E_z \quad (3.52)$$

$$+ \delta(x_i, y_j) \tau \left[-i2k_0 (n_x H_y - n_y H_x) + 2 \left(n_x \frac{\partial}{\partial x} + n_y \frac{\partial}{\partial y} \right) E_z \right]$$

and for the case of the dielectric boundary condition, we can derive

$$-\beta^2 H_x^I = -k_0^2 \epsilon_{rI} H_x^I - \frac{\partial^2}{\partial x^2} H_x^I - \frac{\partial^2}{\partial x \partial y} H_y^I + ik_0 \epsilon_r \frac{\partial}{\partial y} E_z^I \quad (3.53)$$

$$+ \frac{\partial}{\partial x} \delta^I(x_i, y_j) \tau^I \left[n_x^I (H_x^I - H_x^{II}) + n_y^I (H_y^I - H_y^{II}) \right]$$

$$+ \delta^I(x_i, y_j) \tau^I \left[n_x^I \left(\frac{\partial}{\partial x} (H_x^I - H_x^{II}) + \frac{\partial}{\partial y} (H_y^I - H_y^{II}) \right) - ik_0 \epsilon_r n_y^I (E_z^I - E_z^{II}) \right]$$

$$- \delta^I(x_i, y_j) \tau^I \left[n_x^I (\delta^I(x_i, y_j) \tau^I - \delta^{II}(x_i, y_j) \tau^{II}) (n_x^I (H_x^I - H_x^{II}) + n_y^I (H_y^I - H_y^{II})) \right]$$

$$-\beta^2 H_y^I = -k_0^2 \epsilon_{rI} H_y^I - \frac{\partial^2}{\partial x \partial y} H_x^I - \frac{\partial^2}{\partial y^2} H_y^I - ik_0 \epsilon_r \frac{\partial}{\partial x} E_z^I \quad (3.54)$$

$$+ \frac{\partial}{\partial y} \delta^I(x_i, y_j) \tau^I \left[n_x^I (H_x^I - H_x^{II}) + n_y^I (H_y^I - H_y^{II}) \right]$$

$$+ \delta^I(x_i, y_j) \tau^I \left[n_y^I \left(\frac{\partial}{\partial x} (H_x^I - H_x^{II}) + \frac{\partial}{\partial y} (H_y^I - H_y^{II}) \right) + ik_0 \epsilon_r n_x^I (E_z^I - E_z^{II}) \right]$$

$$- \delta^I(x_i, y_j) \tau^I \left[n_y^I (\delta^I(x_i, y_j) \tau^I - \delta^{II}(x_i, y_j) \tau^{II}) (n_x^I (H_x^I - H_x^{II}) + n_y^I (H_y^I - H_y^{II})) \right]$$

$$-\beta^2 E_z^I = -ik_0 \frac{\partial}{\partial y} H_x^I + ik_0 \frac{\partial}{\partial x} H_y^I - \frac{\partial^2}{\partial x^2} E_z^I - \frac{\partial^2}{\partial y^2} E_z^I \quad (3.55)$$

$$+ \tau^I \left[n_x^I \frac{\partial}{\partial x} \delta^I(x_i, y_j) + n_y^I \frac{\partial}{\partial y} \delta^I(x_i, y_j) \right] [E_z^I - E_z^{II}]$$

$$+ \delta^I(x_i, y_j) \frac{\tau^I}{\epsilon_{rI}} \left[-ik_0 (\epsilon_{rI} (n_x^I H_y^I - n_y^I H_x^I) - \epsilon_{rII} (n_x^I H_y^{II} - n_y^I H_x^{II})) \right]$$

$$+ \left(n_x^I \frac{\partial}{\partial x} + n_y^I \frac{\partial}{\partial y} \right) (\epsilon_{rI} E_z^I - \epsilon_{rII} E_z^{II})$$

$$- (\delta^I(x_i, y_j) \tau^I \epsilon_{rI} - \delta^{II}(x_i, y_j) \tau^{II} \epsilon_{rII}) (E_z^I - E_z^{II})].$$

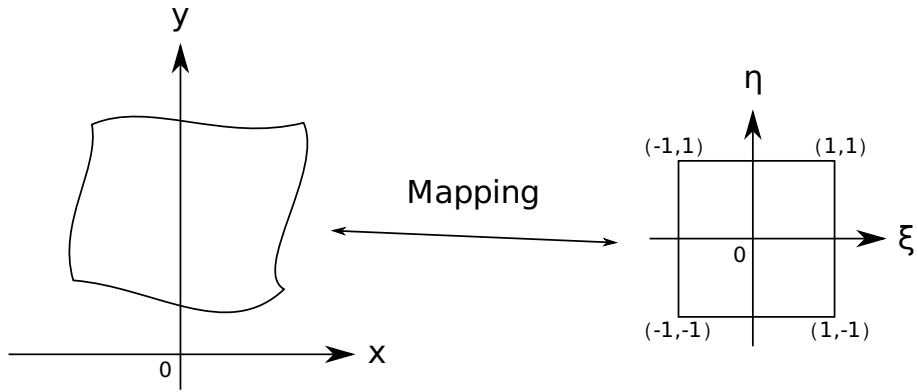


Figure 3.1: Transformation between global and local coordinates.

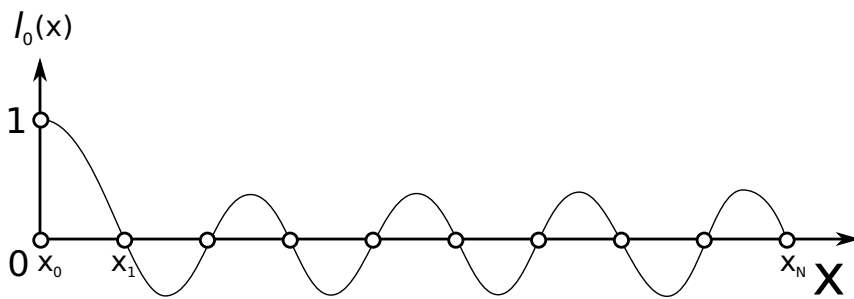


Figure 3.2: The characteristic of $l_0(x)$.

Chapter 4

Mathematical Formulation for 2D Photonic Crystal Analysis

This chapter is devoted to the process of derivation of the formulation for the 2D photonic crystal (PC) problem. Since we have demonstrated the whole process of derivation in details in the last chapter, in this chapter we will only describe some important parts of the whole derivation.

4.1 Equations Used for PC Structure

We start from the Maxwell's curl equations for the TE mode:

$$\epsilon \frac{\partial \tilde{E}_x}{\partial t} = -\frac{\partial \tilde{H}_y}{\partial z} \quad (4.1a)$$

$$\epsilon \frac{\partial \tilde{E}_z}{\partial t} = \frac{\partial \tilde{H}_y}{\partial x} \quad (4.1b)$$

$$\mu_0 \frac{\partial \tilde{H}_y}{\partial t} = \frac{\partial \tilde{E}_z}{\partial x} - \frac{\partial \tilde{E}_x}{\partial z} \quad (4.1c)$$

with the following transformation:

$$\tilde{H}_y = \frac{1}{\sqrt{\mu_0/\epsilon_0}} H_y, \quad \tilde{E}_x = E_x, \quad \tilde{E}_z = E_z \quad (4.2)$$

(4.1) will appear as

$$\frac{\epsilon_r}{c} \frac{\partial E_x}{\partial t} = -\frac{\partial H_y}{\partial z} \quad (4.3a)$$

$$\frac{\epsilon_r}{c} \frac{\partial E_z}{\partial t} = \frac{\partial H_y}{\partial x} \quad (4.3b)$$

$$\frac{1}{c} \frac{\partial H_y}{\partial t} = \frac{\partial E_z}{\partial x} - \frac{\partial E_x}{\partial z} \quad (4.3c)$$

where ϵ_r is relative permittivity defined as $\epsilon_r = \epsilon/\epsilon_0$.

4.2 Well-posedness Analysis

We write (4.3) in matrix form:

$$\frac{M}{c} \frac{\partial \hat{q}}{\partial t} = A_x \cdot \frac{\partial \hat{q}}{\partial x} + A_z \cdot \frac{\partial \hat{q}}{\partial z} \quad (4.4)$$

where $\hat{q} = [E_x \ E_z \ H_y]^T$ and M , A_x , and A_z are defined as

$$M = \begin{bmatrix} \epsilon_r & 0 & 0 \\ 0 & \epsilon_r & 0 \\ 0 & 0 & 1 \end{bmatrix}, A_x = \begin{bmatrix} 0 & 0 & 0 \\ 0 & 0 & 1 \\ 0 & 1 & 0 \end{bmatrix}, A_z = \begin{bmatrix} 0 & 0 & -1 \\ 0 & 0 & 0 \\ -1 & 0 & 0 \end{bmatrix}. \quad (4.5)$$

Let $\hat{q}(x, z, t) = q(x, z) \cdot e^{i\omega t}$ and (4.4) becomes

$$ik_0 M q = A_x \cdot \frac{\partial q}{\partial x} + A_z \cdot \frac{\partial q}{\partial z} \quad (4.6)$$

where $k_0 = \omega/c$.

Now we neglect the low-order terms which do not affect the well-posedness analysis. Then (4.6) becomes

$$0 = A_x \cdot \frac{\partial q}{\partial x} + A_z \cdot \frac{\partial q}{\partial z}. \quad (4.7)$$

Define a new matrix $A(n)$

$$A(n) = n_x A_x + n_z A_z \quad (4.8)$$

where (n_x, n_z) represents the unit normal vector directed outward on the boundary of the considered domain. Since $A(n) = A(n)^T$, there exists a matrix S such that

$$S^T \cdot A(n) \cdot S = \Lambda. \quad (4.9)$$

For a symmetric matrix $A(n)$, we can define such matrix S as

$$S = \begin{bmatrix} \frac{n_z}{\sqrt{2}} & \frac{n_z}{\sqrt{2}} & n_x \\ -\frac{n_x}{\sqrt{2}} & -\frac{n_x}{\sqrt{2}} & n_z \\ \frac{1}{\sqrt{2}} & -\frac{1}{\sqrt{2}} & 0 \end{bmatrix}. \quad (4.10)$$

From (4.10), we have

$$S^T S = I, \quad S^T A(n) S = \begin{bmatrix} -1 & 0 & 0 \\ 0 & 1 & 0 \\ 0 & 0 & 0 \end{bmatrix}$$

where $\sqrt{n_x^2 + n_z^2} = 1$ has been used. We define a new vector R , the characteristic state vector, for latter use

$$R = S^T \cdot q = \begin{bmatrix} \frac{n_z}{\sqrt{2}} E_x - \frac{n_x}{\sqrt{2}} E_z + \frac{1}{\sqrt{2}} H_y \\ \frac{n_z}{\sqrt{2}} E_x - \frac{n_x}{\sqrt{2}} E_z - \frac{1}{\sqrt{2}} H_y \\ n_x E_x + n_z E_z \end{bmatrix} = \begin{bmatrix} R_1 \\ R_2 \\ R_3 \end{bmatrix}. \quad (4.11)$$

4.3 The Energy Method

Based on (4.7), we have the following equations:

$$0 = A_x \frac{\partial q}{\partial x} + A_z \frac{\partial q}{\partial z} \quad (4.12)$$

$$0 = q^* A_x \frac{\partial q}{\partial x} + q^* A_z \frac{\partial q}{\partial z} \quad (4.13)$$

$$0 = \frac{\partial q^*}{\partial x} A_x^* + \frac{\partial q^*}{\partial z} A_z^* = \frac{\partial q^*}{\partial x} A_x + \frac{\partial q^*}{\partial z} A_z, \quad (4.14)$$

$$0 = \frac{\partial q^*}{\partial x} A_x q + \frac{\partial q^*}{\partial z} A_z q. \quad (4.15)$$

Summing up (4.13) and (4.15) and using the local coordinates (ξ, η) transformation shown in Fig. 3.1, we have

$$0 = q^* A_\xi \frac{\partial q}{\partial \xi} + q^* A_\eta \frac{\partial q}{\partial \eta} + \frac{\partial q^*}{\partial \xi} A_\xi q + \frac{\partial q^*}{\partial \eta} A_\eta q \quad (4.16)$$

$$= \frac{\partial}{\partial \xi} (q^* A_\xi q) + \frac{\partial}{\partial \eta} (q^* A_\eta q) \quad (4.17)$$

where

$$A_\xi = A_x \frac{\partial \xi}{\partial x} + A_z \frac{\partial \xi}{\partial z}, \quad A_\eta = A_x \frac{\partial \eta}{\partial x} + A_z \frac{\partial \eta}{\partial z}.$$

Integrating over $\Omega \in \{-1 \leq \xi \leq 1, -1 \leq \eta \leq 1\}$, (4.17) becomes

$$0 = \int_{S=\Omega} \left[\frac{\partial}{\partial \xi} (q^* A_\xi q) + \frac{\partial}{\partial \eta} (q^* A_\eta q) \right] \cdot dS \quad (4.18a)$$

$$= \int_{l=\delta\Omega} q^* (n_\xi A_\xi + n_\eta A_\eta) q \cdot dl \quad (4.18b)$$

$$\begin{aligned} &= \int_{-1}^1 |\nabla\eta| [-R_1^* R_1 + R_2^* R_2]_{\eta=-1} \cdot d\xi + \int_{-1}^1 |\nabla\eta| [-R_1^* R_1 + R_2^* R_2]_{\eta=1} \cdot d\xi \\ &\quad + \int_{-1}^1 |\nabla\xi| [-R_1^* R_1 + R_2^* R_2]_{\xi=-1} \cdot d\eta + \int_{-1}^1 |\nabla\xi| [-R_1^* R_1 + R_2^* R_2]_{\xi=1} \cdot d\eta. \end{aligned}$$

For the right side to be zero, we need the condition

$$R_1^* R_1 = R_2^* R_2 \quad \text{at boundary.} \quad (4.19)$$

And we must follow (4.19) when we design the boundary condition to make the equations be well-posed.

4.4 Characteristic Representations of Physical Boundary Conditions

We now consider the representations of physical boundary conditions for PC structure. Unlike the waveguide problem, there are only two types of boundary conditions, the dielectric boundary condition and the periodic boundary condition, involved in the PC structure. Consider an interface separating two domains, and define the unit vector $\vec{n} = (n_x, n_z)$ pointing from the first domain to the second domain. Then from (4.11), we can rewrite the R variables as

$$R_1 = \frac{1}{\sqrt{2}} \vec{n} \times \vec{E}_{\parallel} + \frac{1}{\sqrt{2}} \vec{H}_{\perp} \quad (4.20a)$$

$$R_2 = \frac{1}{\sqrt{2}} \vec{n} \times \vec{E}_{\parallel} - \frac{1}{\sqrt{2}} \vec{H}_{\perp} \quad (4.20b)$$

where the subscript of \vec{E}_{\parallel} means the direction of the electric field is in the x - z plane, and the subscript of \vec{H}_{\perp} means the direction of magnetic field is perpendicular to xz plane. We ignore R_3 because its corresponding eigenvalue is zero.

For the case of dielectric boundary condition, we have (considering isotropic non-magnetic media)

$$\vec{n} \times \vec{E}_{\parallel}^I = \vec{n} \times \vec{E}_{\parallel}^{II}, \quad \vec{E}_{\perp}^I = \vec{E}_{\perp}^{II} \quad (4.21a)$$

$$\vec{n} \cdot \epsilon_I \vec{E}_{\parallel}^I = \vec{n} \cdot \epsilon_{II} \vec{E}_{\parallel}^{II} \quad (4.21b)$$

$$\vec{n} \times \vec{H}_{\parallel}^I = \vec{n} \times \vec{H}_{\parallel}^{II}, \quad \vec{H}_{\perp}^I = \vec{H}_{\perp}^{II} \quad (4.21c)$$

$$\vec{n} \cdot \vec{H}_{\parallel}^I = \vec{n} \cdot \vec{H}_{\parallel}^{II} \quad (4.21d)$$

where the superscripts I and II denote the variables are defined in different regions.

From (4.20), we have

$$R_1^I = \frac{1}{\sqrt{2}} \vec{n}^I \times \vec{E}_{\parallel}^I + \frac{1}{\sqrt{2}} \vec{H}_{\perp}^I \quad (4.22a)$$

$$R_2^{II} = \frac{1}{\sqrt{2}} \vec{n}^{II} \times \vec{E}_{\parallel}^{II} - \frac{1}{\sqrt{2}} \vec{H}_{\perp}^{II}. \quad (4.22b)$$

Because \vec{n}^I and \vec{n}^{II} are in opposite directions, letting $\vec{n} = \vec{n}^I = -\vec{n}^{II}$ and adding (4.22a) to (4.22b), we obtain

$$R_1^I + R_2^{II} = \frac{1}{\sqrt{2}} \vec{n} \times (\vec{E}_{\parallel}^I - \vec{E}_{\parallel}^{II}) + \frac{1}{\sqrt{2}} (\vec{H}_{\perp}^I - \vec{H}_{\perp}^{II}).$$

By using (4.21a) and (4.21c), the above equation becomes

$$R_1^I = -R_2^{II}.$$

Consequently, we have the characteristic representation

$$\left(R_{1BC}^{I/II} = -R_{2BC}^{II/I}, \quad R_{2BC}^{I/II} = -R_{1BC}^{II/I} \right). \quad (4.23)$$

Because of the periodic geometry character of the PC structure, the field distribution should satisfy Bloch theorem

$$\psi(\vec{r} + \vec{n}a) = e^{-j(\vec{n} \cdot \vec{k})a} \psi(\vec{r}) \quad (4.24)$$

or

$$\psi(x + n_x a, z + n_z a) = e^{-j(n_x k_x + n_z k_z)a} \psi(x, z) \quad (4.25)$$

where a is the lattice constant of the PC and \vec{k} is the wave vector in the x - z plane. And (4.23) should be modified to be

$$\begin{pmatrix} R_{1BC}^{I/II} = -e^{-j(n_x k_x + n_z k_z)a} R_2^{II/I} \\ R_{2BC}^{I/II} = -e^{-j(n_x k_x + n_z k_z)a} R_1^{II/I} \end{pmatrix} \quad (4.26)$$

as the periodic boundary condition.

4.5 Design of the Scheme

In this section, we will add boundary conditions to the governing equations. Start from (4.6) with boundary terms for a grid point (x_i, z_j)

$$ik_0 M q|_{(x_i, z_j)} = A_x \frac{\partial q}{\partial x} \Big|_{(x_i, z_j)} + A_z \frac{\partial q}{\partial z} \Big|_{(x_i, z_j)} - \delta(x_i, z_j) \tau S B (R - R_{BC}) \quad (4.27)$$

where $i, j \in \{0, 1, \dots, N\}$ represents the numbering of grid points, $\delta(x_i, z_j)$ is defined as

$$\delta(x_i, z_j) = \delta_{0i} + \delta_{Ni} + \delta_{0j} + \delta_{Nj}$$

τ is a real constant number with its values to be determined latter, S is a matrix defined in (4.10), B is the boundary inflow/outflow operator defined as

$$B = \begin{bmatrix} b_1 & 0 & 0 \\ 0 & b_2 & 0 \\ 0 & 0 & 0 \end{bmatrix} \quad (4.28)$$

where b_1 and b_2 are both real, R is the characteristic state vector defined in (4.11), and R_{BC} is defined in the previous section for every physical boundary condition.

Next, we ignore the low-order terms of (4.27), and use (4.13) and (4.15) to obtain

$$0 = q^*|_{(x_i, y_j)} A_x \frac{\partial q}{\partial x} \Big|_{(x_i, y_j)} + q^*|_{(x_i, y_j)} A_y \frac{\partial q}{\partial y} \Big|_{(x_i, y_j)} - \delta(x_i, y_j) \tau (R^* B R) \quad (4.29)$$

$$0 = \frac{\partial q}{\partial x} \Big|_{(x_i, y_j)} A_x q^*|_{(x_i, y_j)} + \frac{\partial q}{\partial y} \Big|_{(x_i, y_j)} A_y q^*|_{(x_i, y_j)} - \delta(x_i, y_j) \tau (R^* B R). \quad (4.30)$$

Summing up (4.29) and (4.30), integrating the equation in the discrete form, and basing on (4.18), we have

$$\begin{aligned}
0 &= \sum_{j=0}^N w_{zj} \sum_{i=0}^N w_{xi} \left[\frac{\partial}{\partial x} (q^* A_x q) + \frac{\partial}{\partial z} (q^* A_z q) - 2\delta(x_i, z_j) \tau (R^* B R) \right] \\
&= \left(\sum_{\substack{i=0 \\ z=-1}}^N + \sum_{\substack{i=0 \\ z=1}}^N \right) w_{xi} |\nabla \eta| [-R_1^* R_1 + R_2^* R_2] + \left(\sum_{\substack{j=0 \\ x=-1}}^N + \sum_{\substack{j=0 \\ x=1}}^N \right) w_{zj} |\nabla \xi| [-R_1^* R_1 + R_2^* R_2] \\
&\quad - \left(w_{z0} \sum_{\substack{i=0 \\ z=-1}}^N + w_{zN} \sum_{\substack{i=0 \\ z=1}}^N \right) w_{xi} 2\tau (R^* B R) - \left(w_{x0} \sum_{\substack{j=0 \\ x=-1}}^N + w_{xN} \sum_{\substack{j=0 \\ x=1}}^N \right) w_{zj} 2\tau (R^* B R)
\end{aligned} \tag{4.31}$$

where \sum is the discrete form of integral and w_{xi} and w_{zj} are the weights of the discrete integrals (which will be delivered in Chapter 5). The values of w_{xi} and w_{zj} depend on the numerical method employed. Write (4.31) as

$$\begin{aligned}
0 &= \sum_{\substack{i=0 \\ z=-1}}^N w_{xi} [(-|\nabla \eta| - 2w_{y0} \tau b_1) R_1^* R_1 + (|\nabla \eta| - 2w_{y0} \tau b_2) R_2^* R_2] \\
&\quad + \sum_{\substack{i=0 \\ z=1}}^N w_{xi} [(-|\nabla \eta| - 2w_{yN} \tau b_1) R_1^* R_1 + (|\nabla \eta| - 2w_{yN} \tau b_2) R_2^* R_2] \\
&\quad + \sum_{\substack{j=0 \\ x=-1}}^N w_{yj} [(-|\nabla \xi| - 2w_{x0} \tau b_1) R_1^* R_1 + (|\nabla \xi| - 2w_{x0} \tau b_2) R_2^* R_2] \\
&\quad + \sum_{\substack{j=0 \\ x=1}}^N w_{yj} [(-|\nabla \xi| - 2w_{xN} \tau b_1) R_1^* R_1 + (|\nabla \xi| - 2w_{xN} \tau b_2) R_2^* R_2].
\end{aligned} \tag{4.32}$$

In order to make the right of (4.32) to be zero, we define

$$\tau = \begin{cases} \frac{1}{2w_{z0}} |\nabla \eta|, & \text{when } z = -1 \\ \frac{1}{2w_{zN}} |\nabla \eta|, & \text{when } z = 1 \\ \frac{1}{2w_{x0}} |\nabla \xi|, & \text{when } x = -1 \\ \frac{1}{2w_{xN}} |\nabla \xi|, & \text{when } x = 1 \end{cases} \tag{4.33}$$

and

$$\left(b_1 = -1, \quad b_2 = 1 \right). \tag{4.34}$$

Substituting the values in (4.34) into (4.28), the matrix B is determined.

4.6 The Final Form of The Three-Equation Version

Now we substitute all variables obtained to form a standard eigenvalue problem.

We start with the dielectric boundary condition. First, substituting the matrices M , A_x , A_z , S , and B into (4.27), and replacing $(R - R_{BC})$ with (4.23), we can obtain the following three equations

$$ik_0 E_x^I = \frac{-1}{\epsilon_{rI}} \frac{\partial H_y^I}{\partial z} + \delta^I(x_i, z_j) \frac{\tau^I}{\epsilon_{rI}} [n_z (H_y^I - H_y^{II})] \quad (4.35a)$$

$$ik_0 E_z^I = \frac{1}{\epsilon_{rI}} \frac{\partial H_y^I}{\partial x} - \delta^I(x_i, z_j) \frac{\tau^I}{\epsilon_{rI}} [n_x (H_y^I - H_y^{II})] \quad (4.35b)$$

$$ik_0 H_y^I = \frac{\partial E_z^I}{\partial x} - \frac{\partial E_x^I}{\partial z} + \delta^I(x_i, z_j) \tau^I [n_z (E_x^I - E_x^{II}) - n_x (E_z^I - E_z^{II})]. \quad (4.35c)$$

We can do the same procedure for the periodic boundary condition and obtain

$$ik_0 E_x^I = \frac{-1}{\epsilon_{rI}} \frac{\partial H_y^I}{\partial z} + \delta^I(x_i, z_j) \frac{\tau^I}{\epsilon_{rI}} [n_z (H_y^I - e^{-j(n_x k_x + n_z k_z)a} H_y^{II})] \quad (4.36a)$$

$$ik_0 E_z^I = \frac{1}{\epsilon_{rI}} \frac{\partial H_y^I}{\partial x} - \delta^I(x_i, z_j) \frac{\tau^I}{\epsilon_{rI}} [n_x (H_y^I - e^{-j(n_x k_x + n_z k_z)a} H_y^{II})] \quad (4.36b)$$

$$ik_0 H_y^I = \frac{\partial E_z^I}{\partial x} - \frac{\partial E_x^I}{\partial z} + \delta^I(x_i, z_j) \tau^I [(n_z E_x^I - n_x E_z^I) - e^{-j(n_x k_x + n_z k_z)a} (n_z E_x^{II} - n_x E_z^{II})]. \quad (4.36c)$$

Similarly, for TM mode we can derive for the dielectric boundary condition:

$$ik_0 H_x^I = -\frac{\partial E_y^I}{\partial z} + \delta^I(x_i, z_j) \tau^I [n_z (E_y^I - E_y^{II})]$$

$$ik_0 H_z^I = \frac{\partial E_y^I}{\partial x} - \delta^I(x_i, z_j) \tau^I [n_x (E_y^I - E_y^{II})]$$

$$ik_0 E_y^I = \frac{1}{\epsilon_{rI}} \frac{\partial H_x^I}{\partial z} - \frac{1}{\epsilon_{rI}} \frac{\partial H_z^I}{\partial x} + \delta^I(x_i, z_j) \frac{\tau^I}{\epsilon_{rI}} [n_z (H_x^I - H_x^{II}) - n_x (H_z^I - H_z^{II})]$$

and for the periodic boundary condition:

$$\begin{aligned}
ik_0 H_x^I &= -\frac{\partial E_y^I}{\partial z} + \delta^I(x_i, z_j) \tau^I [n_z (E_y^I - e^{-j(n_x k_x + n_z k_z)a} E_y^{II})] \\
ik_0 H_z^I &= \frac{\partial E_y^I}{\partial x} - \delta^I(x_i, z_j) \tau^I [n_x (E_y^I - e^{-j(n_x k_x + n_z k_z)a} E_y^{II})] \\
ik_0 E_y^I &= \frac{1}{\epsilon_{rI}} \frac{\partial H_z^I}{\partial x} - \frac{1}{\epsilon_{rI}} \frac{\partial H_x^I}{\partial z} \\
&\quad + \delta^I(x_i, z_j) \frac{\tau^I}{\epsilon_{rI}} [(n_z H_x^I - n_x H_z^I) - e^{-j(n_x k_x + n_z k_z)a} (n_z H_x^{II} - n_x H_z^{II})].
\end{aligned}$$

4.7 The Final Form of the One-Equation Version

We have demonstrated the formulations for the PC problem in the previous section. In fact, we can decrease the number of equations from three to one. First, we start from (4.35) by writing it in the continuous form

$$ik_0 E_x^I(x, z) = \frac{-1}{\epsilon_{rI}} \frac{\partial}{\partial z} H_y^I(x, z) + \delta^I(x, z) \frac{\tau^I}{\epsilon_{rI}} [n_z (H_y^I - H_y^{II})] \quad (4.39a)$$

$$ik_0 E_z^I(x, z) = \frac{1}{\epsilon_{rI}} \frac{\partial}{\partial x} H_y^I(x, z) - \delta^I(x, z) \frac{\tau^I}{\epsilon_{rI}} [n_x (H_y^I - H_y^{II})] \quad (4.39b)$$

$$\begin{aligned}
ik_0 H_y^I(x, z) &= \frac{\partial}{\partial x} E_z^I(x, z) - \frac{\partial}{\partial z} E_x^I(x, z) \\
&\quad + \delta^I(x, z) \tau^I [n_z (E_x^I - E_x^{II}) - n_x (E_z^I - E_z^{II})]
\end{aligned} \quad (4.39c)$$

where $\delta(x, z)$ is defined as

$$\delta(x, z) = l_0(x) + l_N(x) + l_0(z) + l_N(z).$$

We multiply (4.39c) with ik_0 and replace $ik_0 E_x(x, z)$ and $ik_0 E_z(x, z)$ with (4.39a) and (4.39b), respectively, to obtain

$$\begin{aligned}
-k_0^2 H_y^I(x, z) &= \frac{1}{\epsilon_{rI}} \frac{\partial^2}{\partial x^2} H_y^I(x, z) + \frac{1}{\epsilon_{rI}} \frac{\partial^2}{\partial z^2} H_y^I(x, z) \\
&\quad - \left(n_x \frac{\partial}{\partial x} + n_z \frac{\partial}{\partial z} \right) \delta^I(x, z) \frac{\tau^I}{\epsilon_{rI}} [H_y^I - H_y^{II}] \\
&\quad - \delta^I(x, z) \tau^I \left[\left(n_x \frac{\partial}{\partial x} + n_z \frac{\partial}{\partial z} \right) \left(\frac{H_y^I}{\epsilon_{rI}} - \frac{H_y^{II}}{\epsilon_{rII}} \right) \right. \\
&\quad \quad \left. - \left(\frac{\delta^I(x, y) \tau^I}{\epsilon_{rI}} - \frac{\delta^{II}(x, y) \tau^{II}}{\epsilon_{rII}} \right) (H_y^I - H_y^{II}) \right].
\end{aligned} \quad (4.40)$$

Finally, we rewrite (4.40) in simplified form

$$\begin{aligned}
-k_0^2 H_y^I &= \frac{1}{\epsilon_{rI}} \nabla^2 H_y^I - (\vec{n} \cdot \nabla \delta^I) \frac{\tau^I}{\epsilon_{rI}} [H_y^I - H_y^{II}] \\
&\quad - \delta^I \tau^I \left[\vec{n} \cdot \nabla \left(\frac{H_y^I}{\epsilon_{rI}} - \frac{H_y^{II}}{\epsilon_{rII}} \right) - \left(\frac{\delta^I \tau^I}{\epsilon_{rI}} - \frac{\delta^{II} \tau^{II}}{\epsilon_{rII}} \right) (H_y^I - H_y^{II}) \right].
\end{aligned} \tag{4.41}$$

For the periodic boundary condition, we can get

$$\begin{aligned}
-k_0^2 H_y^I &= \frac{1}{\epsilon_{rI}} \nabla^2 H_y^I - (\vec{n} \cdot \nabla \delta^I) \frac{\tau^I}{\epsilon_{rI}} [H_y^I - AH_y^{II}] \\
&\quad - \delta^I \tau^I \left[\vec{n} \cdot \nabla \left(\frac{H_y^I}{\epsilon_{rI}} - A \frac{H_y^{II}}{\epsilon_{rII}} \right) - \left(\frac{\delta^I \tau^I}{\epsilon_{rI}} - \frac{\delta^{II} \tau^{II}}{\epsilon_{rII}} \right) (H_y^I - AH_y^{II}) \right]
\end{aligned} \tag{4.42}$$

where $A = e^{-j(n_x k_x + n_z k_z)a}$.

The above is for TE mode. For the TM mode, we can derive

$$\begin{aligned}
-k_0^2 E_y^I &= \frac{1}{\epsilon_{rI}} \nabla^2 E_y^I - (\vec{n} \cdot \nabla \delta^I) \frac{\tau^I}{\epsilon_{rI}} [E_y^I - E_y^{II}] \\
&\quad - \delta^I \frac{\tau^I}{\epsilon_{rI}} \left[\vec{n} \cdot \nabla (E_y^I - E_y^{II}) - (\delta^I \tau^I - \delta^{II} \tau^{II}) (E_y^I - E_y^{II}) \right]
\end{aligned} \tag{4.43}$$

for the dielectric boundary condition and

$$\begin{aligned}
-k_0^2 E_y^I &= \frac{1}{\epsilon_{rI}} \nabla^2 E_y^I - (\vec{n} \cdot \nabla \delta^I) \frac{\tau^I}{\epsilon_{rI}} [E_y^I - AE_y^{II}] \\
&\quad - \delta^I \frac{\tau^I}{\epsilon_{rI}} \left[\vec{n} \cdot \nabla (E_y^I - AE_y^{II}) - (\delta^I \tau^I - \delta^{II} \tau^{II}) (E_y^I - AE_y^{II}) \right]
\end{aligned} \tag{4.44}$$

for the periodic boundary condition.

Chapter 5

Pseudospectral Method and Shifted Inverse Power Method

This chapter is devoted to the introduction to the numerical methods we use for numerical analysis, including the pseudospectral method and the shifted inverse power method (SIPM).

5.1 The Pseudospectral Method

The spectral method [*Hendiksen et al.*, 2007] is known as high-efficiency and high-accuracy method in numerical computation. The basic idea of the spectral method is to use a set of interpolation polynomials to approximate a function of interest. There are two types of spectral method: Galerkin methods and collocation methods (which we call pseudospectral methods). We usually use pseudospectral methods since it is simpler than the other.

For interpolation polynomials, there are mainly three kinds of polynomials used in this method: Fourier, Legendre, and Chebyshev polynomials. The collocation points are different in each polynomial method. We will only describe the Legendre collocation method in detail since we only use this polynomial in our research.

5.1.1 Overview of the Pseudospectral Method

Assume we want to solve the equation:

$$Lu(x) = f(x) \tag{5.1}$$

where L is a differential operator, $u(x)$ is the solution to the differential equation, and $f(x)$ is a known function. Since $u(x)$ is an unknown function, one of possible ways to solve it is to use a set of functions, called basis functions, to approximate $u(x)$. In other words, we can let

$$u(x) \approx u_N(x) = \sum_{k=0}^N u_k \phi_k(x). \quad (5.2)$$

where $\phi_k(x)$'s are the basis functions and u_k 's are complex numbers. By substituting (5.2) into (5.1), we can define a residual function as

$$R_N(x) = Lu_N(x) - f(x). \quad (5.3)$$

Now the question becomes: how to minimize the residual function.

For the pseudospectral method, we let the residual function to be zero at the $N + 1$ collocation points $x_i, i = 0, 1, \dots, N$, so that

$$Lu_N(x_i) = f(x_i), \quad i = 0, 1, \dots, N. \quad (5.4)$$

Therefore,

$$\sum_{k=0}^N u_k L\phi_k(x_i) = f(x_i), \quad i = 0, 1, \dots, N \quad (5.5)$$

which is an algebraic system with $N + 1$ coefficients, $u_k, k = 0, 1, \dots, N$, to be determined. In other words, we transform the differential equation problem into an algebraic equation problem. The collocation points and differential operators will be delivered in the next subsection for Legendre functions.

5.1.2 The Pseudospectral Legendre Method

The Legendre polynomial of order N , $P_N(x)$, is defined as

$$P_N(x) = \frac{1}{2^N N!} \frac{d^N (x^2 - 1)^N}{dx^N}, \quad |x| \leq 1. \quad (5.6)$$

We consider the collocation method that is the same as described by *Hesthaven and Gottlieb*, [1996] with the collocation points given as the Legendre-Gauss-Lobatto

points, defined as the roots of the polynomial $(1 - x^2)P'_N(x)$. There exists no analytical formula for these roots.

The choice of Gauss-Lobatto points is for the purpose of using the Gauss-Lobatto quadrature formula which means that if $f(x)$ is a polynomial of degree $2N - 1$, then

$$\sum_{i=0}^N f(x_i)w_i = \int_{-1}^1 f(\xi)d\xi \quad (5.7)$$

where x_i 's are the Legendre-Gauss-Lobatto collocation points, and the Gauss-Lobatto weights, w_i , are given as

$$w_i = -\frac{2}{N+1} \frac{1}{P_N(x_i)P'_{N-1}(x_i)}, \quad 1 \leq i \leq N-1 \quad (5.8a)$$

$$w_0 = w_N = \frac{2}{N(N+1)}. \quad (5.8b)$$

In the pseudospectral Legendre method or the Legendre collocation method, the function $f(x)$ is approximated by Legendre-Lagrange interpolating polynomials. Thus, we can construct an N th order global Legendre interpolant, L_N , to obtain an approximation to the function as

$$(L_N f)(x) = \sum_{i=0}^N f(x_i)g_i(x) \quad (5.9)$$

where the interpolating Legendre-Lagrange polynomial $g_i(x)$ is given as

$$g_i(x) = -\frac{(1-x^2)P'_N(x)}{N(N+1)(x-x_i)P_N(x_i)} \quad (5.10)$$

Note that by this construction,

$$(L_N f)(x_i) = f(x_i). \quad (5.11)$$

The spatial derivatives of $(L_N f)(x_i)$ can be achieved by a matrix operator, with the matrix entries given as

$$D_{ij} = g'_j(x_i) = \begin{cases} -\frac{N(N+1)}{4}, & i = j = 0 \\ \frac{P_N(x_i)}{P_N(x_j)} \frac{1}{x_i - x_j}, & i \neq j \\ \frac{N(N+1)}{4}, & i = j = N \\ 0, & i = j \in [1, N-1] \end{cases} \quad (5.12)$$

such that the derivative of $f(x)$ at a collocation point, x_i , is approximated as

$$\frac{df(x_i)}{dx} \approx \frac{d(L_N f)(x_i)}{dx} = \sum_{j=0}^N D_{ij} f(x_j). \quad (5.13)$$

We can use (5.13) for 1D waveguide problems, but for 2D waveguide and PC problems we must introduce transfinite elements.

5.1.3 Curvilinear Representation of The Pseudospectral Method

Consider a 2D setting and define the approximation to $f(x, y)$ as

$$f(x, y) \approx \sum_{i=0}^N \sum_{j=0}^N f(x_i, y_j) g_i(x) g_j(y) \quad (5.14)$$

where the Legendre-Gauss-Lobatto grid y_i has been introduced. The approach has the benefit that the derivatives can be calculated through the 1D formula and thus the differential formula at the 2D collocation points arranged in a rectangular domain can be expressed as in the following matrix multiplication form

$$\frac{\partial \bar{f}_{\text{rect}}}{\partial x} = \bar{\bar{D}}_{(N+1) \times (N+1)} \bar{f}_{\text{rect}} \quad (5.15a)$$

$$\frac{\partial \bar{f}_{\text{rect}}}{\partial y} = \bar{f}_{\text{rect}} \bar{\bar{D}}_{(N+1) \times (N+1)}^T \quad (5.15b)$$

where

$$\bar{\bar{D}}_{(N+1) \times (N+1)} = \begin{bmatrix} D_{00} & D_{01} & \cdots & D_{0N} \\ D_{10} & D_{11} & \cdots & D_{1N} \\ \vdots & \vdots & \cdots & \vdots \\ D_{N0} & D_{N1} & \cdots & D_{NN} \end{bmatrix}. \quad (5.16)$$

The entries of $\bar{\bar{D}}_{(N+1) \times (N+1)}$ have been defined in (5.12). \bar{f}_{rect} is an $(N+1) \times (N+1)$ matrix with entries $f(x_i, y_j)$, $i = 0, 1, 2, \dots, N$, and $j = 0, 1, 2, \dots, N$, corresponding to collocation points in rectangular arrangement. However, the employment of matrix products is still restricted by the nature of rectangular grids. And since we define (5.6) in the range $x \in [-1, 1]$, (5.15) can only be adopted in a unit square $[-1, 1] \times [-1, 1]$ area which restricts our computation. In order to surpass this restriction, we must introduce the transfinite transformation.

By applying the transfinite blending function presented by *Doncker* [2000], each curvilinear quadrilateral in Cartesian (x, y) coordinates can be mapped into a unit square area $[-1, 1] \times [-1, 1]$ in curvilinear (ξ, η) coordinates under the transformation

$$\xi = \xi(x, y), \quad \eta = \eta(x, y). \quad (5.17)$$

And we define four new matrices,

$$\bar{M}_{\xi x} = \begin{bmatrix} \partial\xi(x_0, y_0)/\partial x & \partial\xi(x_0, y_1)/\partial x & \cdots & \partial\xi(x_0, y_N)/\partial x \\ \partial\xi(x_1, y_0)/\partial x & \partial\xi(x_1, y_1)/\partial x & \cdots & \partial\xi(x_1, y_N)/\partial x \\ \vdots & \vdots & \cdots & \vdots \\ \partial\xi(x_N, y_0)/\partial x & \partial\xi(x_N, y_1)/\partial x & \cdots & \partial\xi(x_N, y_N)/\partial x \end{bmatrix} \quad (5.18a)$$

$$\bar{M}_{\eta x} = \begin{bmatrix} \partial\eta(x_0, y_0)/\partial x & \partial\eta(x_0, y_1)/\partial x & \cdots & \partial\eta(x_0, y_N)/\partial x \\ \partial\eta(x_1, y_0)/\partial x & \partial\eta(x_1, y_1)/\partial x & \cdots & \partial\eta(x_1, y_N)/\partial x \\ \vdots & \vdots & \cdots & \vdots \\ \partial\eta(x_N, y_0)/\partial x & \partial\eta(x_N, y_1)/\partial x & \cdots & \partial\eta(x_N, y_N)/\partial x \end{bmatrix} \quad (5.18b)$$

$$\bar{M}_{\xi y} = \begin{bmatrix} \partial\xi(x_0, y_0)/\partial y & \partial\xi(x_0, y_1)/\partial y & \cdots & \partial\xi(x_0, y_N)/\partial y \\ \partial\xi(x_1, y_0)/\partial y & \partial\xi(x_1, y_1)/\partial y & \cdots & \partial\xi(x_1, y_N)/\partial y \\ \vdots & \vdots & \cdots & \vdots \\ \partial\xi(x_N, y_0)/\partial y & \partial\xi(x_N, y_1)/\partial y & \cdots & \partial\xi(x_N, y_N)/\partial y \end{bmatrix} \quad (5.18c)$$

$$\bar{M}_{\eta y} = \begin{bmatrix} \partial\eta(x_0, y_0)/\partial y & \partial\eta(x_0, y_1)/\partial y & \cdots & \partial\eta(x_0, y_N)/\partial y \\ \partial\eta(x_1, y_0)/\partial y & \partial\eta(x_1, y_1)/\partial y & \cdots & \partial\eta(x_1, y_N)/\partial y \\ \vdots & \vdots & \cdots & \vdots \\ \partial\eta(x_N, y_0)/\partial y & \partial\eta(x_N, y_1)/\partial y & \cdots & \partial\eta(x_N, y_N)/\partial y \end{bmatrix}. \quad (5.18d)$$

From the fundamental differential principle, the approximations for the derivatives of $f(x, y)$ in the (ξ, η) coordinates can be written as

$$\frac{\partial \bar{f}_{\text{cur}}}{\partial x} = \bar{M}_{\xi x} \bullet (\bar{D} \bar{f}_{\text{cur}}) + (\bar{f}_{\text{cur}} \bar{D}^T) \bullet \bar{M}_{\eta x} \quad (5.19a)$$

$$\frac{\partial \bar{f}_{\text{cur}}}{\partial y} = \bar{M}_{\xi y} \bullet (\bar{D} \bar{f}_{\text{cur}}) + (\bar{f}_{\text{cur}} \bar{D}^T) \bullet \bar{M}_{\eta y} \quad (5.19b)$$

where " \bullet " symbols Schur product defined as $(A \bullet B)_{ij} = a_{ij}b_{ij}$, and $\bar{\bar{D}}$ equals $\bar{\bar{D}}_{(N+1) \times (N+1)}$ defined in (5.16). Here the matrix $\bar{\bar{f}}_{\text{cur}}$ is in general different from $\bar{\bar{f}}_{\text{rect}}$ in (5.15) in that the latter has been defined on rectangular grids while the former is on deformed locations of grids adapted to the shape of the sub-domain.

Since we want to form a standard eigenvalue problem, the unknown function must be a vector. Unfortunately, $\bar{\bar{f}}_{\text{cur}}$ is an $(N+1) \times (N+1)$ matrix, so we must convert (5.19) into a resolvable form. First, we rearrange the $(N+1) \times (N+1)$ matrix $\bar{\bar{f}}_{\text{cur}}$ into the $[(N+1)(N+1)]$ column vector \tilde{f}_{cur} as below

$$\bar{\bar{f}}_{\text{cur}} = \begin{bmatrix} f_{00} & f_{01} & \cdots & f_{0N} \\ f_{10} & f_{11} & \cdots & f_{1N} \\ \vdots & \vdots & \cdots & \vdots \\ f_{N0} & f_{N1} & \cdots & f_{NN} \end{bmatrix}_{(N+1) \times (N+1)} \Rightarrow \tilde{f}_{\text{cur}} = \begin{bmatrix} f_{00} \\ f_{10} \\ \vdots \\ f_{N0} \\ f_{01} \\ \vdots \\ f_{NN} \end{bmatrix}_{[(N+1)(N+1)] \times 1}.$$

Then, we define $\tilde{M}_{\xi x}$, $\tilde{M}_{\eta x}$, $\tilde{M}_{\xi y}$, and $\tilde{M}_{\eta y}$ as

$$\begin{aligned} \tilde{M}_{\xi x} &= \text{diag} \left(\frac{\partial \xi(x_0, y_0)}{\partial x}, \frac{\partial \xi(x_1, y_0)}{\partial x}, \dots, \frac{\partial \xi(x_N, y_0)}{\partial x}, \frac{\partial \xi(x_0, y_1)}{\partial x}, \dots, \frac{\partial \xi(x_N, y_N)}{\partial x} \right) \\ \tilde{M}_{\eta x} &= \text{diag} \left(\frac{\partial \eta(x_0, y_0)}{\partial x}, \frac{\partial \eta(x_1, y_0)}{\partial x}, \dots, \frac{\partial \eta(x_N, y_0)}{\partial x}, \frac{\partial \eta(x_0, y_1)}{\partial x}, \dots, \frac{\partial \eta(x_N, y_N)}{\partial x} \right) \\ \tilde{M}_{\xi y} &= \text{diag} \left(\frac{\partial \xi(x_0, y_0)}{\partial y}, \frac{\partial \xi(x_1, y_0)}{\partial y}, \dots, \frac{\partial \xi(x_N, y_0)}{\partial y}, \frac{\partial \xi(x_0, y_1)}{\partial y}, \dots, \frac{\partial \xi(x_N, y_N)}{\partial y} \right) \\ \tilde{M}_{\eta y} &= \text{diag} \left(\frac{\partial \eta(x_0, y_0)}{\partial y}, \frac{\partial \eta(x_1, y_0)}{\partial y}, \dots, \frac{\partial \eta(x_N, y_0)}{\partial y}, \frac{\partial \eta(x_0, y_1)}{\partial y}, \dots, \frac{\partial \eta(x_N, y_N)}{\partial y} \right) \end{aligned}$$

where $\text{diag}(a, b, \dots)$ represents a diagonal matrix which has a, b, \dots as the diagonal elements of the matrix and zero otherwise. Next, we rewrite (5.19) with slight modification

$$\frac{\partial \tilde{f}_{\text{cur}}}{\partial x} = \tilde{D}_x \tilde{f}_{\text{cur}} \quad (5.20a)$$

$$\frac{\partial \tilde{f}_{\text{cur}}}{\partial y} = \tilde{D}_y \tilde{f}_{\text{cur}}. \quad (5.20b)$$

In (5.20), the definitions of \tilde{D}_x and \tilde{D}_y are

$$\tilde{D}_x = \tilde{M}_{\xi x} [I_{(N+1) \times (N+1)} \otimes \bar{\bar{D}}] + \tilde{M}_{\eta x} [\bar{\bar{D}} \otimes I_{(N+1) \times (N+1)}] \quad (5.21a)$$

$$\tilde{D}_y = \tilde{M}_{\xi y} [I_{(N+1) \times (N+1)} \otimes \bar{\bar{D}}] + \tilde{M}_{\eta y} [\bar{\bar{D}} \otimes I_{(N+1) \times (N+1)}] \quad (5.21b)$$

where $I_{(N+1) \times (N+1)}$ represents an identity matrix with dimension $(N+1) \times (N+1)$ and \otimes symbols Kronecker product defined as

$$\bar{\bar{A}} \otimes \bar{\bar{B}} = \begin{bmatrix} a_{00}\bar{\bar{B}} & a_{01}\bar{\bar{B}} & \cdots & a_{0N}\bar{\bar{B}} \\ a_{10}\bar{\bar{B}} & a_{11}\bar{\bar{B}} & \cdots & a_{1N}\bar{\bar{B}} \\ \vdots & \vdots & \cdots & \vdots \\ a_{N0}\bar{\bar{B}} & a_{N1}\bar{\bar{B}} & \cdots & a_{NN}\bar{\bar{B}} \end{bmatrix}. \quad (5.22)$$

And we can use (5.20) to construct the matrix we need for 2D waveguide and PC problems.

5.2 The Shifted Inverse Power Method

The shifted inverse power method (SIPM) is a numerical method to solve the eigenvalue problem. It is widely used because of its fast convergent property. We have developed some techniques to improve its practicability.

5.2.1 The Algorithm of SIPM

Consider an eigenvalue problem:

$$Ax = \mu x \quad (5.23)$$

where A is a known square matrix, x is an eigenvector, and μ is the corresponding eigenvalue. We can use the SPIM to find x and μ . The algorithm of the SIPM is

given below:

$$\text{choose } \mu^*, x^{(0)} \quad (5.24)$$

for $n = 1$ to max_it

$$(A - \mu^* I)x^{(n+1)} = x^{(n)} \quad (5.25)$$

$$\mu^{(n)} = \frac{\theta(x^{(n)})}{\theta(x^{(n+1)})} + \mu^*$$

$$x^{(n+1)} = \frac{x^{(n+1)}}{|x^{(n+1)}|}$$

where max_it represents the maximum iteration time, I is an identity matrix whose dimension is the same as A , and $\theta(x)$ is an arbitrary linear function which follows the rule: $\theta(\alpha x + \beta y) = \alpha\theta(x) + \beta\theta(y)$. Please note that (5.25) is to solve a linear system. Usually we use the LU decomposition method to solve this linear system. But since the matrix A we deal with is always a sparse matrix, it is not so appropriate to use LU decomposition because it will consume enormous memory space. Instead of using the LU method, we choose to use iterative methods to solve the linear system with the benefit that they allow us to allocate only the entries which are nonzero.

5.2.2 The Iterative Method

The iterative method includes a wide range of techniques that use successive approximations to solve a linear system. They can be classified as:

- Stationary iterative methods
 - The Jacobi method
 - The Gauss-Seidel method
 - The symmetric successive overrelaxation method
- Nonstationary iterative methods
 - Conjugate gradient method (CG)
 - MINRES and SYMMLQ

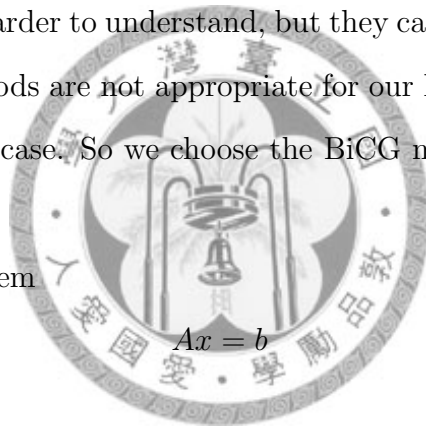
- CG on the normal equations, CGNE and CGNR
- Generalized minimal residual (GMRES)
- BiConjugate gradient (BiCG)
- Quasi-minimal residual (QMR)
- Conjugate gradient squared method (CGS)
- BiConjugate gradient stabilized (Bi-CGSTAB)
- Chebyshev iteration.

Stationary methods are older, simpler to understand and implement, but usually not as effective. Nonstationary methods appeared from relatively recent development; their analysis is usually harder to understand, but they can be highly effective. From our test, stationary methods are not appropriate for our linear system because they do not converge in every case. So we choose the BiCG method as our linear solver algorithm.

Consider a linear system

$$Ax = b$$

(5.26)



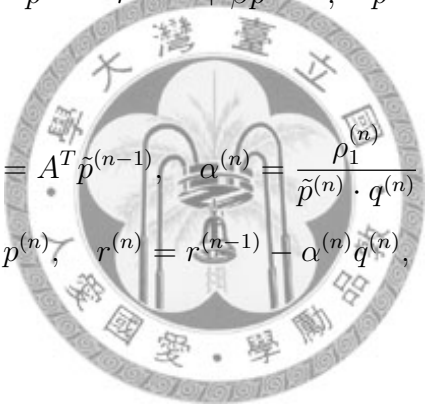
where A is a known square matrix, x is an unknown vector, and μ is a known vector.

We can use the BiCG to find x . The algorithm of BiCG is as follows.

```

choose  $x^{(0)}$ 
 $r^{(0)} = b - Ax^{(0)}$ ,  $\tilde{r}^{(0)} = r^{(0)}$ 
for  $n = 1$  to max_it
 $\rho_1^{(n)} = r^{(n-1)} \cdot \tilde{r}^{(n-1)}$ 
if  $i = 1$  then
 $p^{(1)} = r^{(0)}$ ,  $\tilde{p}^{(1)} = \tilde{r}^{(0)}$ 
else
 $\beta^{(n)} = \frac{\rho_1^{(n)}}{\rho_2^{(n-1)}}$ ,  $p^{(n)} = r^{(n-1)} + \beta p^{(n-1)}$ ,  $\tilde{p}^{(n)} = \tilde{r}^{(n-1)} + \beta \tilde{p}^{(n-1)}$ 
endif
 $q^{(n)} = Ap^{(n)}$ ,  $\tilde{q}^{(n)} = A^T \tilde{p}^{(n-1)}$ ,  $\alpha^{(n)} = \frac{\rho_1^{(n)}}{\tilde{p}^{(n)} \cdot q^{(n)}}$ 
 $x^{(n)} = x^{(n-1)} + \alpha^{(n)} p^{(n)}$ ,  $r^{(n)} = r^{(n-1)} - \alpha^{(n)} q^{(n)}$ ,  $\tilde{r}^{(n)} = \tilde{r}^{(n-1)} - \alpha^{(n)} \tilde{q}^{(n)}$ 
 $\rho_2^{(n)} = \rho_1^{(n)}$ 
end

```



By using the BiCG method, we do not need large memory space to do the calculation.

In fact, all analysis cases in this thesis can be run under a normal personal computer with 4GB memory.

5.2.3 Guessing the Initial Eigenvector Using Former Data

This technique is to modify step (5.24). Step (5.24) requires us to guess the initial eigenvector. For higher-degree of polynomials, the initial eigenvector can be obtained from interpolating the eigenvector at lower degree.

For example, if we want to solve the 2D waveguide problem at the polynomial degree of seven, we can solve the same problem at the polynomial degree of three

first. Then we use the eigenvector computed at degree three to interpolate the initial eigenvector for degree seven. The whole process is shown in Fig. 5.1. Using this technique can speed up the SIPM algorithm since the initial eigenvector is quite accurate.



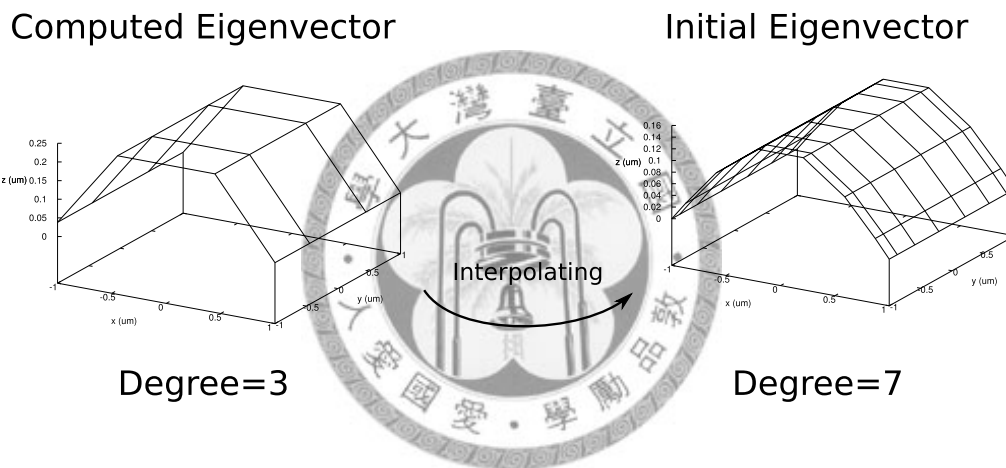


Figure 5.1: Using former data to interpolate initial eigenvector

Chapter 6

Numerical Results For Waveguide Problems

In this chapter, we will analyse several 1D and 2D waveguide structures including slab waveguides, partially filled waveguides, circular waveguides, fiber waveguides, channel waveguides, and rib waveguides using the formulations discussed in previous chapters.

6.1 Symmetric Slab Waveguides

First, we examine the simple symmetric "weakly" guiding slab waveguide. The structure considered is the same as the one considered by *Hadley* [1998], as shown in Fig. 6.1. We take the wavelength to be $1 \mu\text{m}$ and the waveguide width of waveguide is $W=2 \mu\text{m}$. The refractive index for the core area is $n_{core} = \sqrt{11.088}$ and the refractive index for the cladding area is $n_{clad} = \sqrt{11.044}$. The PEC boundary condition is put at the $\pm 15 \mu\text{m}$ positions and the whole structure is divided into five sub-domains. For this structure, the exact effective indices are $n_{eff,exact} = 3.3270509487737$ and 3.3270445145126 for the TE and TM modes, respectively. The effective index is defined as

$$n_{eff} = \frac{\beta}{k_0} \quad (6.1)$$

where β is propagation constant and k_0 is wavenumber in free space.

Because the field profiles of this symmetric structure for TE and TM modes are

almost the same, we just show the field profile of TE mode in Fig. 6.2. Figure 6.3 shows the relative errors in the calculated effective index with respect to the degree of polynomial in each of the five sub-domains. The relative error is defined as

$$R.E. = \frac{n_{eff} - n_{eff,exact}}{n_{eff,exact}}. \quad (6.2)$$

Here $n_{eff,exact}$ represents the calculated effective index. From Fig. 6.3, we can see that both convergence lines for TE and TM modes show spectral convergence characteristics. They reach the orders of 10^{-14} and 10^{-13} , respectively.

6.2 Asymmetric Slab Waveguides

The second case we examine is the asymmetric "strongly" guiding slab waveguide. We take the wavelength to be $1.55 \mu\text{m}$ and the waveguide width $W = 0.75 \mu\text{m}$. The refractive index for the core area is $n_{core} = 3.3704$ and the refractive indices for the cladding areas are $n_{clad1} = 3.17$ and $n_{clad2} = 1.0$. The PEC boundary condition is put at the $-5 \mu\text{m}$ and $2 \mu\text{m}$ positions and the whole structure is divided into five sub-domains. The exact effective indices are $n_{eff,exact} = 3.290296220624705$ and 3.27555088010413 for the TE and TM modes, respectively [Hadley, 1998].

Figures 6.4 and 6.5 illustrate the field profiles for the TE and TM modes. Figure 6.6 shows the relative errors in the effective index for the two modes with respect to the degree of polynomial. It can be seen that because there is an interface with high contrast in the refractive index, we need higher degrees of polynomial (degree = 19 ~ 23) to get the same precision as in the symmetric slab waveguide case ($10^{-13} \sim 10^{-14}$).

6.3 Partially Filled Metallic Waveguides

From now on, we discuss 2D waveguide structures. We first consider a half-filled metallic waveguide structure. Figure 6.7 shows the cross-section of this waveguide. The cross-section is divided into two domains and the width of the waveguide is

twice of the height. For this kind of waveguide, the modes can be classified into longitudinal-section electric (LSE) and longitudinal-section magnetic modes (LSM). The exact value of the effective index can be obtained by solving transcendental equations [Collin, 1960]. Figure 6.8 shows the mesh division. The refractive indices for the dielectric and air regions are $n_1 = 1.5$ and $n_2 = 1.0$, respectively. And we have the PEC boundary condition at all four edges.

The exact value of the effective index is $n_{eff,exact} = 1.27575556678727$ when the wavelength is chosen to be $2\pi \mu\text{m}$. Figure 6.9 shows the relative errors of the calculated effective index for the LSE₁₀ mode obtained using the six-equation and three-equation formulations, respectively. These two convergence lines are quite close to each other in Fig. 6.9 and they are both on the order of $10^{-14} \sim 10^{-15}$ with the ninth degree polynomial in each domain.

6.4 Circular Metallic Waveguides

In order to check if the PEC boundary condition can work on curvilinear boundary, we choose the circular metallic waveguide to do the test. Figure 6.10 shows a quarter of the cross-section of this waveguide. Due to the geometrical symmetry, we only need to consider a quarter of the waveguide cross-section. The radius of this waveguide is $R = 0.5 \mu\text{m}$. Figure 6.11 shows the mesh division. The whole structure is divided into three domains. Two of the three domains are transformed using the curvilinear mapping to match the circular boundary. We put the PEC boundary condition at the circular edge, and the PEC and PMC boundary conditions at the other two edges, respectively.

The exact value of the effective index for the fundamental TE₁₁ mode is $n_{eff,exact} = 0.956102174410419337$ at the wavelength of $0.2 \mu\text{m}$. Figure 6.12 shows the relative errors of the effective index for this fundamental mode with respect to the degree of polynomial for both six-equation and three-equation formulations. It can be seen that both formulations can achieve numerical accuracy on the order of $10^{-13} \sim 10^{-14}$

when we use polynomials of degree=11 ~ 13 in each sub-domain. Notice that the three-equation formulation does not converge when we adopt higher order degrees of polynomial, and we can see this property in other cases. The distributions for all the six field components for this mode are shown in Fig. 6.13.

6.5 Fiber Waveguides

The fiber waveguide is a circular dielectric waveguide which is known to be more complicated than the circular metallic waveguide discussed in the previous subsection in the mode analysis. Figure 6.14 shows a quarter of the cross-section of the fiber waveguide. Just as in the previous case, we only need to consider a quarter of the waveguide cross-section because of geometrical symmetry. The core radius is $R = 0.6 \mu\text{m}$ and the fiber is with high refractive-index difference, namely, the refractive index of the core is $n_{core} = \sqrt{8}$ and that of the surrounding cladding is $n_{space} = 1$. The mesh division for the Legendre method is shown in Fig. 6.15 where five sub-domains are adopted. The radius of the computational window is taken to be $R_{BC} = 2.5 \mu\text{m}$. Note that we must put the boundary of the computational window far enough to avoid significant perturbation of the circular PEC boundary on the calculated mode fields.

The exact effective index for fundamental HE_{11} mode of the fiber waveguide is $n_{eff,exact} = 2.68401932160108$ at the wavelength of $1.5 \mu\text{m}$. Figure 6.16 shows the relative error in the effective index with respect to the degree of polynomial for both six-equation and three-equation formulations. It shows that both formulations can achieve high accuracy with the relative error on the order of 10^{-10} when the degree of 23 is used in each sub-domain. The accuracy of the six-equation formulation can be better than the other of 10^{-11} using the degree of 27. It is again observed that when using higher degrees, the convergence of the three-equation formulation shows some unstable property as in circular metallic waveguide case. Therefore, we can say that the six-equation formulation has better convergent property than the

three-equation one. Figure 6.17 shows distributions of all the six field components for this mode, from which, we can see that the fields are well confined in the core region with negligible field near the circular boundary, and the PEC boundary of the computational window is appropriately located.

6.6 Channel Waveguides with Sharp Corners

The channel waveguides with sharp dielectric corners is a simple structure. Here we consider a square channel waveguide. Figure 6.19 shows a quarter of its cross-section as the computational domain with the considered boundary conditions. Again, because of the geometrical symmetry, we only need to consider a quarter of the whole structure. Although the geometry is simple, there exists no analytical exact mode solutions and exact effective index values are not available. The width of corner waveguide is assumed to be $1\mu\text{m}$. The refractive index of the core is $n_{core} = 1.5$ and that of the surrounding space is $n_{space} = 1$. We put PEC boundary conditions at two edges of the computational domain and the PMC boundary conditions at the other two, as shown in Fig. 6.18. Figure 6.19 shows the mesh division where four domains are adopted.

Although the exact effective index is not available, *Hadley* [2002] has conducted an elaborative numerical analysis by carefully treating the electric field singularity behavior at the sharp corners and provided $n_{eff} = 1.27627404 \pm 10^{-8}$ for the fundamental mode at the wavelength of $1.5\mu\text{m}$. Using *Hadley's* result as a reference, we show in Fig. 6.20 the relative errors of our calculated effective index with respect to the degree of polynomial for both six-equation and three-equation formulations. It is seen that six-equation formulation converges, but the convergent rate of the three-equation formulation appears to be quicker. One thing which is worth being noticed is that we just need $4 \times (7 + 1) \times (7 + 1) = 256$ grid points to reach the 10^{-8} accuracy using the six-equation formulation, compared to $150 \times 150 = 22500$ grid points used by *Hadley* [2002] for reaching the 10^{-7} accuracy. This is quite a

significant advancement in numerical analysis of optical waveguides. We also use the calculated effective index at degree of 45 ($n_{eff} = 1.27627403774$) as the reference and show the corresponding results in Fig. 6.21. From this figure, it is seen that the six-equation formulation can converge faster than the three-equation one at higher degrees. Figures 6.22–6.27 show profiles along $\phi = 45^\circ$ of all the six field components. The figures reveal that even under very low degree of polynomial as degree two, the field profiles have been quite close to those using high degree of polynomial. Finally, we show the distributions of all the six field components in Fig. 6.28 for this channel waveguide. The rapid-varying characteristics of the E_y field component near the corner, due to the field singularity property, as seen in Figs. 6.23 and 6.28, would make the calculated effective index hard to converge to high precision, and we need to use higher degrees of polynomial to better approximate the field profiles.

6.7 Rib Waveguides

We have demonstrated that the new formulations can deal with waveguides with a single corner in the computational domain. We now consider rib waveguides that are multi-corner structure. Figure 6.29 shows a half of the cross-section of the rib waveguide with PECs as the boundaries of the computational domain. This structure can provide x -direction and y -direction confinement by using high refractive-difference in both directions. The refractive indices of the cover, the guiding layer, and the substrate are $n_c = 1$, $n_g = 3.44$, and $n_s = 3.4$. Figure 6.30 shows the mesh division where we divide whole structure into twelve sub-domains.

Again, there exists no exact effective index for the mode on this waveguide, and we use *Hadley's* calculation [*Hadley, 2002*] as the reference value, which for fundamental mode is about $n_{eff} = 3.413132$ when the wavelength is $1.15 \mu\text{m}$. Figure 6.31 shows the relative errors of the effective index with respect to the degree of polynomial for six-equation and three-equation formulations. We can see that the new formulations can easily provide calculated effective indices of accuracy on the

order of 10^{-6} for the multi-corner rib waveguide. Figure 6.32 shows distributions of all the six field components for the fundamental mode of the rib waveguide.



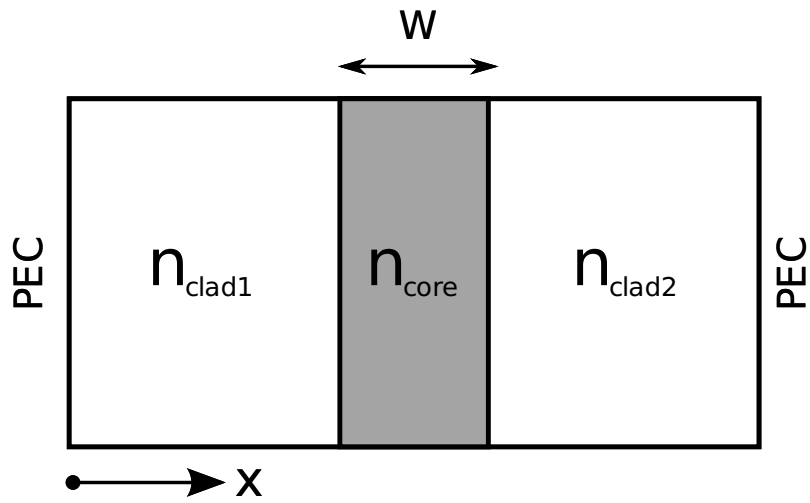


Figure 6.1: Sketch of a slab waveguide.

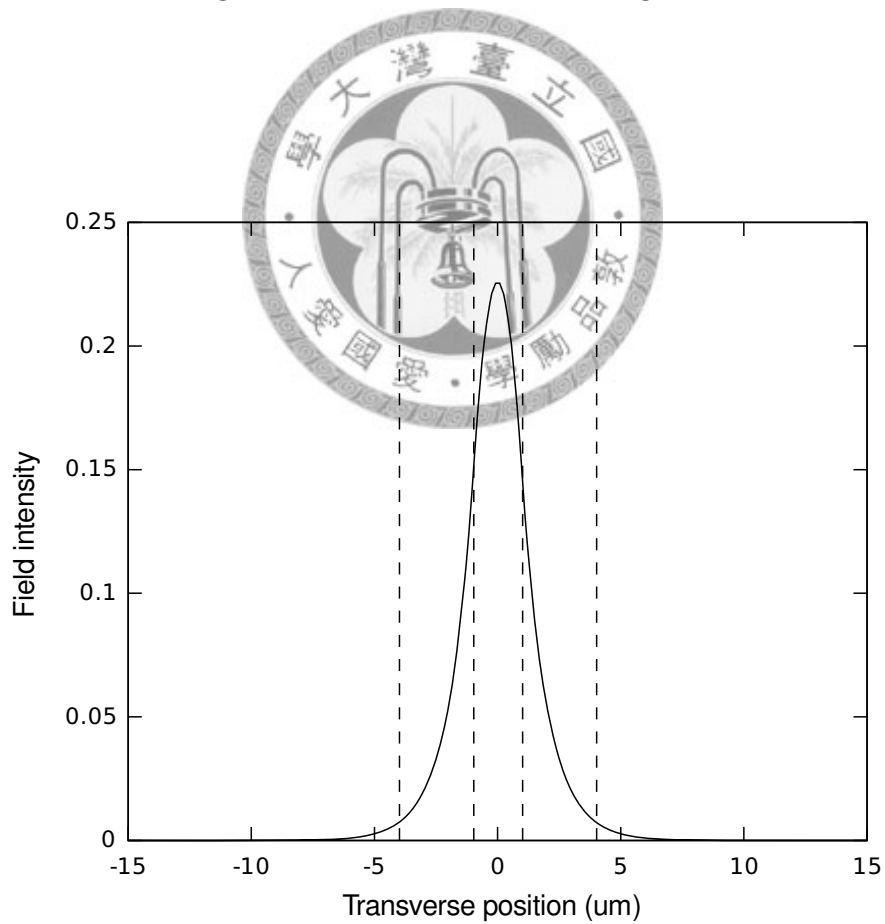


Figure 6.2: Field profile for the TE mode of the symmetric waveguide.

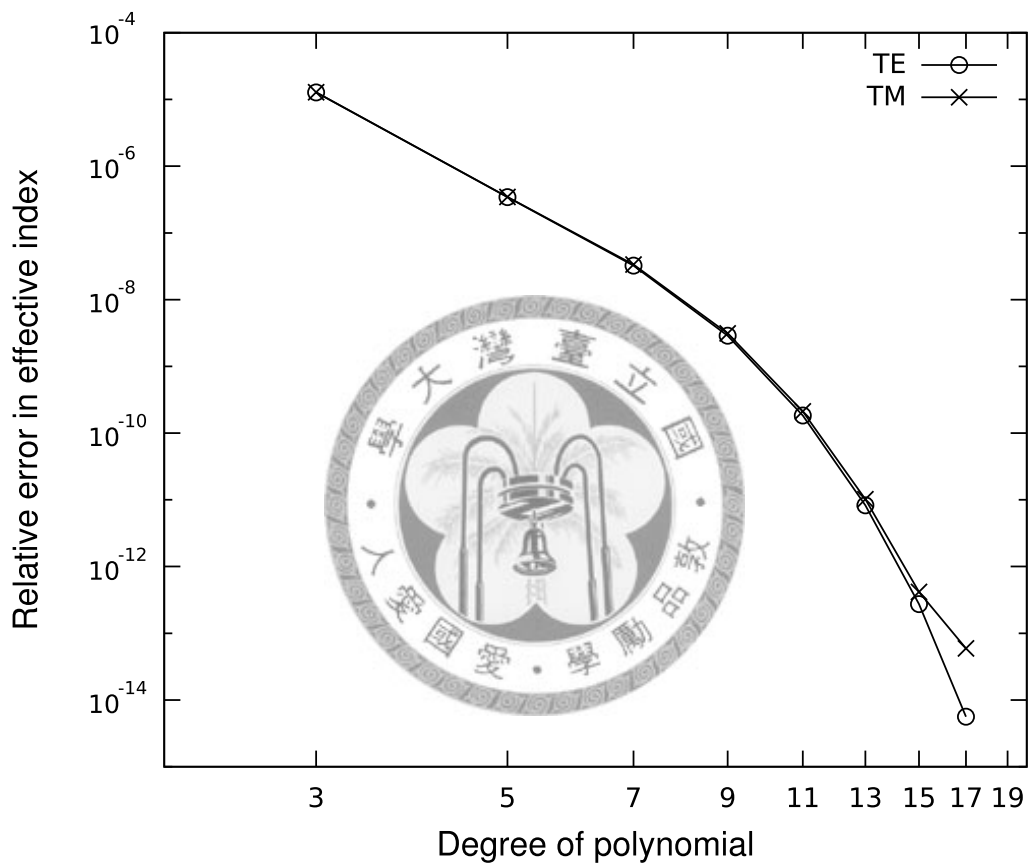


Figure 6.3: Relative errors in the effective index for the TE and TM modes of symmetric slab waveguide with respect to the degree of polynomial in each domain.

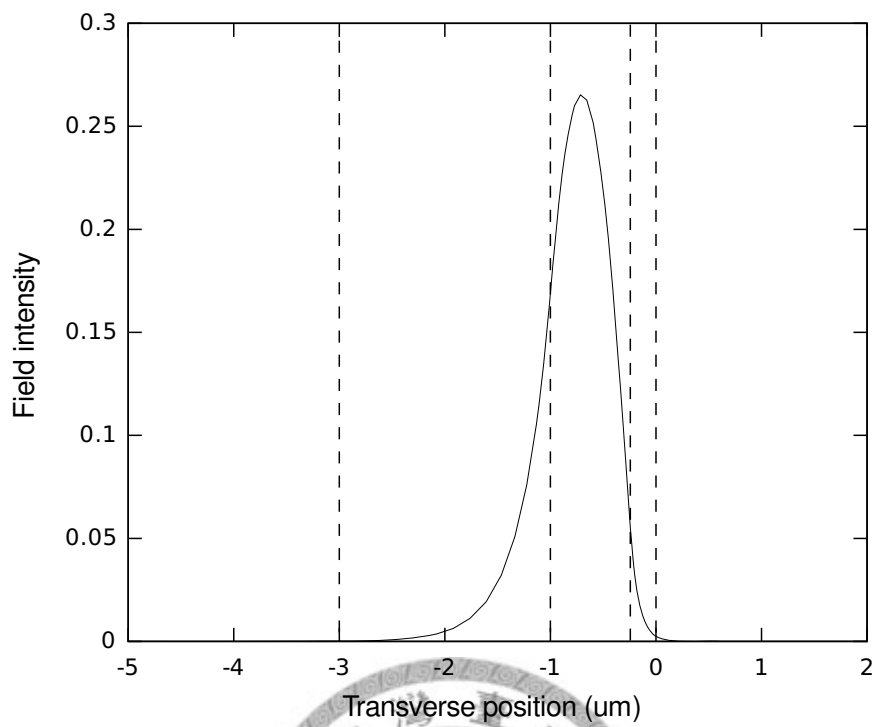


Figure 6.4: Field profile for TE mode of the asymmetric waveguide.

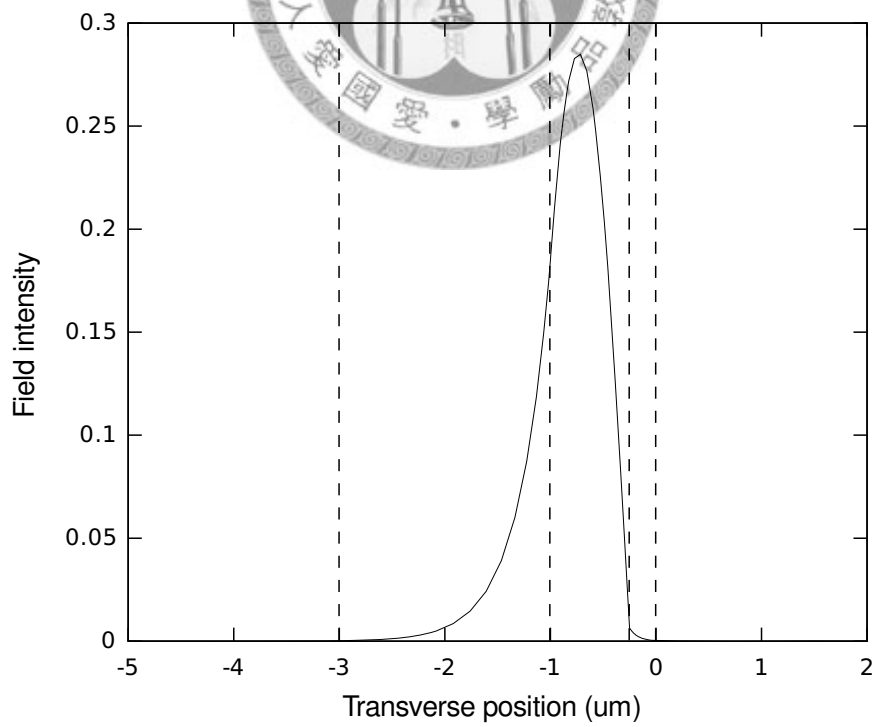


Figure 6.5: Field profile for TM mode of the asymmetric waveguide.

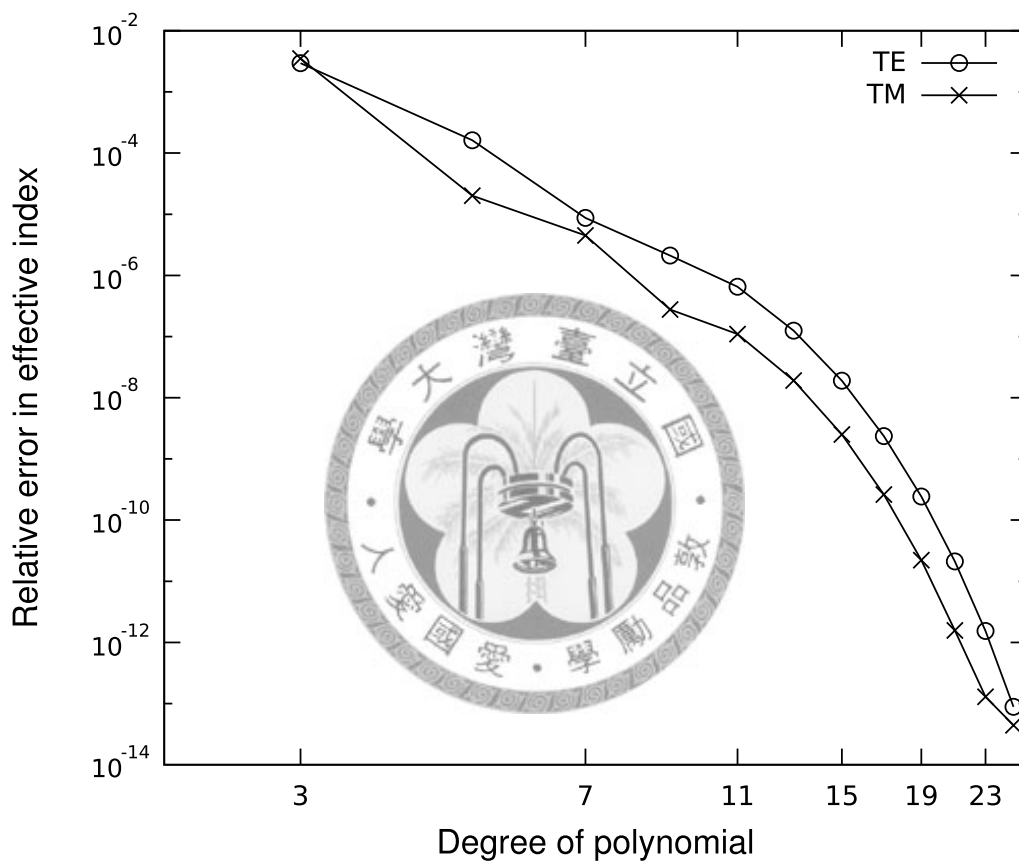


Figure 6.6: Relative errors in the effective index for the TE and TM modes of asymmetric slab waveguide with respect to the degree of polynomial in each domain.

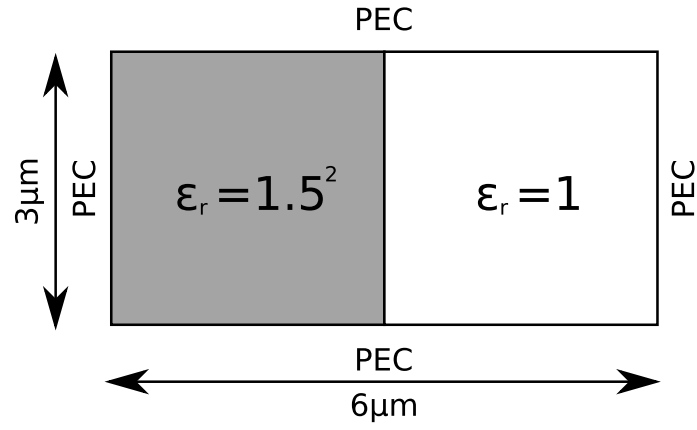


Figure 6.7: Cross-section of a partially filled metallic waveguide.

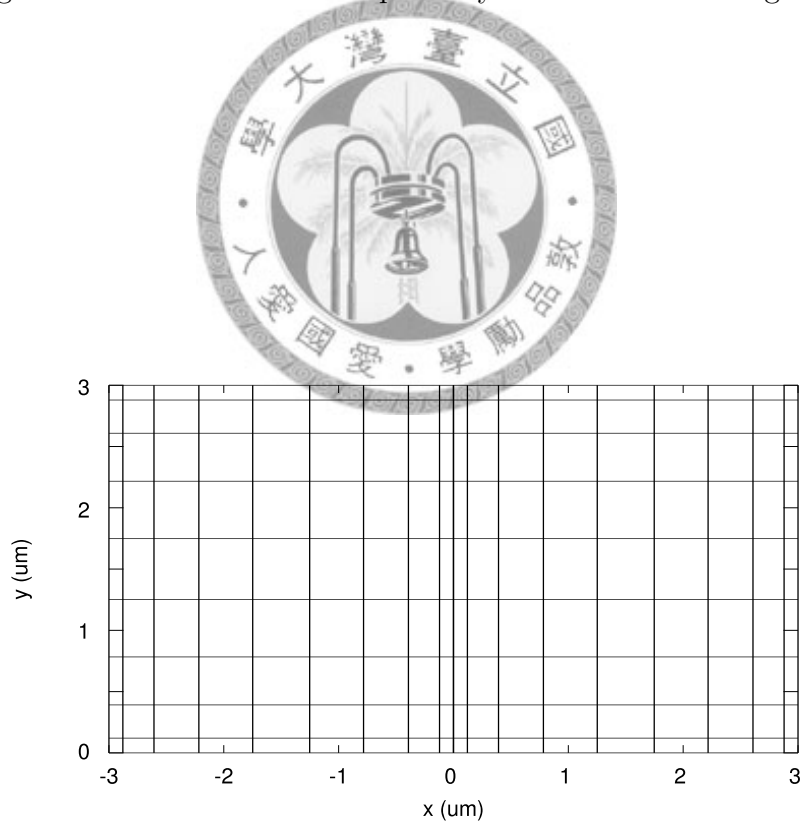


Figure 6.8: Mesh division of the partially filled metallic waveguide of Fig. 6.6.

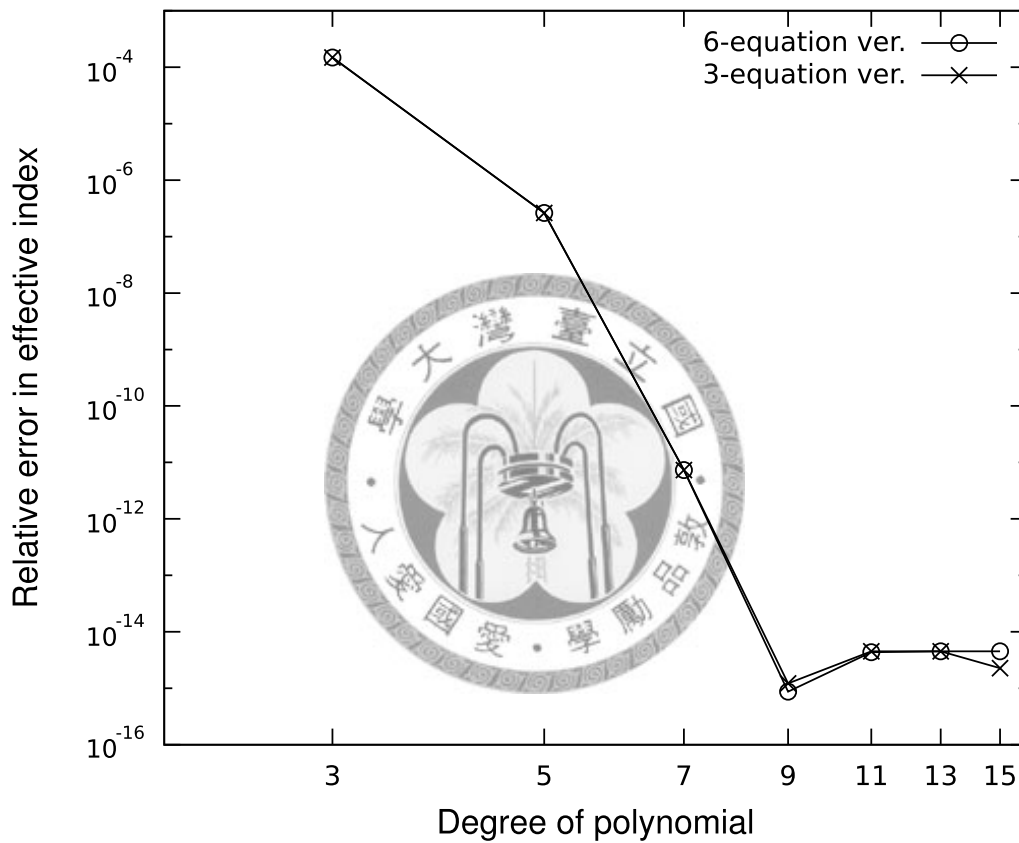


Figure 6.9: Relative error in the effective index for the fundamental LSE_{10} mode of the partially filled metallic waveguide of Fig. 6.7.

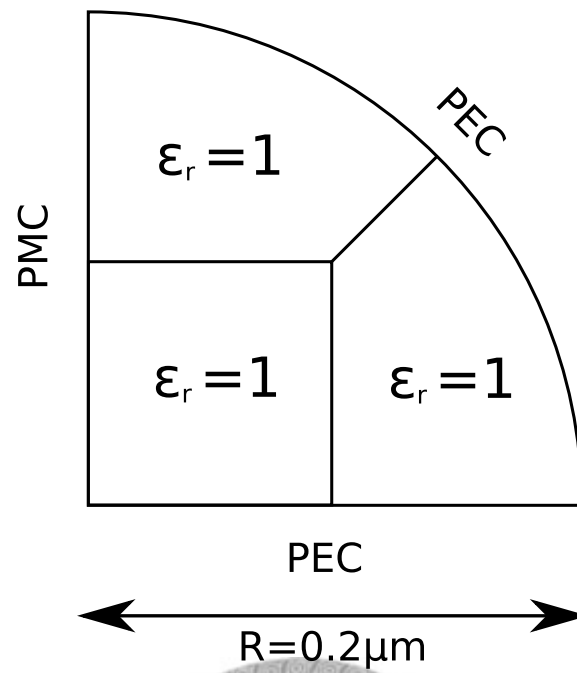


Figure 6.10: Sketch of a quarter of the cross-section of a circular metallic waveguide.

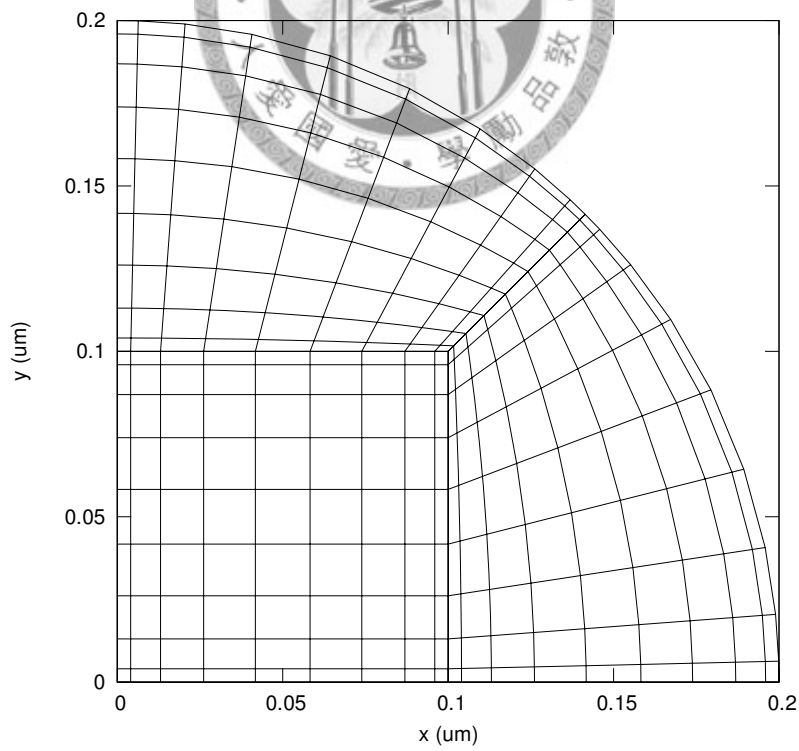


Figure 6.11: Mesh division for the structure of Fig. 6.10.

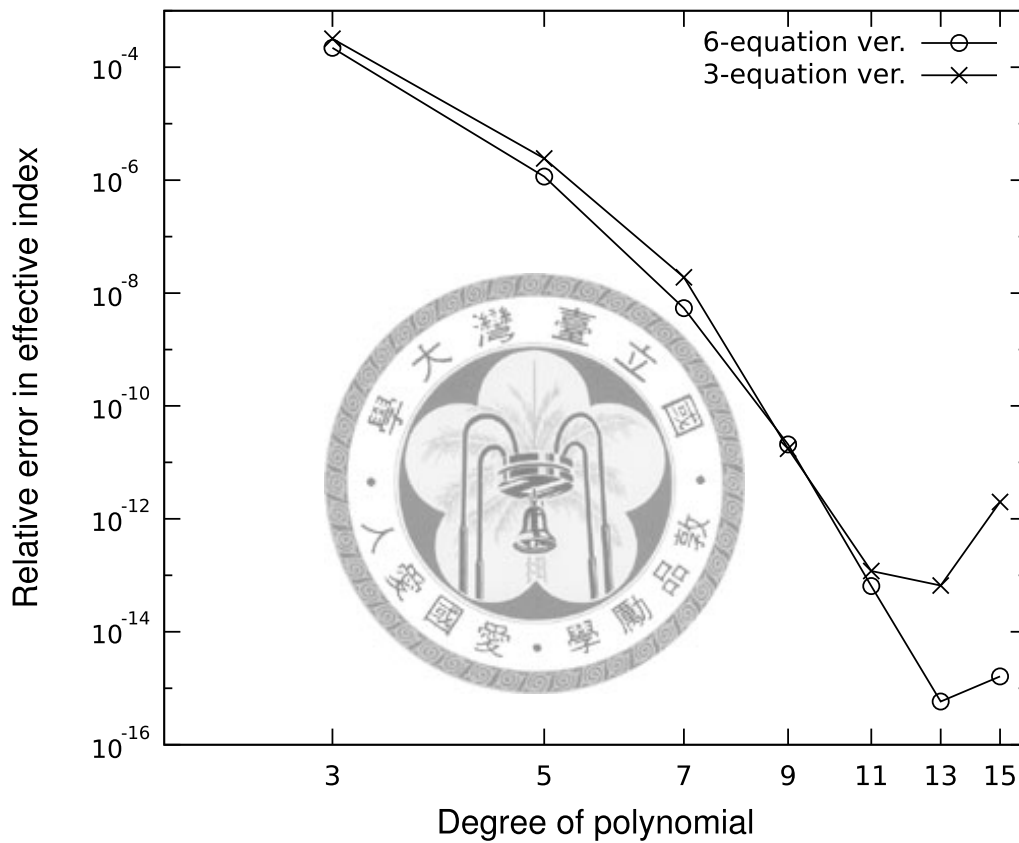


Figure 6.12: Relative errors in the effective index for the fundamental TE_{11} mode of the circular metallic waveguide of Fig. 6.10.

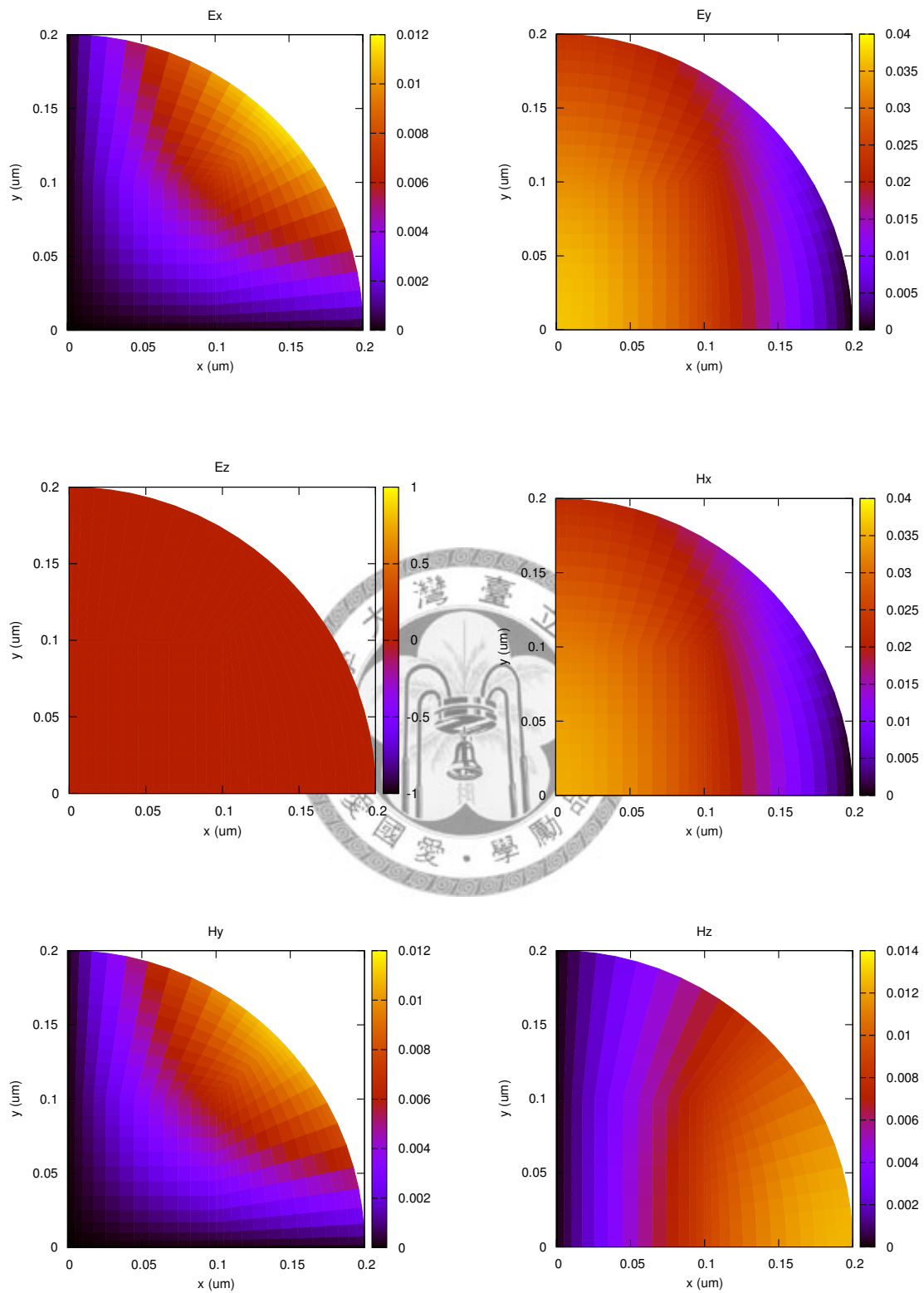


Figure 6.13: Distributions of the six field components of the fundamental (TE_{11}) mode of the circular metallic waveguide of Fig. 6.10.

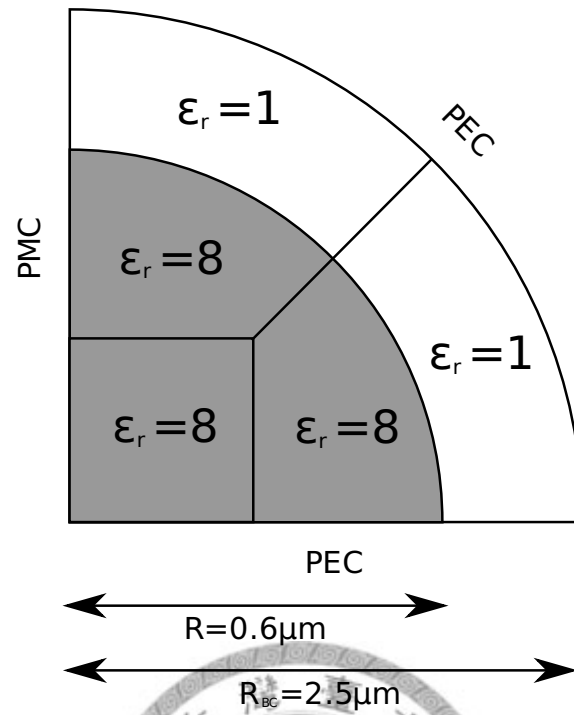


Figure 6.14: Sketch of a quarter of the cross-section of a circular fiber waveguide.

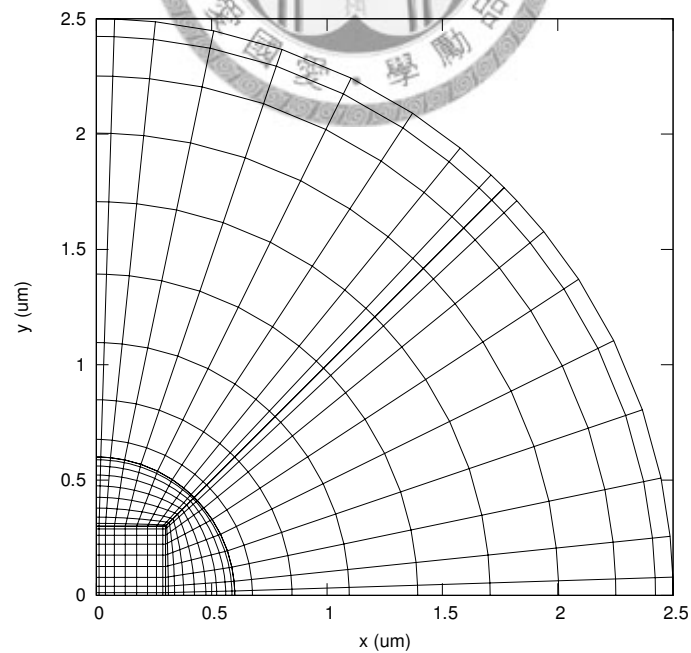


Figure 6.15: Mesh division of for the structure of Fig. 6.14.

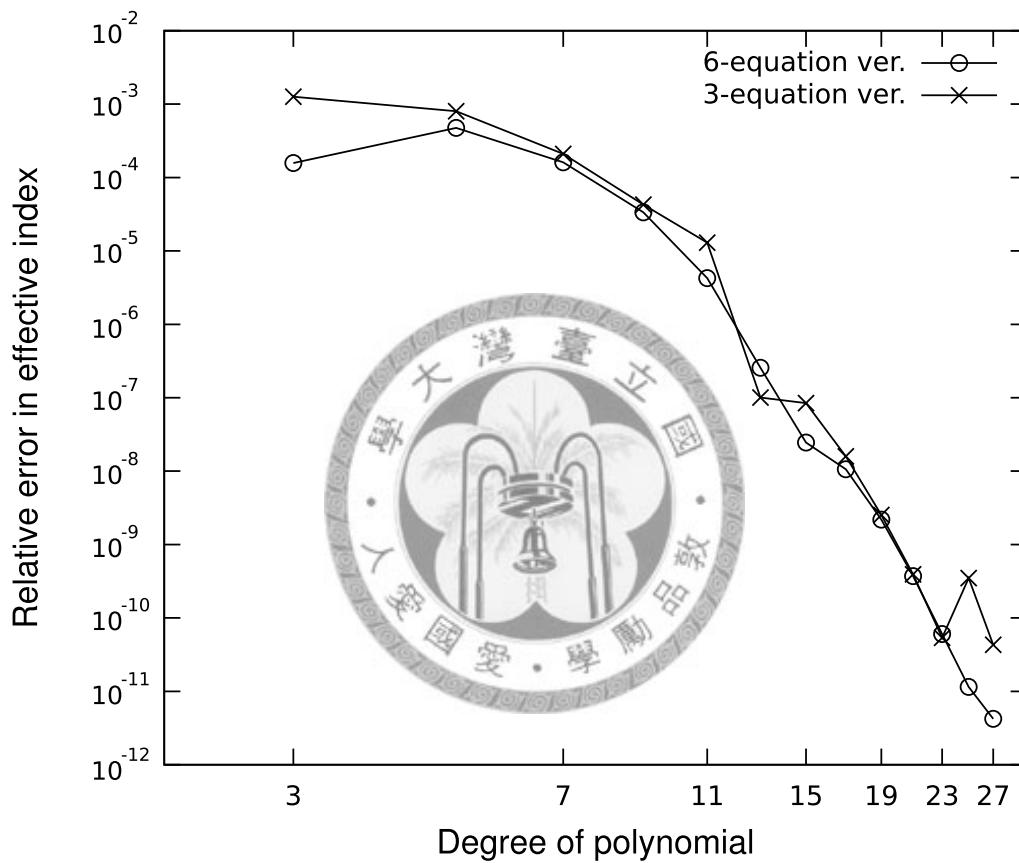


Figure 6.16: Relative errors in the effective index for the fundamental (HE_{11}) mode of the circular fiber waveguide of Fig. 6.14.

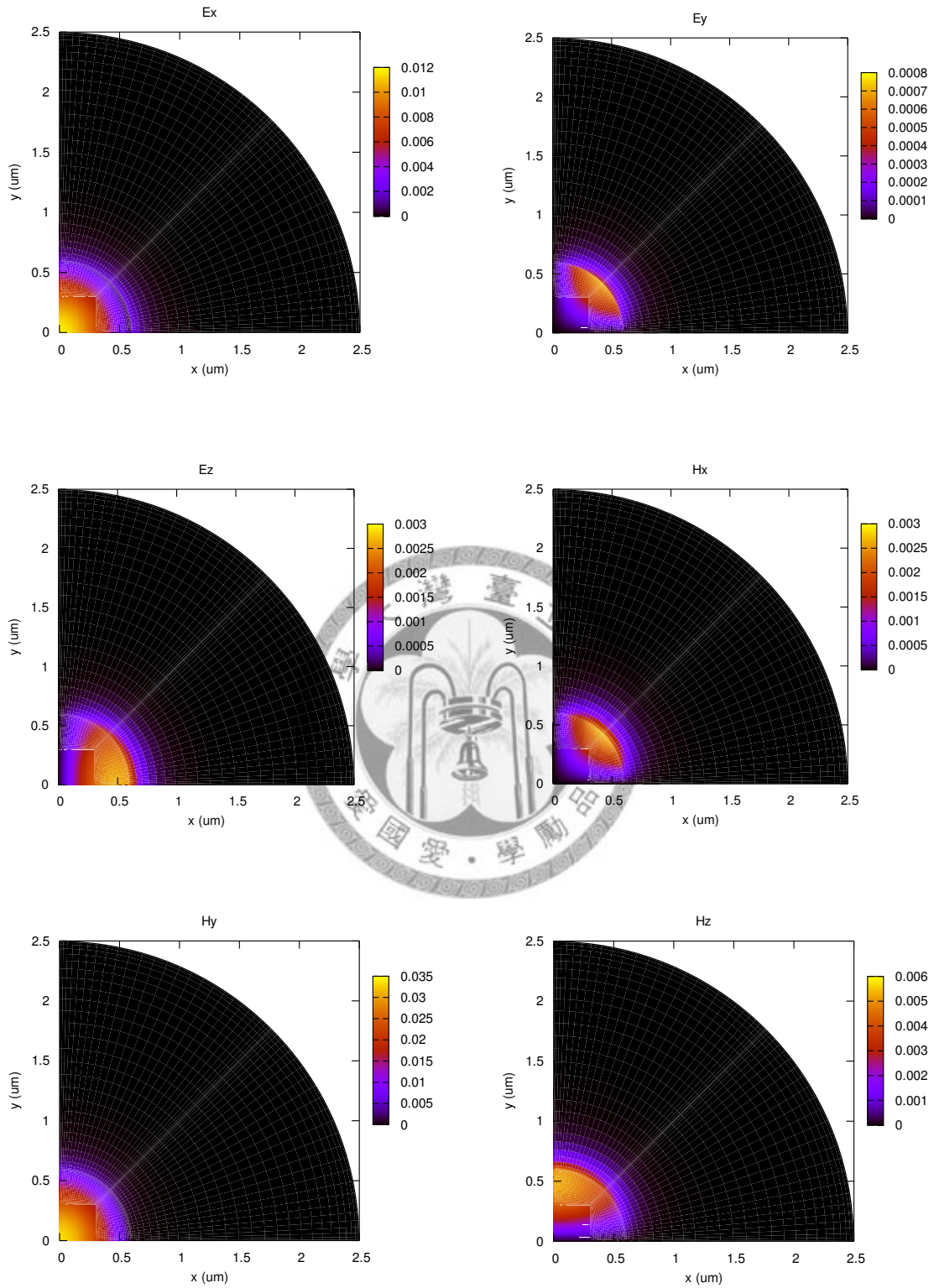


Figure 6.17: Distributions of the six field components of the fundamental (HE_{11}) mode of the circular fiber waveguide of Fig. 6.14.

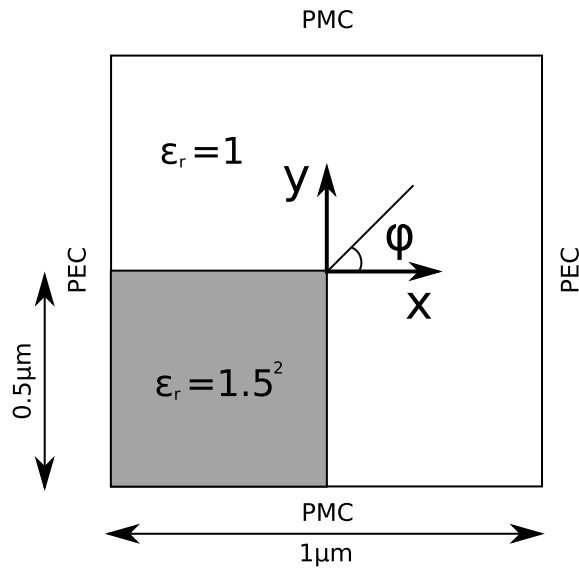


Figure 6.18: Sketch of a quarter of the cross-section of the channel waveguide.

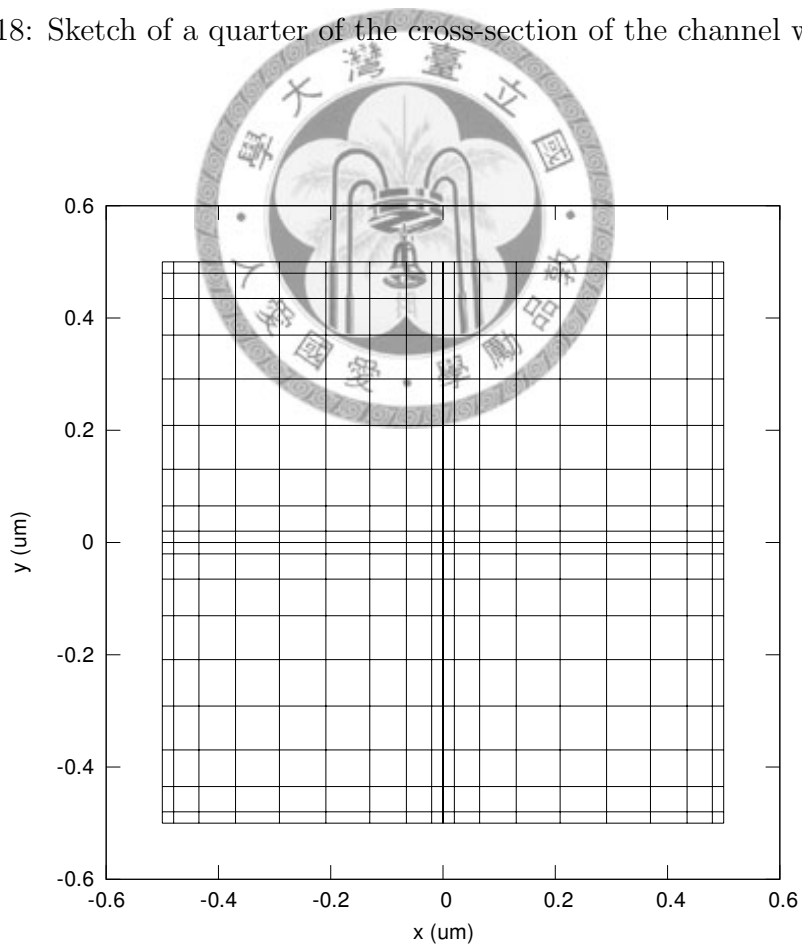


Figure 6.19: Mesh division for the structure of Fig. 6.18.

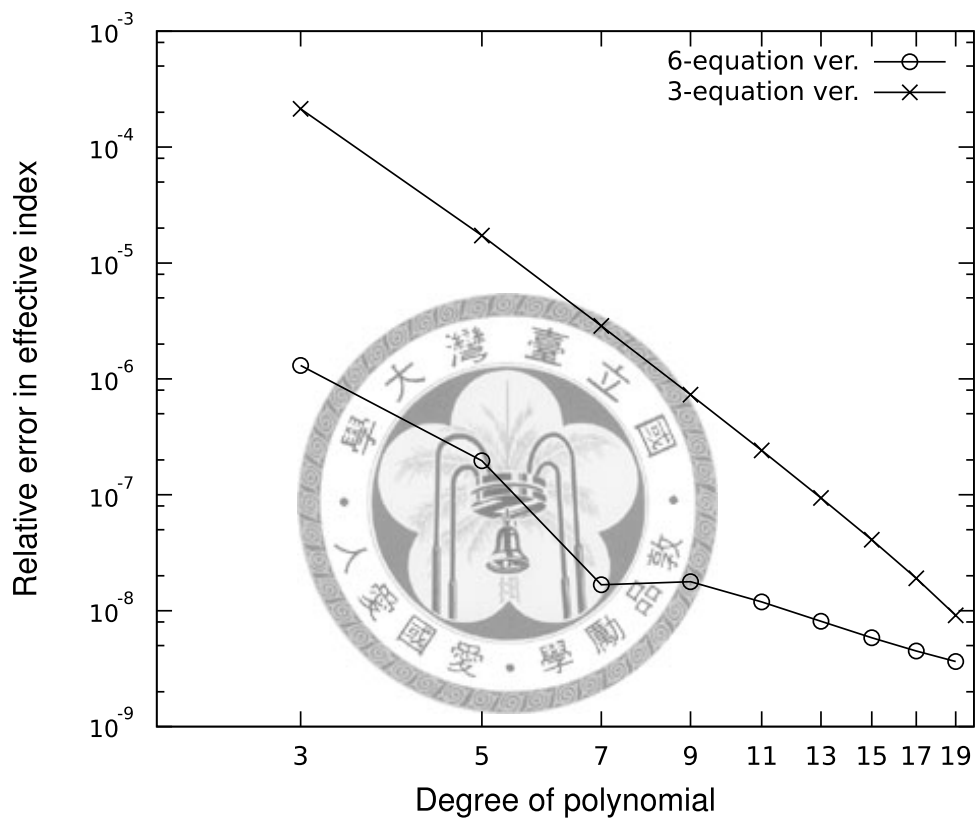


Figure 6.20: Relative errors in the effective index for the fundamental mode of the channel waveguide of Fig. 6.18, as compared to *Hadley's* results [*Hadley*, 2002] ($n_{eff} = 1.27627404$).

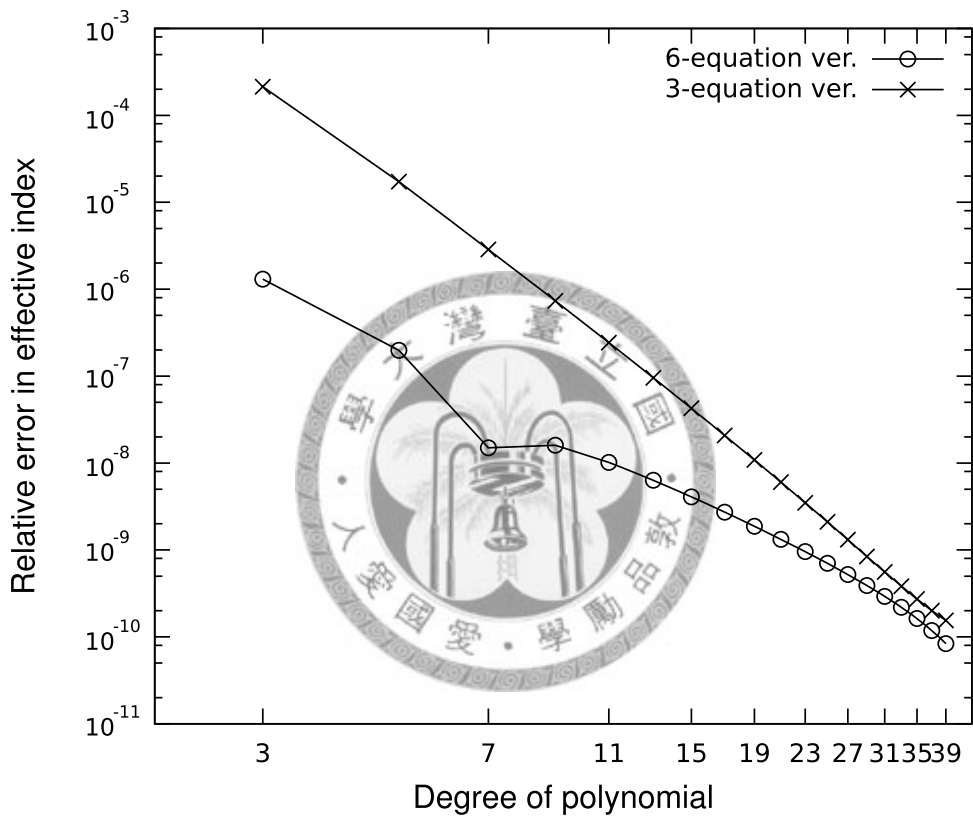


Figure 6.21: Same as Fig. 6.20 but with the reference effective index value being that calculated with degree-45 polynomials ($n_{eff} = 1.27627403774$).

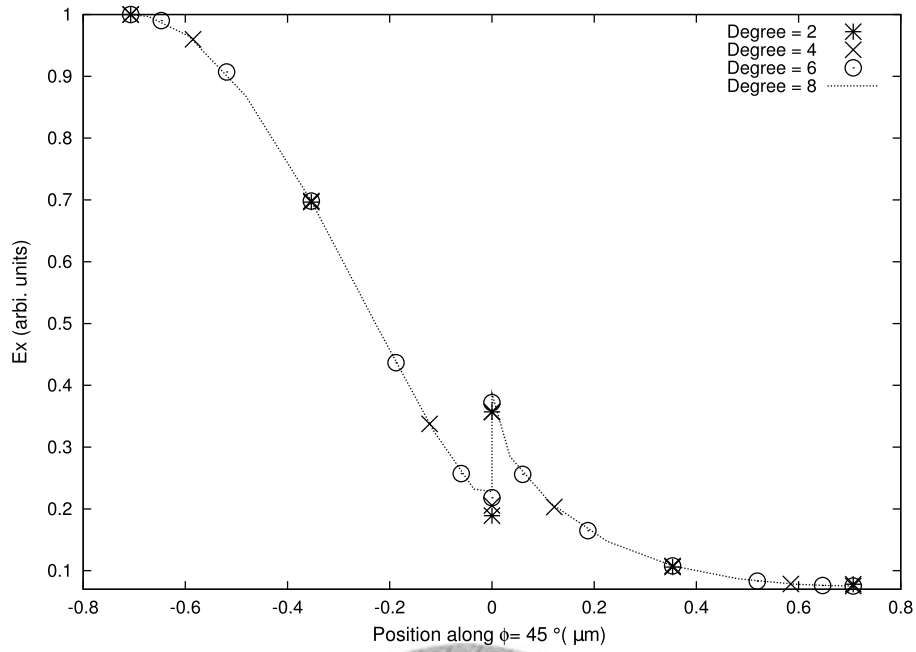


Figure 6.22: Field profiles of E_x along $\phi = 45^\circ$ for the channel waveguide of Fig. 6.18 calculated using various degrees of polynomial.

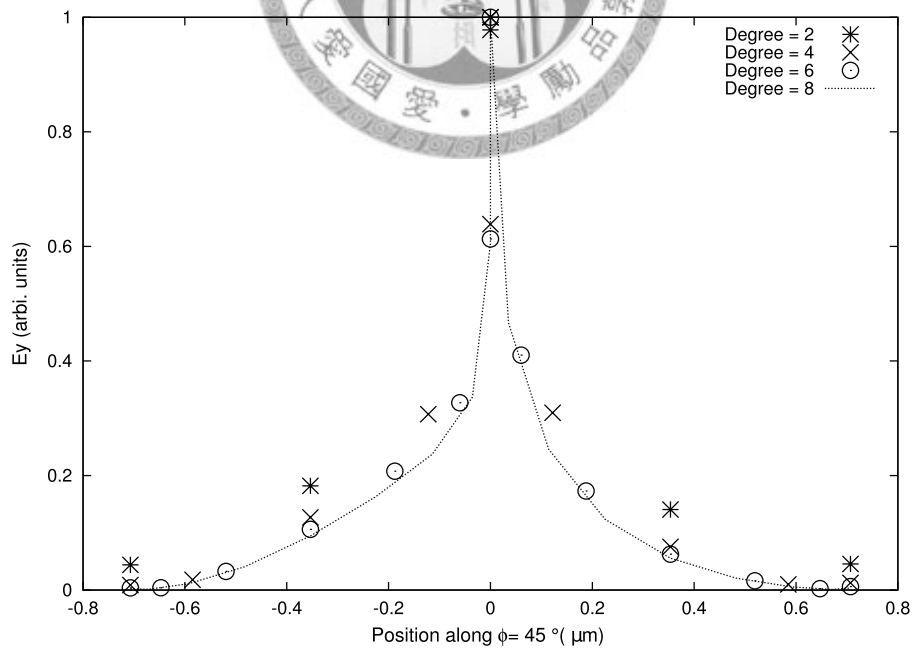


Figure 6.23: Field profiles of E_y along $\phi = 45^\circ$ for the channel waveguide of Fig. 6.18 calculated using various degrees of polynomial.

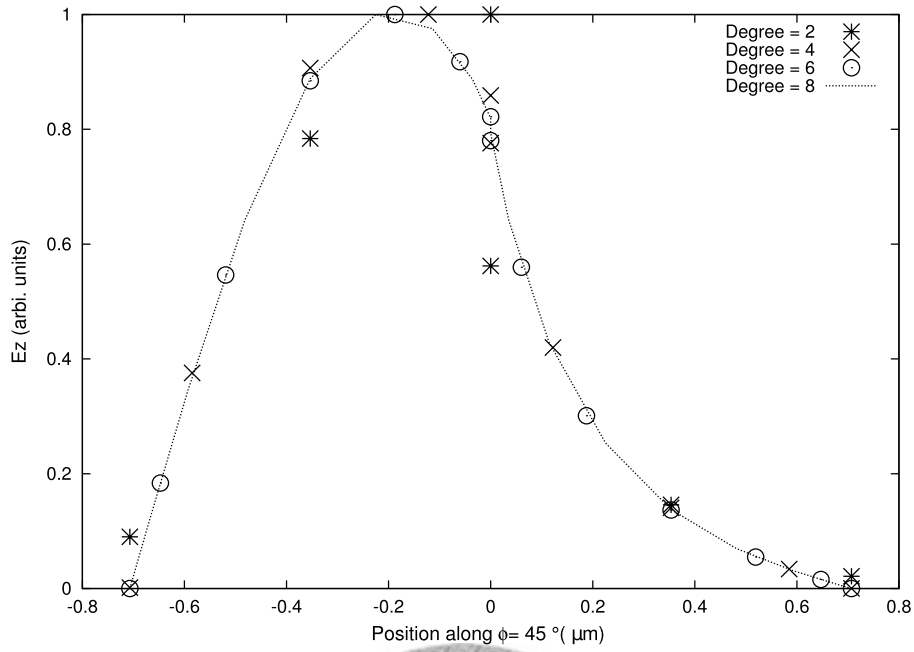


Figure 6.24: Field profiles of E_z along $\phi = 45^\circ$ for the channel waveguide of Fig. 6.18 calculated using various degrees of polynomial.

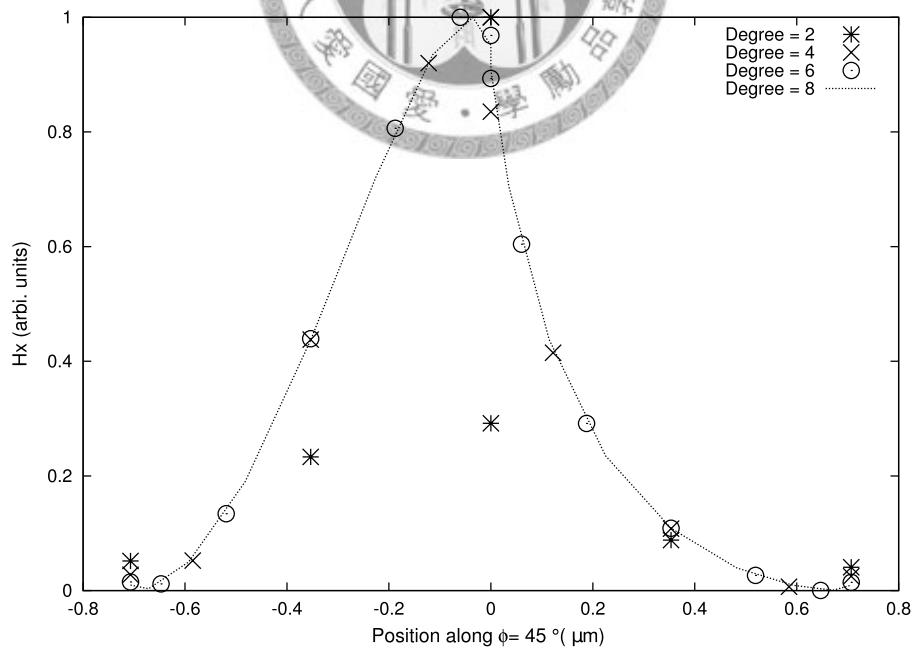


Figure 6.25: Field profiles of H_x along $\phi = 45^\circ$ for the channel waveguide of Fig. 6.18 calculated using various degrees of polynomial.

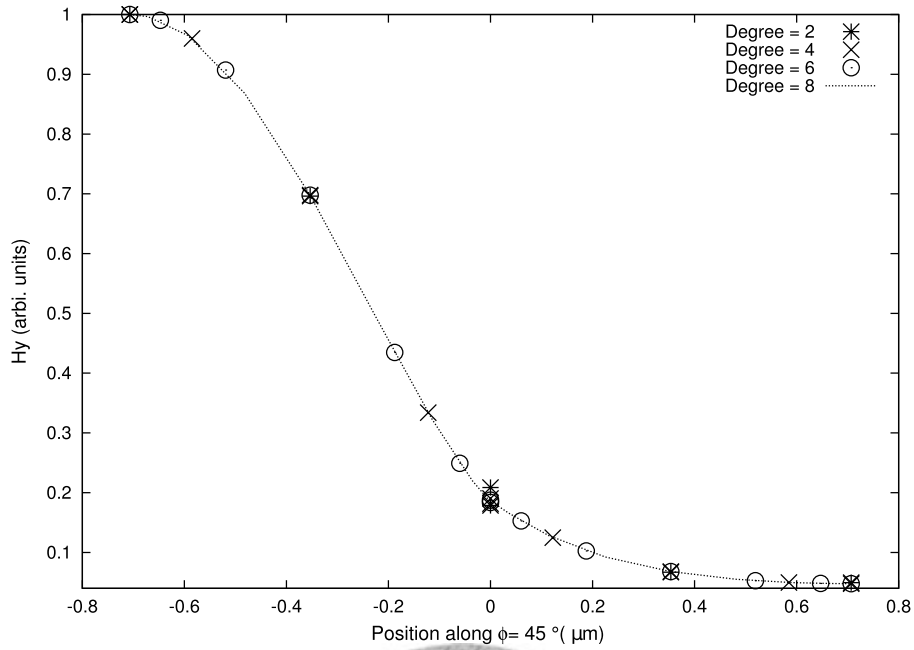


Figure 6.26: Field profiles of H_y along $\phi = 45^\circ$ for the channel waveguide of Fig. 6.18 calculated using various degrees of polynomial.

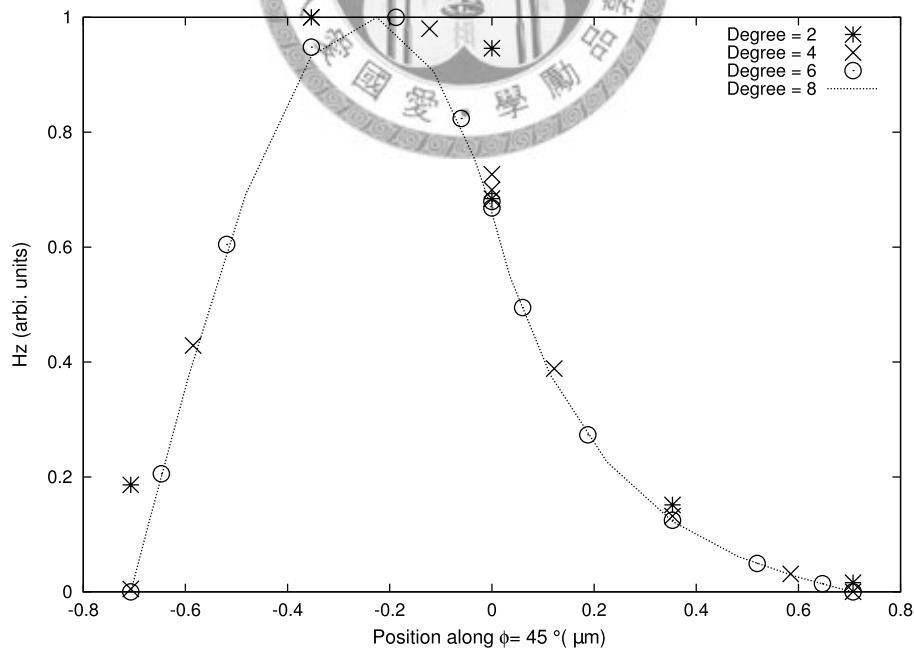


Figure 6.27: Field profiles of H_z along $\phi = 45^\circ$ for the channel waveguide of Fig. 6.18 calculated using various degrees of polynomial.

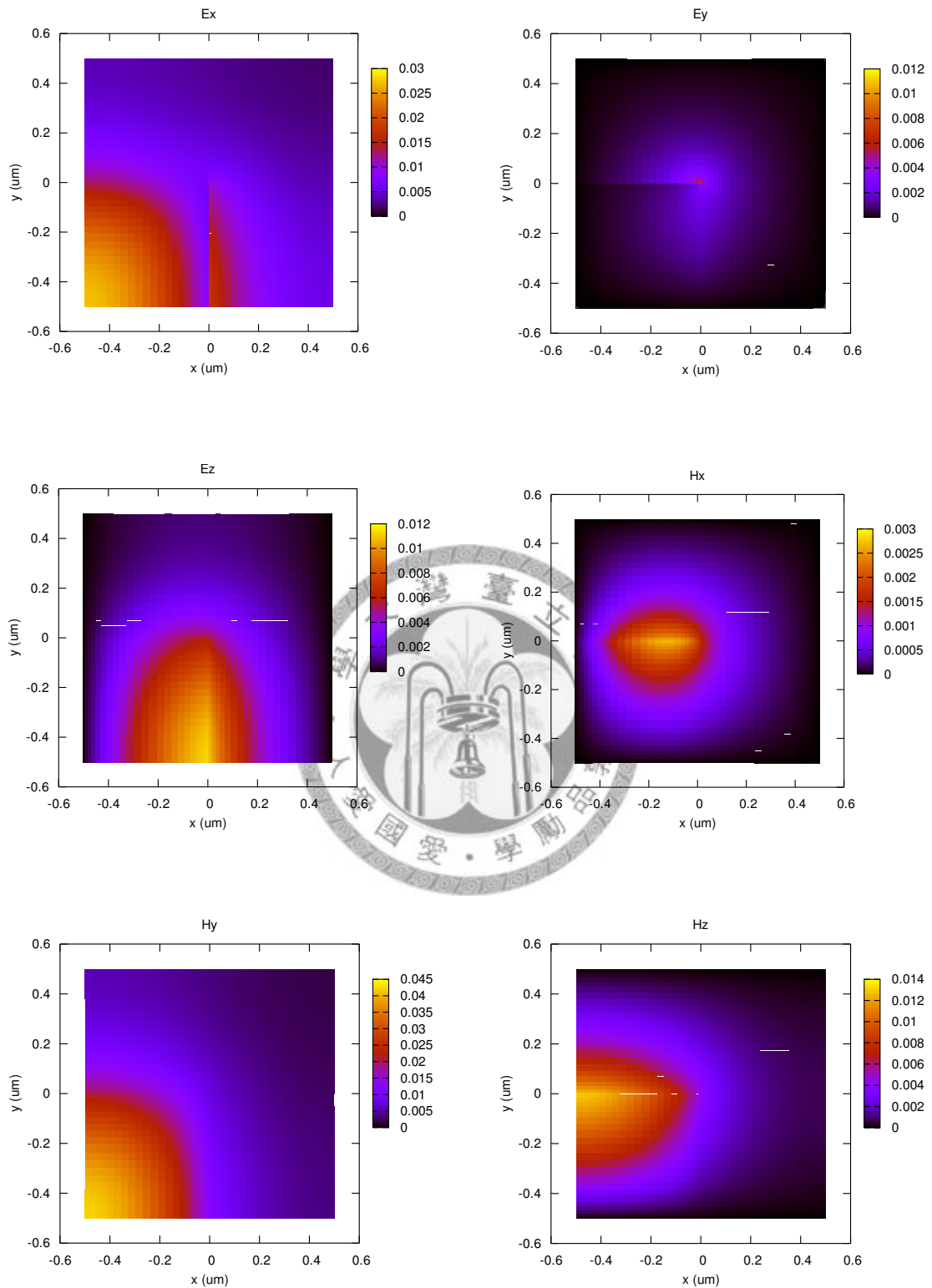


Figure 6.28: Distributions of the six field components of the fundamental mode of the channel waveguide of Fig. 6.18.

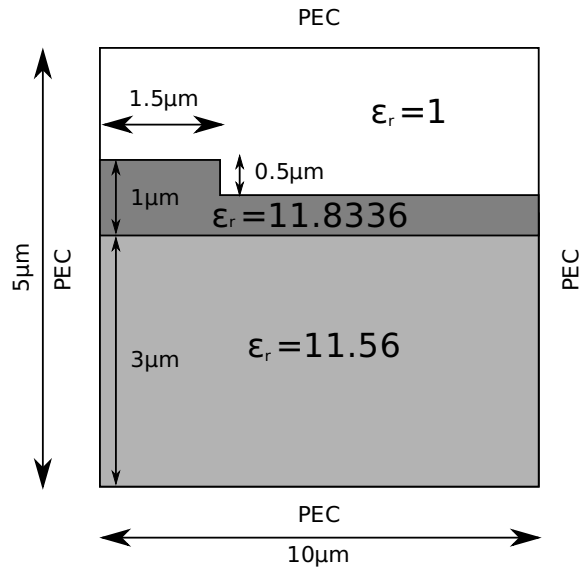


Figure 6.29: Sketch of a half of the cross-section of the rib waveguide.

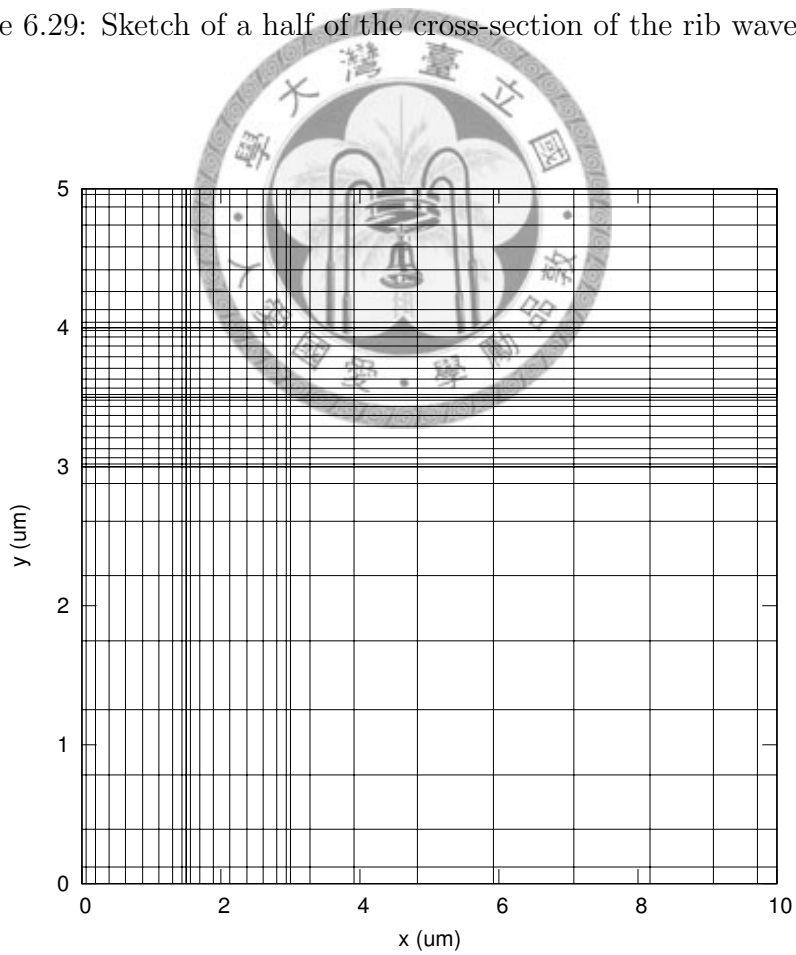


Figure 6.30: Mesh division for the structure of Fig. 6.29.

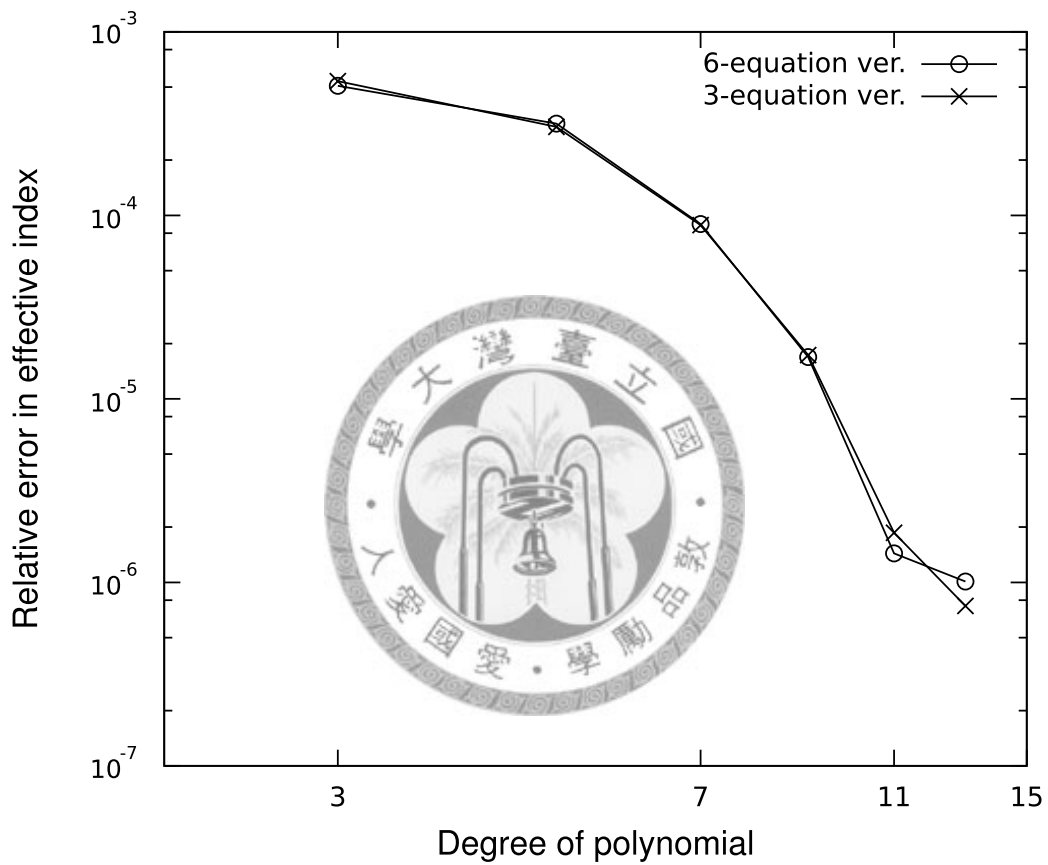


Figure 6.31: Relative error in the effective index for the fundamental mode of the rib waveguide of Fig. 6.29, as compared to *Hadley's* result [*Hadley, 2002*].

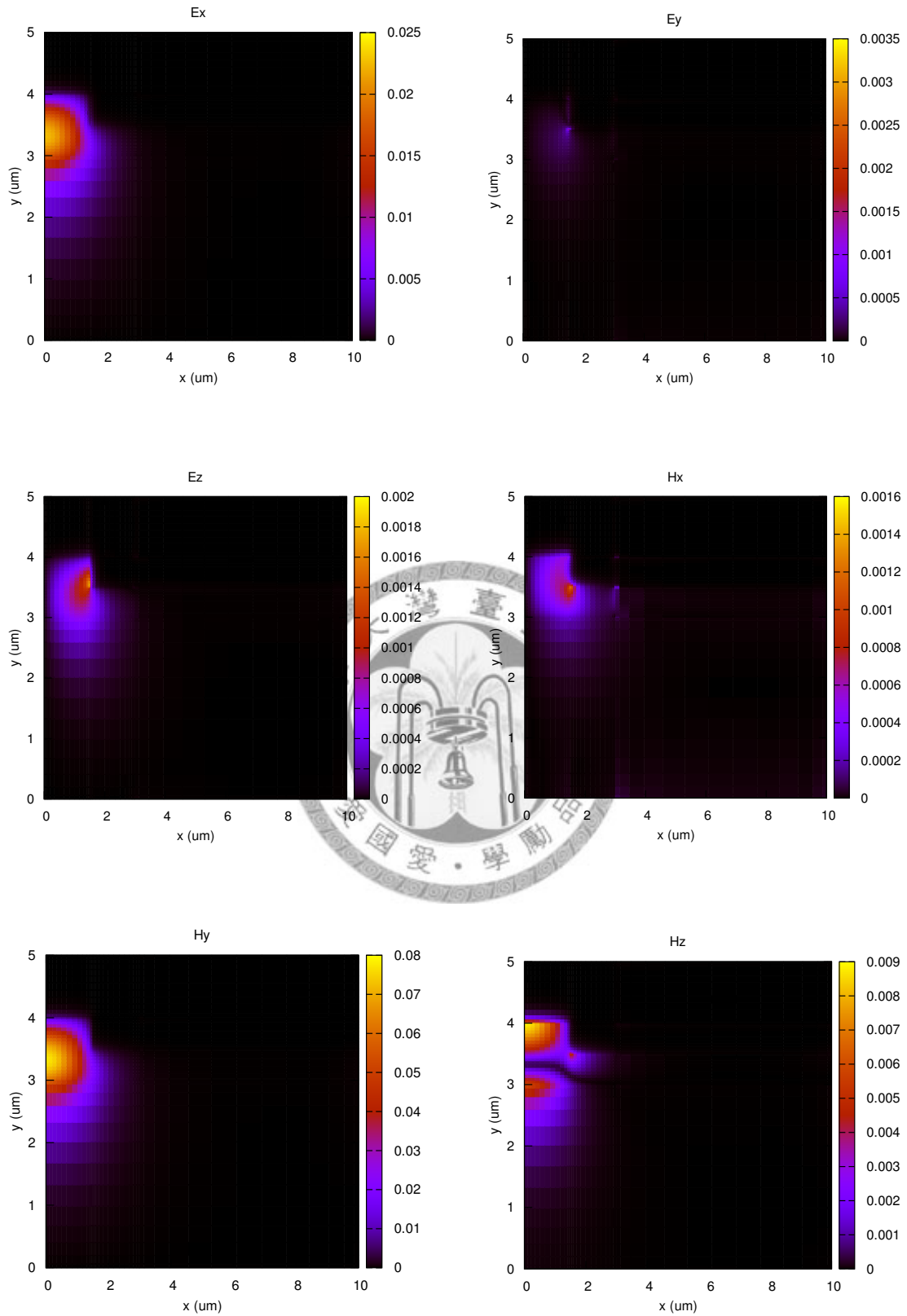


Figure 6.32: Distributions of the six field components of the fundamental mode of the rib waveguide of Fig. 6.29.

Chapter 7

Numerical Results For Photonic Crystal Problems

This chapter is devoted to the analysis of PC structures using the proposed new formulations. We consider two cases, namely, the PC with square lattice and that with triangular lattice.

7.1 Square-Lattice Photonic Crystals

First, We examine a PC with square lattice, with its cross-sections as shown in Fig. 7.1. The structure is formed by parallel alumina rods with refractive index $n = \sqrt{8.9}$ surrounded by air ($n = 1.0$). The radius of each rod is $r = 0.4 \mu\text{m} = 0.2a$, where a is the lattice constant. Figure 7.2 shows the mesh division for the unit cell that is also computational domain, which is divided into thirteen sub-domains. The periodic boundary conditions are put at all four sides, as shown in Fig. 7.1.

The band diagrams for the TE and TM modes are shown in Figs. 7.3 and 7.4, respectively. The results are obtained using the three-equation formulation with degree 13 of polynomial in each sub-domain. The Brillouin zone is shown as the inset in the figures. The normalized frequency is defined as

$$\text{Normalized frequency} = \frac{\omega a}{2\pi c}. \quad (7.1)$$

Using the degree-21 three equation formulation calculation results as the reference, we show in Fig. 7.5 relative errors in the calculated eigen frequency versus

the degree of polynomial for both three-equation and one-equation formulations for the first TE and TM modes at M point where $k_x = \pi/a$ and $k_z = \pi/a$. The spectral convergence behavior is seen for all four situations. Figure 7.6(a), (b), and (c) show the field distributions at M point for the first TE mode and Fig. 7.6(d), (e), and (f) shows those for the first TM mode.

7.2 Triangular-Lattice Photonic Crystals

Next, we analyze the PC with triangular lattice, with its cross-section as shown in Fig. 7.7. The refractive index of each rod is $n = \sqrt{11.4}$, which is surrounded by air. The radius of each rod is $r = 0.4 \mu\text{m} = 0.2a$, where a is lattice constant. Figure 7.8 shows the mesh division for the unit cell where fourteen sub-domains are adopted. The periodic boundary conditions are employed at all six edges.

The band diagrams for TE and TM modes are shown in Figs. 7.9 and 7.10, respectively. The results are obtained using the three-equation formulation with degree 13 of polynomial in each sub-domain. The Brillouin zone is shown at the inset in the figures. Consider the first TE and TM modes at the K point where $k_x = 2\pi/\sqrt{3}a$ at $k_y = 2\pi/3a$. Using the degree-21 three-equation formulation calculation result as the reference, we show in Fig. 7.11 relative errors in the calculated eigen frequency versus the degree of polynomial for both three-equation and one-equation formulations for the first TE and TM modes. Again, the spectral convergence behavior is observed for all four situations. Figure 7.12(a), (b), and (c) illustrate the field distributions at the K point for the first TE mode and Fig. 7.12(d), (e), and (f) illustrate those for the first TM mode.

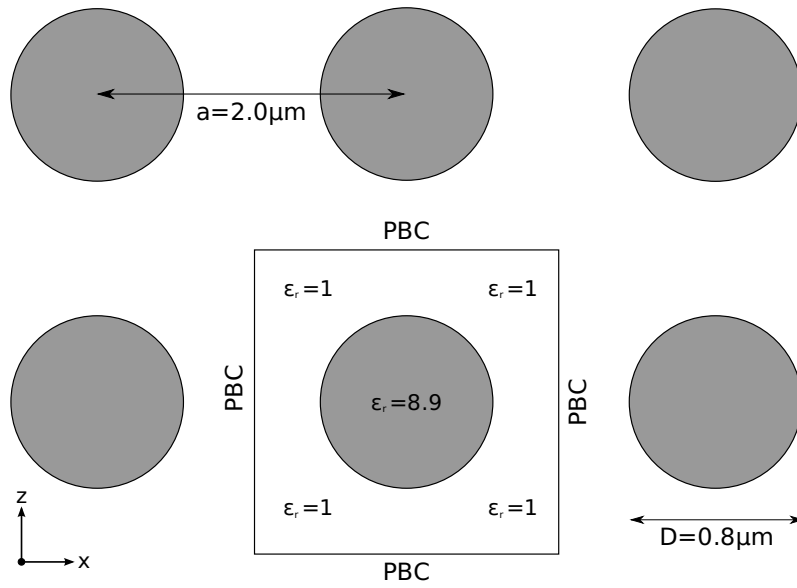


Figure 7.1: Sketch of the cross-section of a PC with square lattice.

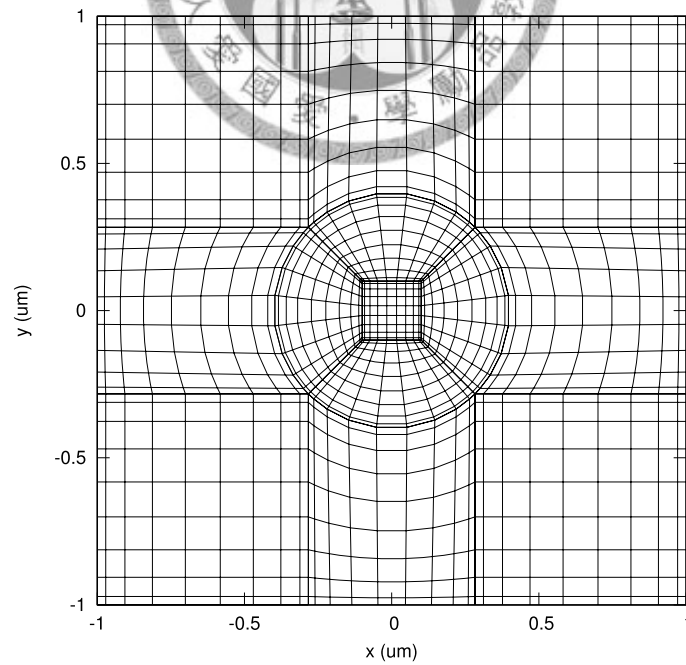


Figure 7.2: Mesh division of the unit cell in Fig. 7.1.

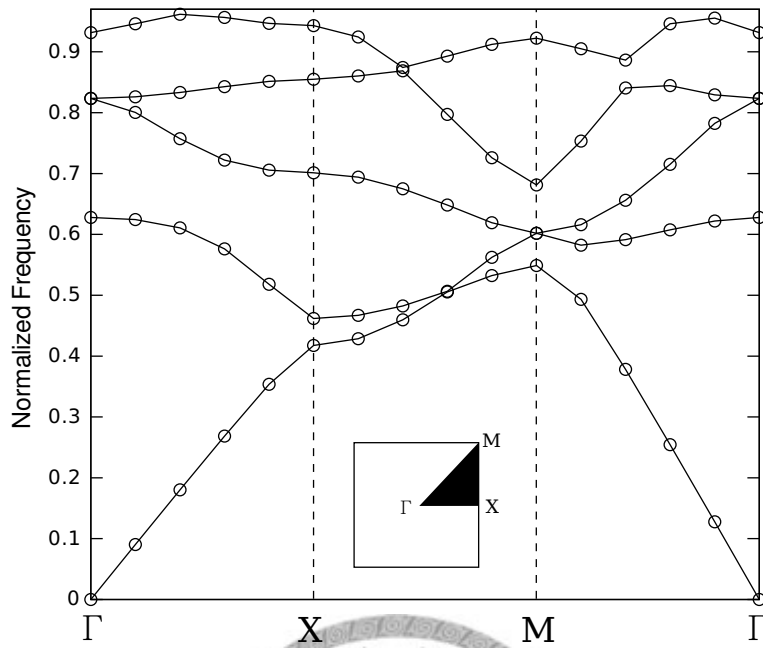


Figure 7.3: Band diagram for TE modes of the square-lattice PC of Fig. 7.1.

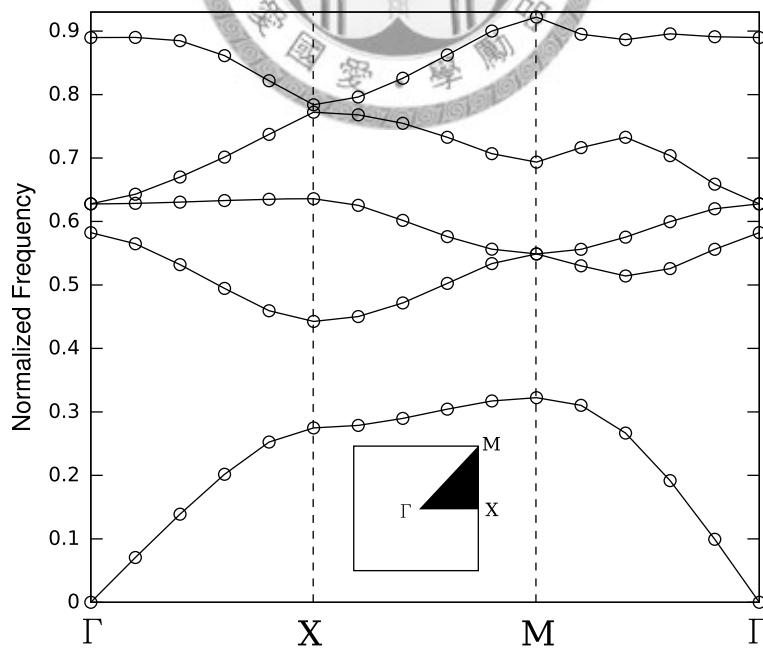


Figure 7.4: Band diagram for TM modes of the square-lattice PC of Fig. 7.1.

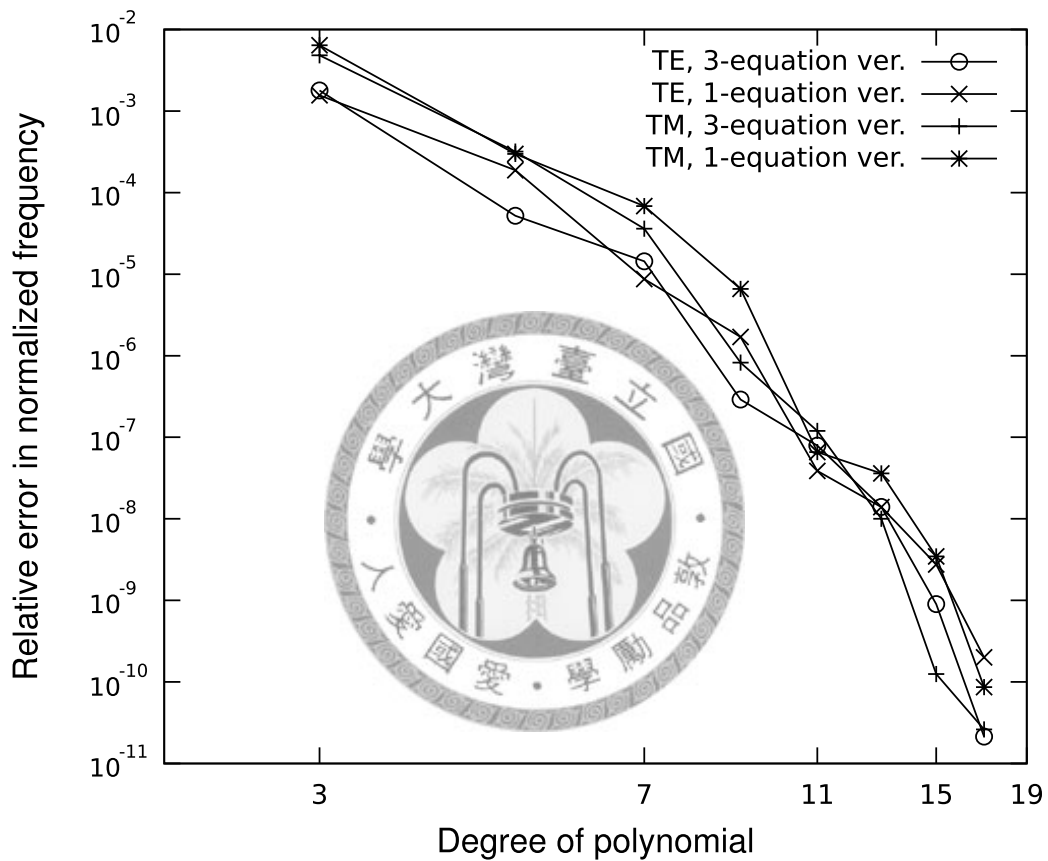


Figure 7.5: Relative errors in the calculated eigen frequency versus the degree of polynomial for the first TE and TM modes of the square-lattice PC of Fig. 7.1 at the M point using the degree-21 three-equation formulation result as reference.

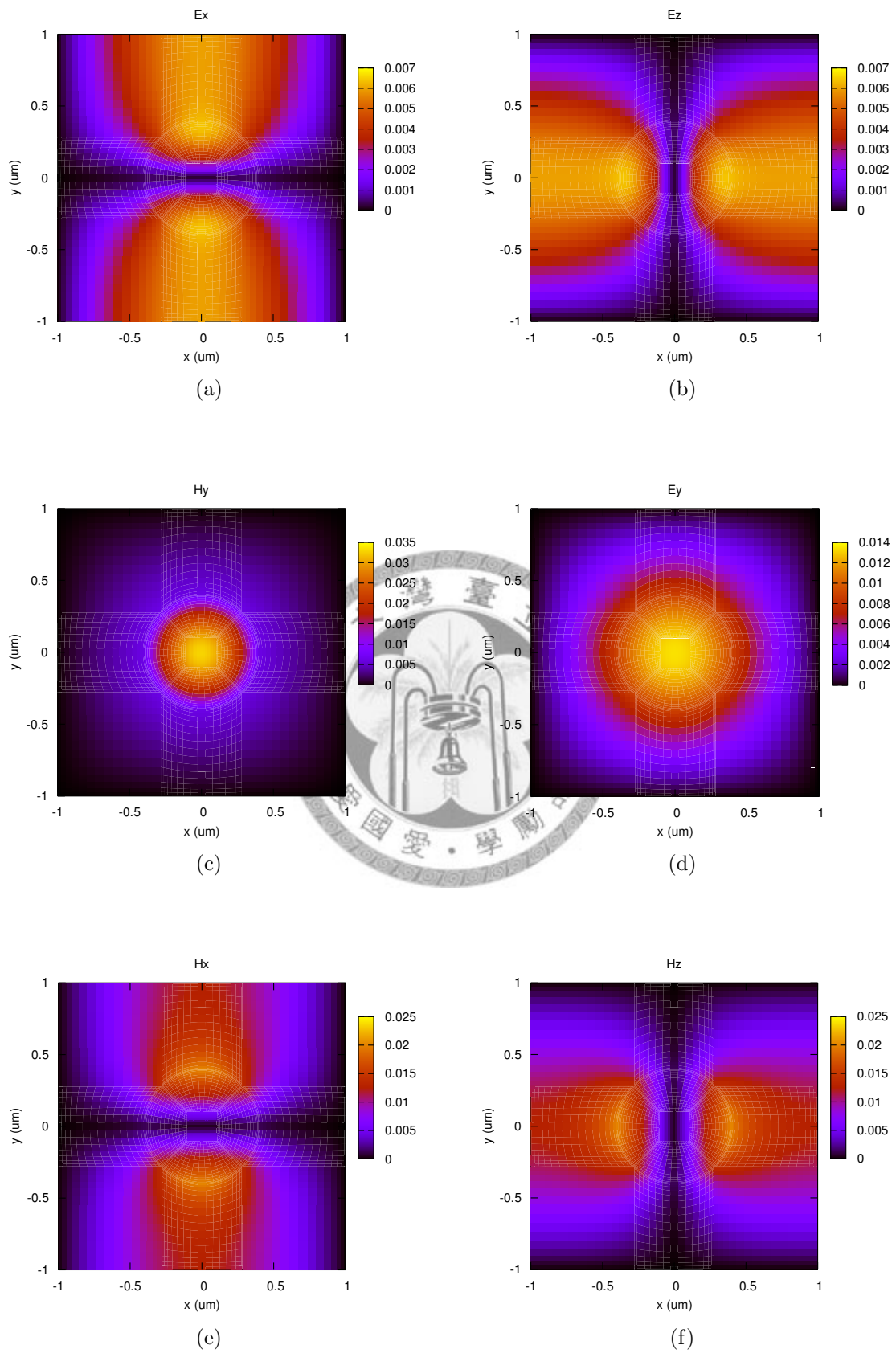


Figure 7.6: (a)(b)(c) Field distributions of the first TE mode at the M point for the square-lattice PC of Fig. 7.1. (d)(e)(f) Field distributions of the first TM mode at the M point for the same PC.

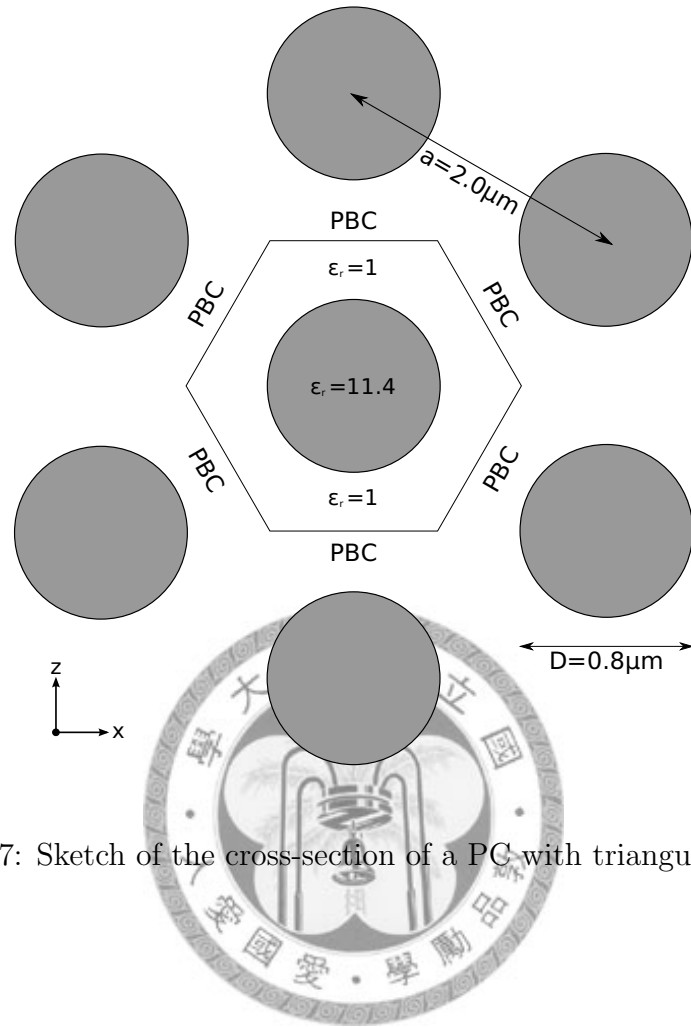


Figure 7.7: Sketch of the cross-section of a PC with triangular lattice.

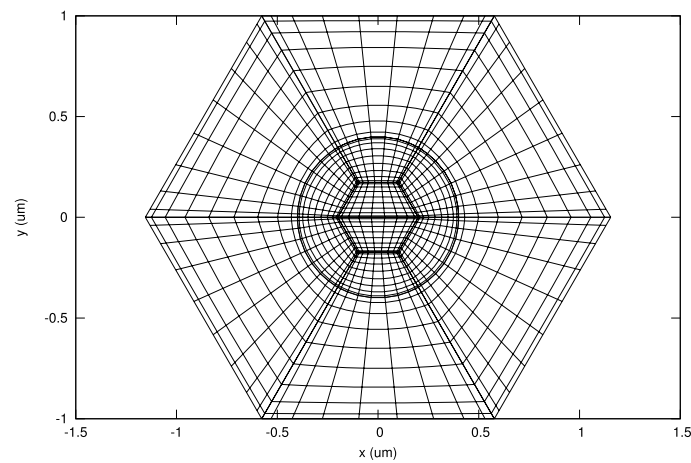


Figure 7.8: Mesh division of the unit cell in Fig. 7.7.

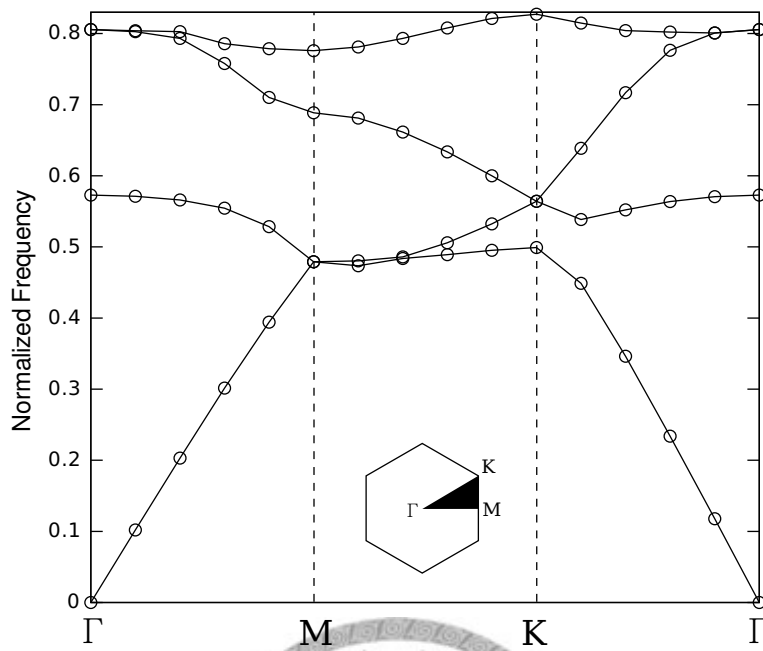


Figure 7.9: Band diagram for TE modes of the triangle-lattice PC of Fig. 7.7.

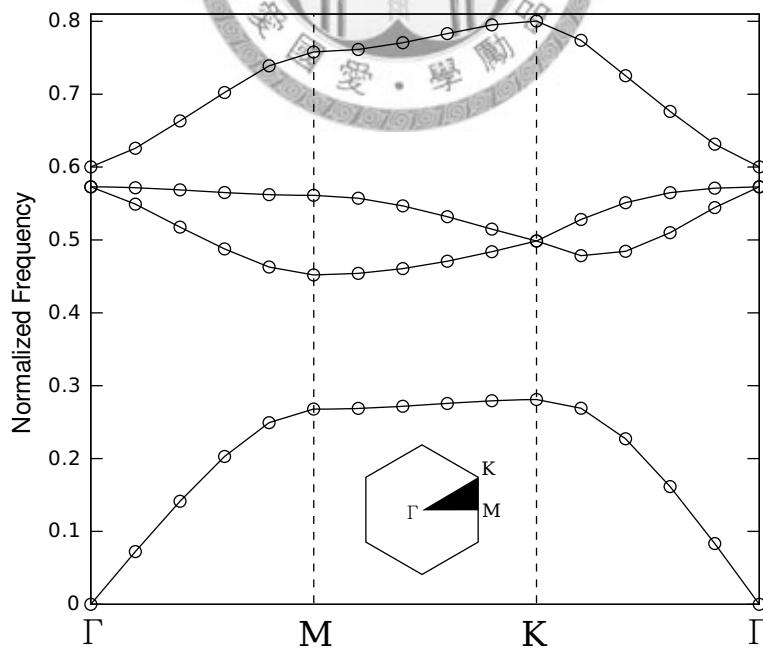


Figure 7.10: Band diagram for TM modes of the triangular-lattice PC of Fig. 7.7.

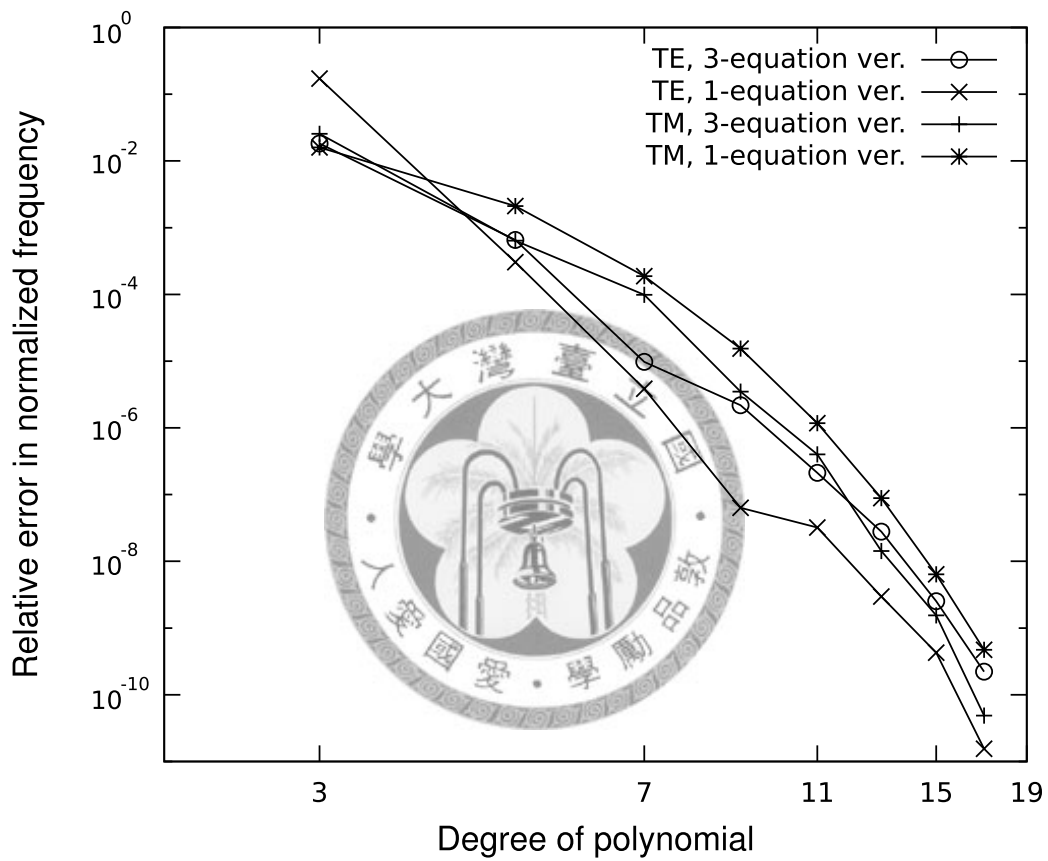


Figure 7.11: Relative errors in the calculated eigen function versus the degree of polynomial of the triangular-lattice PC of Fig. 7.7 at the K point using the degree-21 three-equation formulation result as the reference.

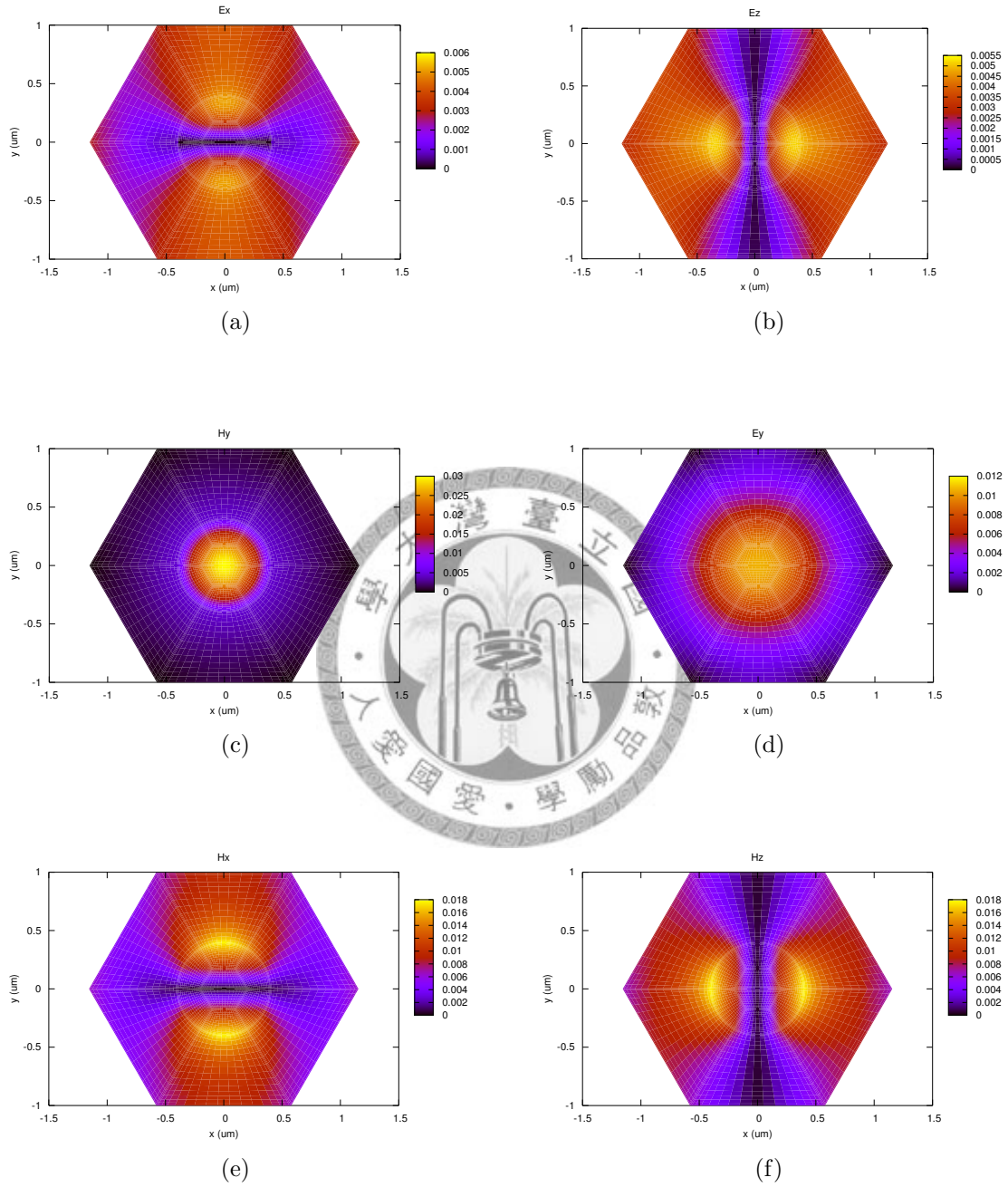


Figure 7.12: (a)(b)(c) Field distributions of the first TE mode at the K point for the triangular-lattice PC of 7.7. (d)(e)(f) Field distributions of the first TM mode of PC at the K point for the same PC.

Chapter 8

Conclusion

New formulations for analyzing 1D and 2D waveguides have been presented in this thesis. The boundary conditions are imposed by the penalty method in each of the 1D, 2D-waveguide, and PC problems. In order to get high-accuracy results, pseudospectral Legendre method is adopted for all three cases.

Since the frequency-domain problem is different from the time-domain problem, we have redrived the penalty-type boundary conditions in Chapters 2–4 for the frequency-domain problems. The derived boundary conditions are very simple, compared to the original ones used in time domain. Although the boundary conditions are simple, they offer enough restrictions for governing equations to calculate the modes. For 2D waveguides, we actually propose two sets of equations: the six-equation form and the three-equation form, and we have proved that both of them can be used to analyze 2D-waveguide problems in Chapter 6. Similarly, we propose the three-equation form and one-equation form for the 2D-PC problem, both of which are proved to be valid in numerical examples in Chapter 7.

In Chapter 5, we briefly describe the pseudospectral Legendre and SIPM numerical methods. Since this thesis does not focus on the fundamental concept of the pseudospectral method, readers can refer to [Boyd, 2000] for more information.

In Chapter 6, in order to examine the feasibility of new 1D and 2D waveguide algorithms, we have analyzed some waveguide structures. For the 1D algorithm, we examine both the symmetric and asymmetric slab waveguides. Compared to the

exact solutions, we find the relative errors in the effective index are both on the order of 10^{-14} . For the 2D algorithm, we first investigate the partial filled waveguide. By comparing with the exact effective index of the LSE_{01} mode, the relative error is found to be on the order of 10^{-15} which is the maximum limit the double precision unit in computer can handle. Next, in order to examine the circular PEC boundary condition, a circular metallic waveguide is investigated. The relative error in the effective index is also on the order of 10^{-15} comparing to the exact solution. The well-known fiber waveguide is also investigated. From comparing with the exact effective index, the numerical errors are found to be on the order of 10^{-11} and 10^{-10} for six-equation and three-equation forms, respectively. Then, we have examined the structures with dielectric corners which have no analytical solutions, i.e., the channel waveguide and the rib waveguide. For the channel waveguide, we found that even using low degree of polynomial, the effective index is quite accurate. The obtained field distributions also show good agreement with those obtained with high degree of polynomial. For the rib waveguide, the error in the effective index can reach the order of 10^{-6} which is the most accurate result we can find in the literature.

In Chapter 7, we examine two 2D-PC structures to check the validity of the algorithm for PCs. We calculate the band diagrams of the square-lattice PC and the triangular-lattice PC for both TE and TM modes. By comparing the band diagrams with the calculations of other methods, the band diagrams are found to have good agreement with the finite-difference frequency-domain (FDFD) analysis [Yu and Chang, 2004] and the plane wave expansion (PWE) method analysis [Johnson and Joannopoulos, 2001].

There is one important issue which we do not consider in this thesis: incorporation of perfectly matched layers (PMLs)[Berenger, 1994] around the computational domain for treating leaky waveguide problems.

In summary, we have successfully implemented pseudospectral mode solvers for 1D waveguides, 2D waveguides, and 2D-PCs using penalty-type boundary condi-

tions.



Bibliography

- [1] Baken, N. H. G, M. B. J. Diemeer, J. M. V. Splunter and H. Blok, “Computational modeling of diffused channel waveguides using a domain integral equation,” *J. Lightwave Technol.*, vol. 8, pp. 576–586, 1990.
- [2] Berenger, J.-P., “A perfectly matched layer for the absorption of electromagnetic waves,” *J. Comput. Phys.*, vol. 114, pp. 185–200, 1994.
- [3] Bierwirth, K., N. Schulz, and F. Arndt, “Finite-difference analysis of rectangular dielectric waveguides structures,” *IEEE Trans. Microwave Theory Tech.*, vol. 34, pp. 1104–1113, 1986.
- [4] Boyd, P. J., *Chebyshev and Fourier Spectral Methods*. New York, NY: Dover Publications, 1999.
- [5] Cendes, Z.J., and P. Silvester, “Numerical solution of dielectric loaded waveguides: Finite-Element Analysis,” *IEEE Trans. Microwave Theory Tech.*, vol. MTT-18, pp. 1124–1131, 1970.
- [6] Chiang, P.J., *Development of Multidomain Pseudospectral Mode Solvers for Optical Waveguides and Photonic Crystals*, M. S. Thesis, Graduate Institute of Electro-Optical Engineering, National Taiwan University, Taipei, Taiwan, January 2007.
- [7] Collin, R., *Field Theory of Guided Waves*. New York: McGraw-Hill, 1960.

- [8] Doncker, Ph. De, “The use of transfinite elements in the methods of moments applied to electromagnetic scattering by dielectric cylinders,” *Progress In Electromagnetics Research*, PIER 25, pp. 77–94, 2000.
- [9] Funaro, D., and D. Gottlieb, “A new method of imposing boundary conditions in pseudospectral approximations of hyperbolic equations,” *Math. Comp.*, vol. 51, pp. 599–613, 1988.
- [10] Hadley, G. R., “Low-truncation-error finite difference equations for photonics simulation I: Beam propagation,” *J. Lightwave Technol.*, vol. 16, pp. 134–141, 1998.
- [11] Hadley, G. Ronald, “High-accuracy finite-difference equations for dielectric waveguide analysis: II. Dielectric corners,” *J. Lightwave Technol.*, vol. 20, pp. 1219–1231, 2002.
- [12] Hadley, G. R., and R. E. Smith, “Full-vector waveguide modeling using an iterative finite-difference method with transparent boundary conditions,” *J. Lightwave Technol.*, vol. 13, pp. 465–469, 1999.
- [13] Hesthaven, J. S., and D. Gottlieb, “A stable penalty method for the compressible Navier-Stokes equations. I. Open boundary conditions,” *SIAM J Sci. Comput.*, vol. 17, pp. 579–612, 1996.
- [14] Hesthaven, J. S., P. G. Dinesen, and J. P. Lynov, “Spectral collocation time-domain modeling of diffractive optical elements,” *J. Comput. Phys.*, vol. 155, pp. 287–306, 1999.
- [15] Hesthaven, J., S. Gottlieb, and D. Gottlieb, *Spectral Methods for Time-dependent Problems*. Cambridge University Press, 2007.

- [16] Johnson, S. G., and J. D. Joannopoulos, “Block-iterative frequency-domain methods for Maxwell’s equations in a planewave basis,” *Opt. Express*, vol. 8, pp. 173–190, 2001.
- [17] Lee, J. F., D. K. Sun, and Z. J. Cendes, “Full-wave analysis of dielectric waveguides using tangential vector finite elements,” *IEEE Trans. Microwave Theory Tech.*, vol. 39, pp. 1262–1271, 1991.
- [18] Lüsse, P., P. Stuwe, J. Schüle, and H.-G. Unger, “Analysis of vectorial mode fields in optical waveguides by an new finite difference method,” *J. Lightwave Technol.*, vol. 12, pp. 487–493, 1994.
- [19] Orszag, S. A., and G. S. Patterson, “Numerical simulation of three-dimensional homogeneous isotropic turbulence,” *Phys. Rev. Lett.*, vol. 28, pp. 76–79, 1972.
- [20] Rahman, B. M. A., and J. B. Davis, “Finite-element analysis of optical and microwave waveguides problems,” *IEEE Trans. Microwave Theory Tech.*, vol. MTT-32, pp. 20–28, 1984.
- [21] Spicopoulos, T., V. Teodoridis, and F. E. Gardiol, “Dyadic Green function for the electromagnetic field in multilayered isotropic media: an operator approach,” *Inst. Elec. Eng. Proc.*, vol. 132, pp. 392–335, 1985.
- [22] Stern, M. S., P. C. Kendall, and P. W. A. McIlroy, “Analysis of the aspectral index method for vector modes of rib waveguides,” *Inst. Elec. Eng. Proc. -J.*, vol. 137, pp. 21–26, 1990.
- [23] Sudbo, A. S., “Why are accurate computations of mode fields in rectangular dielectric waveguides difficult?,” *J. Lightw. Technol.*, vol. 10, pp. 418–419, 1992.
- [24] Teng, C. H., B. Y. Lin, H. C. Chang, H. C. Hsu, C. N. Lin, and K. A. Feng, “A Legendre pseudospectral penalty scheme for solving time-domain Maxwell’s equations,” *J. Sci. Comput.*, 2008. (in press)

- [25] Thomas, N., P. Sewell, and T. M. Benson, “A new full-vectorial higher order finite-difference scheme for the modal analysis of rectangular dielectric waveguides,” *J. Lightwave Technol.*, vol. 25, pp. 2563–2570, 2007.
- [26] Wu, J. L., *Development of Multidomain Pseudospectral Mode Solvers for Optical Waveguides and Photonic Crystals*, M. S. Thesis, Graduate Institute of Communication Engineering, National Taiwan University, Taipei, Taiwan, June 2003.
- [27] Yang, B., and J. S. Hesthaven, “A pseudospectral method for time-domain computation of electromagnetic scattering by bodies of revolution,” *IEEE Trans. Antennas Propagat.*, vol. 47, pp. 132–141, 1999.
- [28] Yu, C. P., and H. C. Chang, “A compact finite-difference frequency-domain method for the analysis of two-dimensional photonic crystals,” *Opt. Express*, vol. 12, pp. 1397–1408, 2004.

